7-2-2011

Microwave techniques and applications for semiconductor quantum dot mode-locked lasers
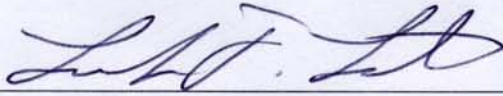
Chang-Yi Lin

Chang-Yi Lin
_____
Candidate

Optical Science and Engineering Program, Physics and Astronomy Department
_____
Department
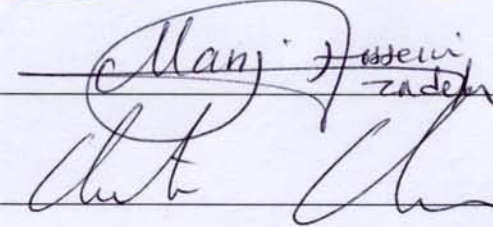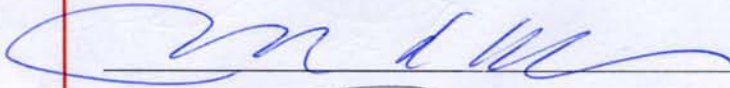
This dissertation is approved, and it is acceptable in quality
and form for publication:

Approved by the Dissertation Committee:

_____, Chairperson

MICROWAVE TECHNIQUES AND APPLICATIONS FOR SEMICONDUCTOR QUANTUM DOT MODE-LOCKED LASERS

BY

CHANG-YI LIN

B.S., Physics, National Cheng Kung University, Taiwan, 2004
M.S., Optical Science and Engineering, University of New Mexico, USA, 2008

DISSERTATION

Submitted in Partial Fulfillment of the
Requirements for the Degree of

Doctor of Philosophy
Optical Science and Engineering

The University of New Mexico
Albuquerque, New Mexico

May 2011

ACKNOWLEDGMENTS

I would like to thank Prof. Luke F. Lester, my advisor and dissertation committee chair, for his direction and guidance through the duration of my Ph.D. life. His expertise and ability to teach concepts in the research field will remain with me as I continue my career.

I also thank my committee members, Prof. Christos G. Christodoulou, Prof. Mansoor Sheik-Bahae, and Prof. Mani Hossein-Zadeh, for their valuable recommendations pertaining to this study and assistance in my professional development.

I would like to thank Dr. Frédéric Grillot, our visiting scholar, for his expertise and support in the laboratory and his eagerness to see me succeed. His great efforts make this dissertation work possible.

I wish to acknowledge my gratitude to my research group members for their guidance and assistance. I thank Dr. Yongchun Xin, Dr. Yan Li, Dr. Kai Yang, Dr. Mark Crowley, Junghoon Kim, Nader Naderi, Nishant Patel, David Murrell, Furqan L. Chiragh, Mohamed El-Emawy, Therese Saiz, William Zortman, Mike Pochet, and Ravi Raghunathan for their help in the laboratory and understanding the field. In addition, special thanks to Dr. Li Wang for providing customized optical fibers in experiments.

Last, but not least, I would like to thank my parents. Without their hard work, I would not have had the opportunities to enhance my education and achieve what I have now. I would also like to thank my brother, Che-Hsuan, for all of his encouragement. To my fiancee, Pei-Hua, your thoughtful understanding and company are the best support for my achievement today. I can never thank you enough for what you have done for me.

MICROWAVE TECHNIQUES AND APPLICATIONS FOR SEMICONDUCTOR QUANTUM DOT MODE-LOCKED LASERS

BY

CHANG-YI LIN

ABSTRACT OF DISSERTATION

Submitted in Partial Fulfillment of the
Requirements for the Degree of

Doctor of Philosophy
Optical Science and Engineering

The University of New Mexico
Albuquerque, New Mexico

May 2011

MICROWAVE TECHNIQUES AND APPLICATIONS FOR SEMICONDUCTOR QUANTUM DOT MODE-LOCKED LASERS

By

Chang-Yi Lin

B.S., Physics, National Cheng Kung University, Taiwan, 2004

M.S., Optical Science and Engineering, University of New Mexico, 2008

Ph.D, Optical Science and Engineering, University of New Mexico, 2011

ABSTRACT

Semiconductor mode-locked lasers (MLLs) are important as compact and cost-effective sources of picosecond or sub-picosecond optical pulses with moderate peak powers. They have potential use in various fields including optical interconnects for clock distribution at an inter-chip/intra-chip level as well as high bit-rate optical time division multiplexing (OTDM), diverse waveform generation, and microwave signal generation. However, there are still several challenges to conquer for engineering applications. Semiconductor MLLs sources have generally not been able to match the noise performance and pulse quality of the best solid-state mode-locked lasers. For improving the characteristics of semiconductor mode-locked lasers, research on both the material/device design and stabilization mechanism is necessary.

In this dissertation, by extending the net-gain modulation phasor approach based on a microwave photonics perspective, a convenient, yet powerful analytical model is derived and experimentally verified for the cavity design of semiconductor two-section passive MLLs. This model will also be useful in designing the next generation quantum dot (QD)

MLL capable of stable operation from 20°C to 100°C for optical interconnects applications.

The compact optical generation of microwave signals using a monolithic passive QD MLL is investigated. Relevant equations for the efficient conversion of electrical to optical to electrical (EOE) energy are derived and the device principles are described. In order to verify the function of a QD MLL as an RF signal generator, the integration with a rectangular patch antenna system is also studied. Furthermore, combined with the reconfigurable function, the multi-section QD MLL will be a promising candidate of the compact, efficient RF signal source in wireless, beam steering, and satellite communication applications.

The noise performance is a key element for semiconductor MLLs in OTDM communications. The external stabilization methods to improve the timing stability in passive MLLs have been studied and an all-microwave measurement technique has also been developed to determine the pulse-to-pulse rms timing jitter. Compared to the conventional optical cross-correlation technique, the new method provides an alternative and simple approach to characterize the timing jitter in a passive MLL. The average pulse-to-pulse rms timing jitter is reduced to 32 fs/cycle under external optical feedback stabilization.

TABLE OF CONTENTS

LIST OF FIGURES

x

LIST OF TABLES

Chapter 1

Introduction

1.1 Motivation

Semiconductor mode-locked lasers (MLLs) are important as compact, reliable and cost-effective sources of picosecond or sub-picosecond optical pulses with moderate peak powers. They have potential use in various fields including optical communications and clock distribution, photonic analog-to-digital converters, electro-optic sampling systems, diverse waveform generation, and microwave signal generation [1-5]. The advantages of using semiconductor diode lasers as optical pulse sources are that they are compact, available over a wide range of wavelengths using bandgap engineering, allow integration with other optoelectronic devices, and are electrically pumped.

On the other hand, solid-state lasers based on vibronic gain materials, such as Yb:KGW, Ti:Sapphire and Cr:Forsterite, have achieved the best performance in terms of high peak output power, femtosecond optical pulse durations, and low timing jitter. For example, 3.9 kW of peak power with a pulse duration of 281-fs has been reported using a Yb:KGW laser [6]. Using a Kerr-lens mode-locking scheme, an optical pulse as short as 5-fs can has been produced by a Ti:sapphire laser system[7]. These solid-state laser systems, however, exhibit several intrinsic limitations that have prevented their widespread use in industrial applications. The cost of ultrafast solid-state lasers is high and the system architecture is complicated and cumbersome. Also, the size of these

systems is still very bulky, thus integration with other optoelectronic devices for a compact setup is practically impossible. Ultrafast solid-state lasers are multi-element systems, comprised of a nonlinear crystal, lenses, output couplers and mirrors that all must be accurately aligned to achieve optimal performance. Most of these lasers also incorporate a dispersion compensation mechanism in order to achieve femtosecond pulse durations. Furthermore, the crystals used in these laser systems have usually low gain, and therefore the necessary minimum crystal length limits the obtainable pulse repetition frequency. In ultrafast solid-state lasers, electrical control of the output characteristics such as pulse duration and emission wavelength is also hard to achieve.

In contrast, semiconductor laser diodes can be compact, electrically pumped, easily fabricated, and can also be integrated with other optoelectronic devices to create a monolithic system. Monolithic picosecond pulse diode lasers have been proposed using a wide range of schemes such as gain-switching, Q-switching, and mode-locking [8]. Mode locking is usually the preferred technique for generating shorter optical pulses and higher repetition rates. It is more feasible to achieve mode-locking, particularly passive mode-locking, in a semiconductor laser by employing the ultrashort pulse forming element directly into the device structure during the fabrication process. Being much cheaper to fabricate and operate, semiconductor lasers also offer the potential for direct cost savings and lower power consumption in a number of applications that conventionally rely on solid-state laser systems. Furthermore, due to their short cavity length, these lasers provide an alternative option for the generation of high-repetition rate pulse trains.

The use of semiconductor MLLs is not limited to optical communication system applications. Compact optical generation of microwave signals can also be achieved

using a semiconductor MLL. It combines the optical pulse generation of a passive MLL with the high-speed characteristics of the saturable absorber (SA) to produce a microwave signal directly from the same laser diode. From the RF point of view, the SA behaves as a p-i-n photodetector. When an optical pulse train passes through the SA, an electrical pulse is directly generated at the same repetition rate as the optical pulses using only a DC bias. As shown by research at UNM, this compact RF signal generator can then be integrated with a reconfigurable antenna that accesses the various frequencies available from the pulsed source [5].

Despite several advantages of using a semiconductor laser that were described above, there are still several challenges to conquer for practical usage in applications. Semiconductor MLLs sources have generally not been able to match the noise performance and pulse quality of the best solid-state mode-locked laser [9]. Semiconductor MLLs also suffer from having a larger timing jitter, impaired stability, wider pulse width, asymmetric pulses, chirped spectra and lower peak power. For improving the characteristics of semiconductor mode-locked lasers, research on both the material/device design and stabilization mechanism is necessary.

1.2. Overview of semiconductor quantum dot lasers

1.2.1 A brief history of semiconductor quantum dot lasers

The first semiconductor lasers were developed with GaAs and GaAsP alloys by several groups in 1962 [9, 10]. These lasers had an extremely low efficiency due to the homostructure layouts that have no method of confining carriers in the active region and could only be operated under pulsed conditions and at low temperatures. In the past 40

years, the performance of semiconductor lasers has been improved dramatically with the development of new structure designs and processing techniques. For instance, double heterostructure (DH) lasers were reported by Alferov, Hayashi and Panish in the late 60s [11-13]. The threshold current density was significantly decreased by two orders of magnitude by applying a lower bandgap layer (active layer) surrounded between two higher bandgap semiconductor material layers. Such a design results in enhanced electronic and optical confinement due to a higher bandgap semiconductor that exhibits a lower refractive index.

Another revolutionary step happened when it was realized that the confinement of electrons in lower dimensional semiconductor structures can lead to completely new material properties compared to bulk material systems. As the thickness of the active layer drops near or below 10 nm, the distribution of available energy states for electrons and holes confined in the active region changes from quasi-continuous to discrete. This is the so-called quantum size effect. The electrons are strongly confined in one dimension, while moving freely in the remaining two dimensions. This is the case of a quantum well (QW) system. The idea that the quantum size effect could be used in semiconductor lasers was first suggested by Henry and Dingle in 1975 [14]. Until the late 1970s and early 1980s, Dupuis and Tsang *et. al*. demonstrated the earliest QW lasers grown by metal-organic chemical vapor deposition (MOCVD) and molecular-beam epitaxy (MBE) techniques, respectively [15, 16].   Over the past thirty years, QW lasers have been fully developed with further threshold current reduction and wider wavelength coverage by changing the QW thickness [17-19]. The progress of QW lasers motivated further efforts

to investigate semiconductor materials with multi-dimensional carrier confinement for better device performance.

The theory describing the quantum dot (QD) was first proposed by Arakawa *et al* in 1982 as an extension of the QW and was called the "multidimensional quantum well" [20]. These theoretical models were based on lattice-matched heterostructures and an equilibrium carrier distribution. However, the challenge in realizing QD lasers with superior operation to that of quantum well lasers is in creating a high areal density QD structure in the active region with sufficient uniformity. Many scientists believed these models were too ideal and strongly doubted that real QD lasers would demonstrate the predicted advantages. Until the early 1990s, it was realized that self-assembly on surfaces due to the strain caused by the lattice mismatch can be used to form high density QD layers [21-23]. In 1994, the first self-assembled QD lasers, with fully quantized energy levels in both bands and a strongly inhomogeneously-broadened gain spectrum, were reported [24]. Since then, QD devices based on self-assembly have been remarkably improved and are used in a broad array of applications such as mode-locked lasers, super-luminescent light emitting diodes, detectors, and solar cells [25-28]. Fig. 1.1 shows the evolution of the threshold current density of semiconductor lasers from the DH structure to QD material.

1.2.2 Epitaxy and formation of self-assembled quantum dots

While there are several different ways to form QDs, self-assembled QDs grown by MBE are the most frequently used and have produced most of the devices with superior lasing characteristics. Self-assembled QD growth is realized from lattice mismatched combinations of semiconductor materials and the most common mode used for growth is

the Stranski-Krastanow (S-K) mode. S-K growth mode occurs in the case of moderate lattice mismatch (>1.8%) starting with a few monolayers of layer-by-layer growth (wetting layer) followed by the formation of 3-D islands (QDs). The driving force for the self-assembled 3-D island (QDs) is the elastic relaxation on the island facet edges, minimization of the surface energy of facets and the interaction between neighboring islands via the substrate. Fig 1.2 illustrates the 2-D wetting layer and 3-D island formation in S-K mode that is responsible for forming the InAs QDs on a GaAs substrate [29].

The threshold current density has been shown to be low due to the QD's delta-like density of states [30]. However, it is clear that decreasing the state density has the negative side effect of reducing the maximum optical gain that is undesirable for device applications. In addition, if the dots do not fill a plane, the efficiency of the carrier capture is hampered. Thus, the research group in UNM has proposed a new semiconductor design — the dots-in-a-well (DWELL) laser to improve the injection efficiency and QD density control [31]. In the DWELL layout, a layer of quantum dots is placed inside a quantum well, the QW could first capture the carriers and then turn them into the 2-D plane to enhance capture into the QDs. Thus, the fill factor is effectively 100%, and the internal quantum efficiency of the DWELL laser should be superior to a conventional QD laser [31]. This is supported by the photoluminescence experiment reported by Lester et al. [32], in which the photoluminescence intensity was observed to increase by at least an order of magnitude when the dots were grown in an InGaAs quantum well as compared to grown directly on a GaAs waveguide. On the other hand, in order to improve the maximum optical gain, multiple DWELL layers can be designed and

built to increase the dot density and internal quantum efficiency and maintain the dot uniformity compared to ref. [33]. From Liu et al. [31], for instance, the ground state saturated modal gain for the 3-DWELL lasers improves to 12.5 cm^{-1}, more than three times the one of the corresponding 1-DWELL lasers. The DWELL structure layout has been used in all laser devices studied in this dissertation.
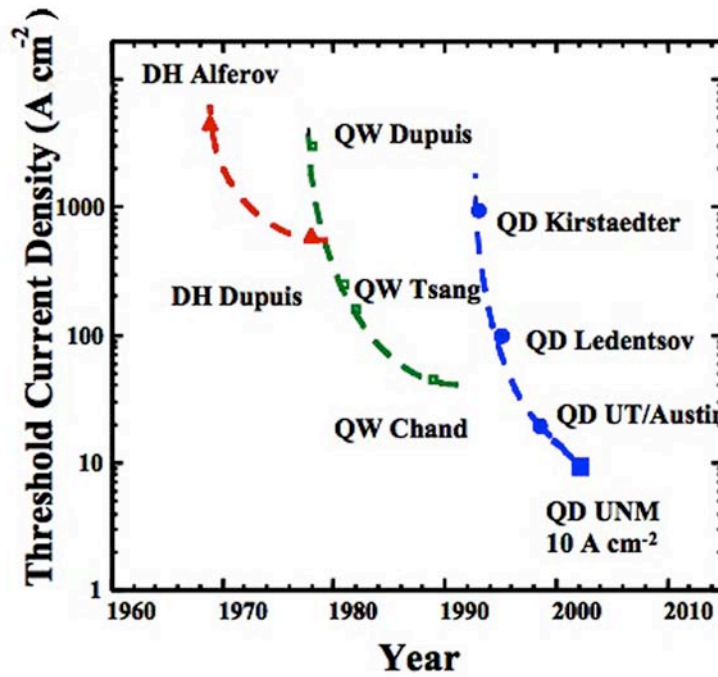
Fig. 1.1 Evolution of the threshold current density of semiconductor lasers.
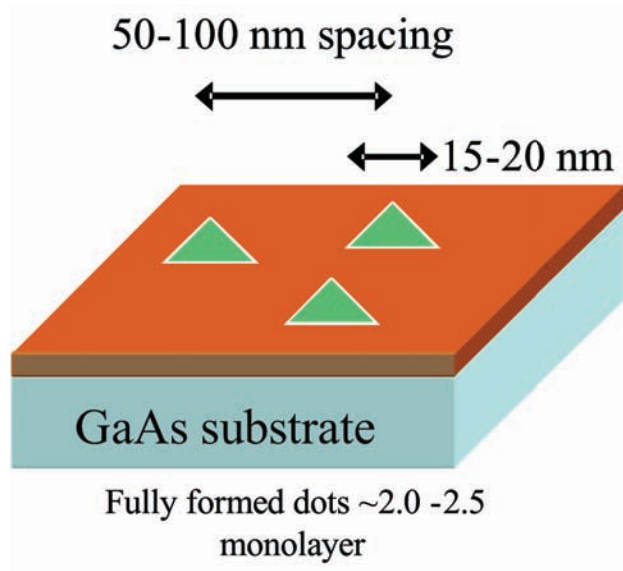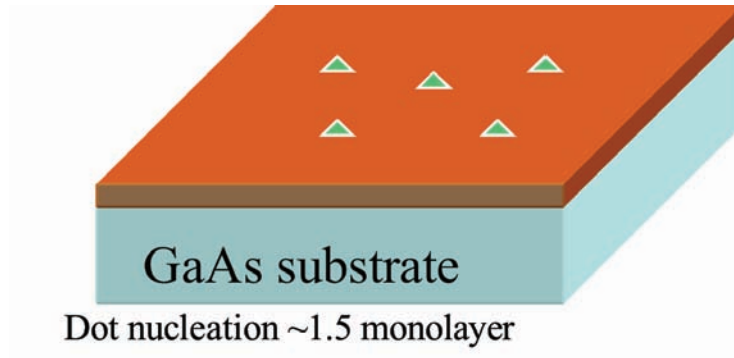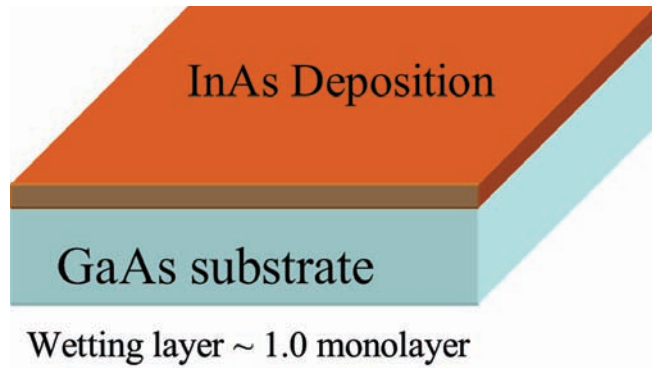
Fig. 1.2 Self-assembly growth technique for InAs quantum dots by S-K mode [29].

1.3. Mode-locking techniques in semiconductor lasers

1.3.1 Mode-locking basics

Mode-locking is a method used to generate ultrashort optical pulses on the order of picoseconds to femtoseconds by locking the phase relationship between longitudinal modes in a laser cavity. A schematic setup with a gain and loss element inside a laser resonator is shown in Fig. 1.3(a) [1]. Usually an intra-cavity loss modulator is used to shape the laser light into short pulses around the minimum of the loss modulation with a period given by the cavity round trip time $T_R = 2L/v_g$, where L is the laser cavity length and v_g the group velocity. There are two major kinds of mode-locking, passive and active, which are distinguished by their pulse-shaping mechanism.

Active mode-locking methods typically involve the use of an external signal to induce a modulation on the intra-cavity light; the laser cavity contains an active element, such as an optical modulator that utilizes the acousto-optic or electro-optic effect. Such an electronically-driven loss modulation produces a sinusoidal loss modulation with a period given by the cavity round-trip time T_R. The saturated gain at steady state only supports net gain around the minimum of the loss modulation. The pulse wings, which do not have any net gain, will be attenuated slightly on each successive round trip and lead to pulse shortening. Fig. 1.3(b) illustrates the pulse generation with the gain and loss saturation and recovery in an active MLL.

In contrast, a passive MLL is driven by the DC current directly and no external RF modulation is used. Passive mode-locking techniques use a nonlinear passive element, such as a saturable absorber, to obtain a self-amplitude modulation of the light inside the

laser cavity that leads to the formation of an ultrashort pulse circulating in the laser. A saturable absorber is called a fast absorber if its recovery time is shorter compared to the duration of pulses produced in the laser. Otherwise, the absorber is called a slow absorber [8].

When a passively mode-locked laser is synchronized to an external clock by modulating a section of the device, hybrid mode-locking is achieved. Hybrid mode-locking is a combination of active and passive mode-locking. With this approach it is possible to control the pulse timing externally, as in an actively mode-locked laser, while also achieving a shorter pulse duration as in a passively mode-locked device. Fig. 1.3(c) shows the pulse generation with the gain and loss saturation and recovery in a passive MLL with a fast absorber [1].

1.3.2 Passive mode-locking dynamics

The passive MLLs that are studied in this dissertation are based on a mutual saturation mode-locking concept [34], known as colliding pulse mode-locking (CPM) [35]. One of the important differences between active and passive MLL is that the pulse shaping in active mode-locking becomes less efficient for short pulses, while the absorber element in passive mode-locking continues trimming the pulse even for very short pulses. Thus, passive mode-locking generally produces shorter pulses than active mode-locking. A schematic plot of a monolithic passive CPM laser is shown in the Fig. 1.4(a). When two counter-propagating pulses collide in the saturable absorber, they will mutually saturate the absorber and produce a much stronger saturation than if the two pulses arrive in sequence. Before the arrival of the optical pulse, the loss and gain values are at their small signal values, and the small signal loss is a little higher than the small signal net

modal gain. In order to generate optical pulses in a passive MLL, the loss has to saturate

faster than the gain, which can be described by the stability condition of a passive MLL:

$$S = \frac{E_{sat,g}}{E_{sat,abs}} = \frac{hvA/\Gamma dg/dN}{n_{tr}hvA} = \frac{1}{n_{tr}\Gamma\frac{dg}{dN}} > 1 \tag{1.1}$$

where $E_{sat,abs}$ is the saturation energy of the absorber, $E_{sat,g}$ is the saturation energy for the

gain section, h is Planck's constant, v is the optical frequency, n_{tr} is the transparency

carrier density, Γ is the optical confinement factor and dg/dN is the differential gain with

respect to carrier density and A is the optical mode cross-sectional area, which is equal in

the absorber and gain sections of a monolithic semiconductor laser [8]. The S is defined

as the stability parameter and is greater than 1 for the case of stable passive mode-

locking. This means that a small transparency density, optical confinement factor and

differential gain are helpful for stable passive mode-locking operation.

The self-colliding pulse mode-locking (SCPM) laser is like folding a CPM laser

from the center except that for the same cavity length the CPM device has twice the

repetition rate of the SCPM laser. The absorber is placed next to a high reflectivity coated

mirror where the optical pulse collides with itself in the saturable absorber for pulse

narrowing. The schematic plot of a monolithic self-colliding pulse mode-locked laser is

shown in Figure 1.4(b). This structure is frequently used to help ensure that the absorber

saturates more easily than the gain medium.
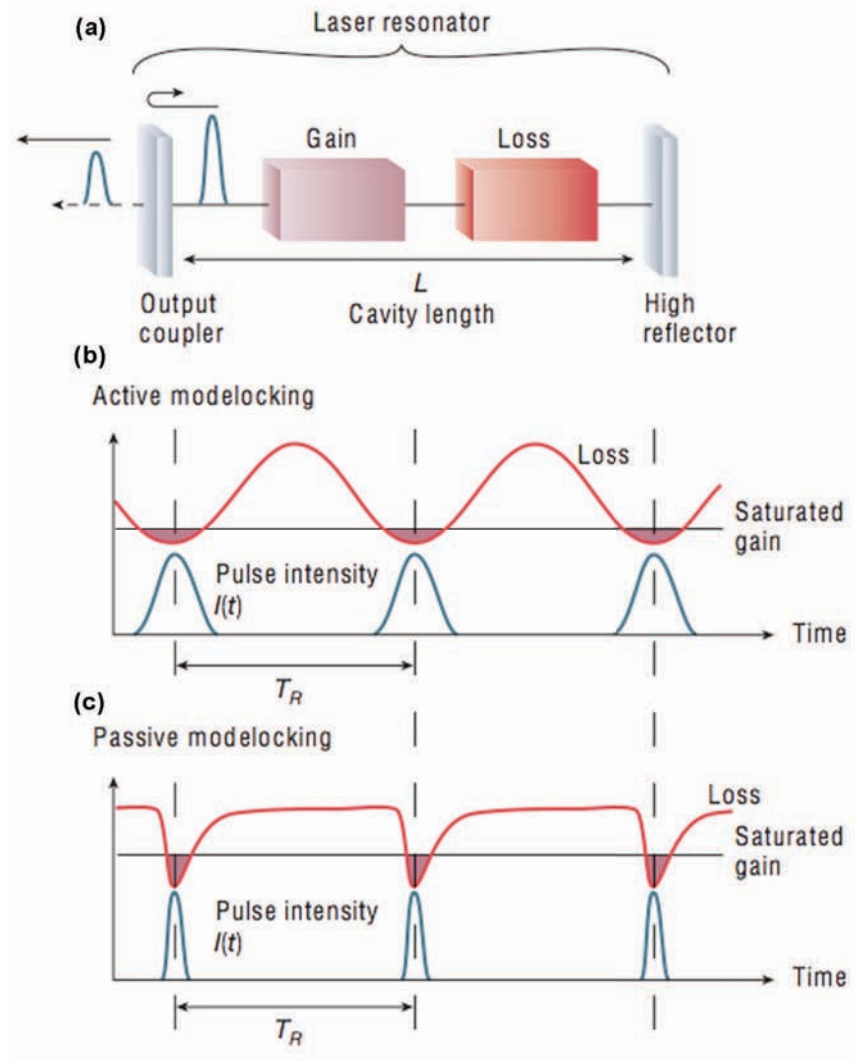
Fig. 1.3 (a) A schematic setup of a mode-locked laser resonator. (b) The pulse generation of an actively mode-locked laser. (c) The pulse generation of a passively mode-locked laser with a fast saturable absorber [1].
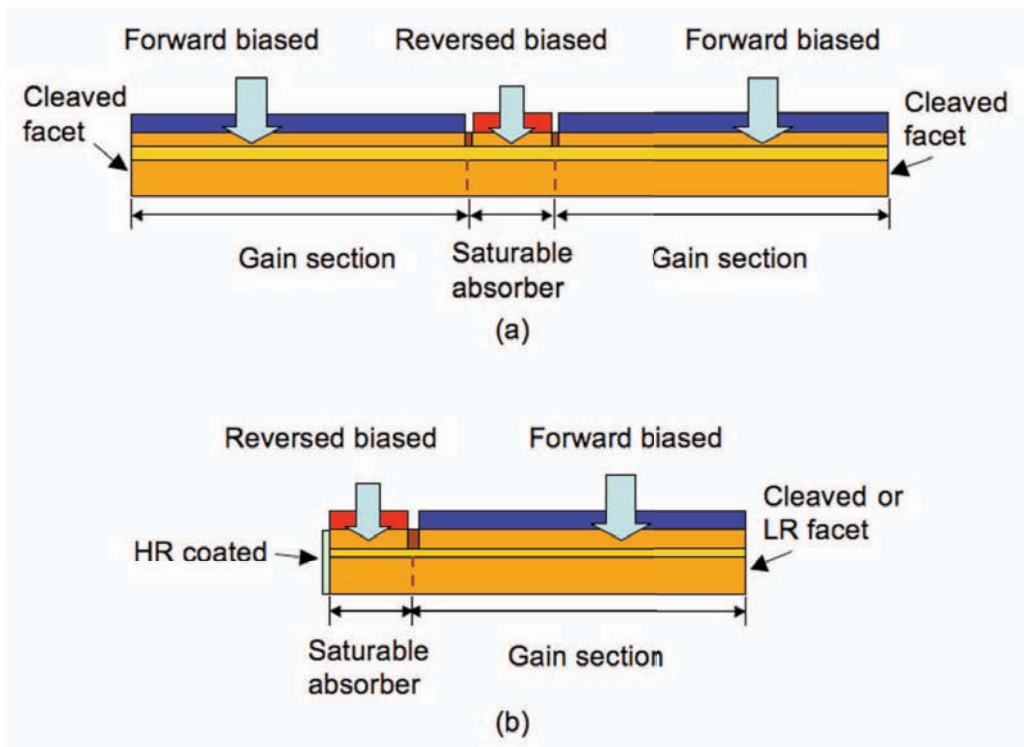
Fig. 1.4 (a) Schematic plot of a monolithic CPM laser. (b) Schematic plot of a monolithic SCPM laser.

1.4 Advantages of using quantum dot structures for mode-locking

Because of the spatial confinement of the electrons and holes on the order of the de Broglie wavelength in lower dimensional semiconductors, extremely different energy-momentum relations in the confinement directions result. Because of this confinement to dimensions on the order of tens of nanometers, the density of states in a QD behave more like an atom with discrete energies and can be represented by a δ function. Quantum dots are occasionally referred to as artificial atoms since the charge carriers occupy only a restricted set of energy levels much like the electrons in an atom. Fig. 1.5 illustrates the density of states functions for bulk, quantum well, quantum wire, and quantum dot active regions. For QDs, the state density is a δ function in energy, which is significantly different from either bulk (0-dimension, continuous) or QW (1-dimension of confinement, step function). The fundamental advantages of using QDs for mode-locking include a low threshold current density, temperature-insensitive operation, ultrafast carrier dynamics, a broad gain bandwidth, and an easily saturated gain and absorption. All these advantages are discussed in detail in the following subsections.

1.4.1 Low threshold current density

Due to the smaller physical volume of the active medium and reduced density of states, a reduction in the threshold current density can be expected in QD materials. Due to the discrete density of states, there are fewer carriers necessary to invert the carrier population, which results in a significantly lower threshold current density in QDs. Because most passive MLLs exhibit mode-locked characteristics near the threshold condition [36], a low threshold current is obviously advantageous for demonstrating a

compact optical source with ultrashort pulses, high efficiency and low power consumption. Furthermore, from the point of view of noise performance, a low threshold current implies less spontaneous emission noise in the cavity, which helps to reduce the phase noise in the passive MLL.
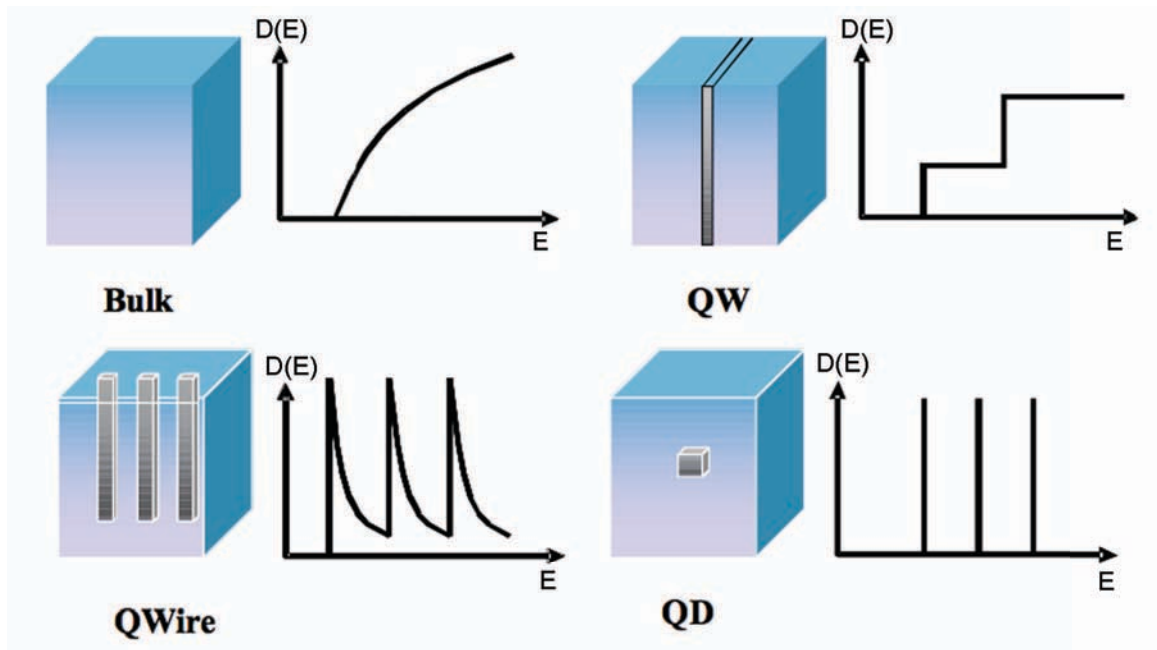
Fig. 1.5 Schematic structures and the corresponding density of states functions of bulk, quantum well, quantum wire, and quantum dot materials [29].

1.4.2 Temperature-insensitive operation

The characteristic temperature, T_0, describes the threshold current dependence of the temperature. Since the threshold current has the empirical relation with the temperature as $I_{th}=I_0 \exp (T/T_0)$, a high T_0 values means little variation of threshold current with temperature change. Also due to the discrete density of states, QD lasers exhibit low temperature sensitivity property [37], making them excellent candidates for optical interconnect applications. If the mode-locking condition in a MLL can be maintained up to 85-100°C, the laser is typically suitable for uncooled applications. Thus, the QD MLL is an attractive source for a cost-effective, compact and low power consumption system.

1.4.3 Ultrafast carrier dynamics

Due to the phonon bottleneck effect, it was thought that the carrier dynamics in QD materials would be significantly slower compared to their QW counterparts when QD materials were first studied [38]. However, the carriers in a QDs actually have access to a number of recombination paths, leading to, ultrafast recovery times under both absorption and gain conditions [39]. Recently, subpicosecond absorption recovery was measured directly in a QD absorption modulator with an applied reverse bias [40] at room temperature. The absorption recovery time as a function of temperature has also been investigated [41]. The measured decrease in absorption recovery time with increasing temperature is in agreement with the thermionic emission model and experimental results of pulsewidth measurements in a passive MLL fabricated from a similar epitaxial structure. These promising results provide evidence for QD materials to be used as ultrafast electro-absorption modulators that can operate at up to 1 THz and beyond.

1.4.4 Ultra-broad gain bandwidth, easily saturated gain and absorption

Due to the reduced δ-function density of states of ideal QDs, the bandwidth of QD materials depends primarily on the inhomogeneous broadening that is caused by QD size fluctuations. Thus, the QD materials can achieve a much wider bandwidth compared with their QW counterparts. For instance, in QW MLLs, it has been shown that there is usually some gain narrowing/filtering effects [42]. With the inhomogeneously-broadened gain bandwidth exhibited in QDs, there is support for more wavelengths and this can work against any pulse broadening that may arise from the spectral narrowing effect. Meanwhile, because of the limited number of available states, the gain and absorption of QDs are easily saturated by increasing the number of injected carriers.

All the above-mentioned properties demonstrated in QDs make them an ideal choice for a passive mode-locking system. Since the first QD MLL was reported in 2001 [36], the research and development in QD MLLs at various operation wavelengths have steadily improved and progressed [25, 43, 44]. In this dissertation, an analytical model is derived based on a microwave photonics perspective to provide a valuable tool for realizing the cavity design of monolithic long-wavelength InAs/InP QDash passively mode-locked lasers. Microwave signal generation from the saturable absorber of a monolithic passive QD MLL is also presented. It confirms that QD MLLs are suitable candidates for the optical generation of RF signals in a compact and efficient semiconductor device. Finally, the timing stability issue in a passive MLL is investigated and characterized with an all-microwave technique. In order to improve the noise performance of the passive MLL, an external optical feedback method is proposed and studied.

1.5 Organization of dissertation

There are four main goals in this dissertation including:

- Determine the cavity geometry guidelines of a passive MLL to improve the mode-locking performance based on a microwave photonics perspective.

- Investigate the optical generation of microwave signals from a monolithic passive QD MLL and study the device's potential as an RF microwave source for hybrid integration with a rectangular patch antenna.

- Characterize the noise performance of a QD MLL through an alternative all-microwave technique that provides a simpler method to obtain the pulse-to-pulse rms timing jitter.

- Utilize an external optical feedback arm to stabilize the passive MLL that usually suffers from the timing stability issue due to the lack of an external reference source.

In chapter 2, by extending the net-gain modulation phasor approach to account for the discrete distribution of the gain and saturable absorber sections in the cavity, a convenient, yet powerful analytical model is derived and experimentally verified for the cavity design of two-section passive quantum dash (QDash) MLLs. The new set of equations are used to predict functional device layouts using the measured modal gain and loss characteristics as input. It is shown to be a valuable tool for realizing the cavity design of monolithic InAs/InP QDash and InAs/GaAs QD passive MLLs.

Chapter 3 investigates the microwave signal generation from the saturable absorber of a monolithic QD MLL. We observe a differential efficiency of 33% that measures the optical to RF power conversion. An optimum extraction efficiency of the saturable

absorber of about 86% is also found. To assess the stability of the device, the mode-locking operation regime of the quantum dot device is analyzed and compared to the QW system. Furthermore, in order to verify the function of a QD MLL as an RF signal generator, the integration with a rectangular patch antenna system was also studied. Our findings confirm that QD MLLs are suitable candidates for the optical generation of RF signals in a compact, efficient semiconductor device and are promising RF microwave sources for hybrid integration with a rectangular patch antenna.

In chapter 4, the effect of external optical feedback on a packaged monolithic QD MLL is presented. The radio-frequency (RF) linewidth narrows from 8 KHz in the free-running situation to a value as low as 170 Hz under relatively low feedback and temperature control. The RF linewidth characterization under resonant feedback at a multiple of the laser cavity length agrees well with the published theory [45]. The timing jitter performance of this device is also characterized at different harmonics in the RF spectrum. An all-microwave technique has been used to determine a pulse-to-pulse rms timing jitter of 32 fs/cycle under external optical feedback. This alternative microwave method provides a simpler approach to characterize the noise performance in a passive MLL.

References:

1. U. Keller, "Recent developments in compact ultrafast lasers, " *Nature*, vol. 424, pp. 831-838 (2003).

2. E. A. Avrutin, J. H. Marsh, and E. L. Portnoi, "Monolithic and multi- gigahertz mode-locked semiconductor lasers: constructions, experiments, models and applications," *IEE Proc., Optoelectron.*, vol. 147, no. 4, pp. 251–278 (2000).

3. D.A.B. Miller, "Device requirements for optical interconnects to silicon chips," *IEEE Proc.*, vol. 97, no. 7, pp. 1166-1185 (2009).

4. C.-Y. Lin, Y.-C. Xin, J. H. Kim, C. G. Christodoulou, and L. F. Lester, "Compact optical generation of microwave signals using a monolithic quantum dot passively mode-locked laser," *IEEE Photonics Journal*, vol. 1, no. 4, pp. 236-244 (2009).

5. J. H. Kim, C. G. Christodoulou, Z. Ku, C.-Y. Lin, Y.-C. Xin, N. A. Naderi, and L. F. Lester, "Hybrid integration of a bowtie slot antenna and a quantum dot mode-locked laser," *IEEE Antenna and Wireless Propagation Lett.*, vol. 8, pp. 1337-1340 (2009).

6. S. Pekarek, C. Fiebig, M. C. Stumpf, A. E. H. Oehler, K. Paschke, G. Erbert, T. Südmeyer, and U. Keller, "Diode-pumped gigahertz femtosecond Yb:KGW laser with a peak power of 3.9 kW," *Opt. Express,* vol. 18, pp. 16320-16326 (2010).

7. R. Ell, U. Morgner, F. X. Kartner, J. G. Fujimoto, E. P. Ippen, V. Scheuer, G. Angelow, T. Tschudi, M. J. Lederer, A. Boiko, and B. Luther-Davies, "Generation of 5-fs pulses and octave-spanning spectra directly from a Ti : sapphire laser," *Opt. Lett.*, vol. 26, pp. 373-375 (2001).

8. P. Vasil'ev, *Ultrafast Diode Lasers: Fundamentals and Applications*. Boston: Artech House, (1995).

9. N. R. Hall, G. E. Fenner, J. D. Kingsley, T. J. Soltys, and R. O. Carlson. "Coherent Light Emission From GaAs Junctions," *Physical Review Letters*, vol 9, no 9, pp. 366–369 (1962).

10. N. Holonyak, Jr. and S. F. Bevacqua, "Coherent (visible) light emission from Ga(As$_{1-x}$P$_x$) junctions," *Appl. Phys. Lett.*, vol 1, pp. 82-83 (1962).

11. Z. I. Alferov, "Nobel Lecture: The double heterostructure concept and its applications in physics, electronics, and technology," *Reviews of Modern Physics*, vol. 73, pp. 767 (2001).

12. I. Hayashi, M. B. Panish, P. W. Foy and S. Sumski, " Junction lasers which operate continuously at room temperature," *Appl. Phys. Lett.,* vol. 17, pp. 109-111 (1970).

13. R. D. Dupuis, and P. D. Dapkus, "Very low threshold Ga$_{1-x}$Al$_x$As-GaAs double-heterostructure lasers grown by metalorganic chemical vapor deposition," *Appl. Phys. Lett.,* vol. 32, pp. 473-475 (1978).

14. R. Dingle, W. Wiegmann, and C. H. Henry, "Quantum States of Confined Carriers in Very Thin Al$_x$Ga$_{1-x}$As-GaAs-Al$_x$Ga$_{1-x}$As Heterostructures," *Phys. Rev. Lett*. vol. 33, pp. 827 – 830 (1974).

15. R. D. Dupuis, P. D. Dapkus, N. Holonyak Jr., E. A. Rezek, R. Chin, "Room Temperature operation of quantum-well Ga1-xAlxAs-GaAs laser diodes grown by metalorganic chemical vapor deposition," *Appl. Phys. Lett*. vol. 32, pp. 295-297 (1978).

16. W. T. Tsang, "Extremely low threshold (AlGa)As modified multiquantum well heterostructure lasers grown by molecular-beam epitaxy," *Appl. Phys. Lett.* vol. 39, pp. 786-788 (1981).

17. W. T. Tsang, "Extremely low threshold (AlGa)As graded-index waveguide separateconfinement heterostructure lasers grown by molecular-beam epitaxy," *Appl. Phys. Lett*. vol. 40, pp. 217-219 (1982).

18. N. Chand, E. E. Becker, J. P. Van der Ziel, S. N. G. Chu, and N. K. Dutta, "Excellent uniformity and very low (less-than-50A/cm2) threshold current density strained InGaAs quantum-well diode-lasers on GaAs substrate," *Appl. Phys. Lett*. vol. 58, pp. 1704-1706 (1991).

19. N. Holonyak, Jr., "Quantum-well and superlattice lasers: Fundamental effects," in Proceedings of the Third (1982) Workshop on the Physics of Submicron Structures, H. Grubin, K. Hess, G. I. Iafrate, and D. K. Ferry, Eds. *New York: Plenum,* pp. 1-18 (1984).

20. Y. Arakawa, and H. Sakaki, "Multidimensional quantum well laser and temperature dependence of its threshold current," *Appl. Phys Lett*., vol. 40, no.11, pp. 939-941 (1982).

21. D. Leonard, S. Fafard, K. Pond, Y. H. Zhang, J. L. Merz, and P. M. Petroff, "Structural And Optical-Properties Of Self-Assembled Ingaas Quantum Dots," *Journal Of Vacuum Science & Technology B*, vol. 12, no. 4, pp. 2516-2520 (1994).

22. D. Bimberg, M. Grundmann, N. N. Ledentsov, S. S. Ruvimov, P. Werner, U. Richter, J. Heydenreich, V. M. Ustinov, P. S. Kopev, and Z. I. Alferov, "Self-organization processes in MBE-grown quantum dot structures," *Thin Solid Films*, vol. 267, no. 1-2, pp. 32-36 (1995).

23. P. M. Petroff and S. P. Denbaars, "MBE And MOCVD Growth And Properties Of Self-Assembling Quantum-Dot Arrays In Iii-V Semiconductor Structures,"

Superlattices And Microstructures, vol. 15, no. 1, pp. 15-21 (1994).

24. N. Kirstaedter, N. N. Ledentsov, M. Grundmann, D. Bimberg, V. M. Ustinov, S. S. Ruvimov, M. V. Maximov, P. S. Kopev, Z. I. Alferov, U. Richter, P. Werner, U. Gosele, and J. Heydenreich, "Low-Threshold, Large T_0 Injection-Laser Emission From (InGa)As Quantum Dots," *Electronics Letters*, vol. 30, no. 17, pp. 1416-1417 (1994).

25. E. U. Rafailov, M. A. Cataluna, and W. Sibbett, "Mode-locked quantum-dot lasers," *Nat. Photonics*, vol. 1, pp.395-401 (2007).

26. Y.-C. Xin, A. Martinez, T. Saiz, A. J. Moscho, Y. Li, T. A. Nilsen, A. L. Gray and L. F. Lester, "1.3-µm quantum-dot multisection superluminescent diodes with extremely broad bandwidth," *IEEE Photonics Technology Letters*, vol. 19, pp. 501-503 (2007).

27. S. Krishna, "Quantum dots-in-a-well infrared photodetectors," *Journal of Physics D-Appl. Phys.*, vol. 38, no. 13, pp.2142-2150 (2005).

28. R. Laghumavarapu, M. El-Emawy, N. Nuntawong, A. Moscho, L. F. Lester, D. L. Huffaker, "Improved device performance of InAs/GaAs quantum dot solar cells with GaP strain compensation layers," *Appl. Phys. Lett*., vol. 91, no. 24, pp. 243115 (2007).

29. Y. Li, "Techniques for high-speed direct modulation of quantum dot lasers," PhD dissertation, University of New Mexico, (2008).

30. K. Mukai, Y. Nakata, H. Shoji, S. Sugawara, K. Ohtsubo, N. Yokoyama, and H. Ishikawa, "Lasing with low-threshold current and high-output power from columnar-shaped InAs/GaAs quantum dots," *Electron. Lett.*, vol. 34, pp. 1588–1590 (1998).

31. G. T. Liu, A. Stintz, H. Li, T. C. Newell, A. L. Gray, P. M. Varangis, K. J. Malloy,

and L. F. Lester, "The Influence of Quantum-Well Composition on the Performance of Quantum Dot Lasers Using InAs/InGaAs Dots-in-a-Well (DWELL) Structures," *IEEE J. Quantum Electron.*, vol. 36, no. 11, pp.1272-1279 (2000).

32. L. F. Lester, A. Stintz, H. Li, T. C. Newell, E. A. Pease, B. A. Fuchs, and K. J. Malloy, "Optical characteristics of 1.24 µm quantum dot lasers," *IEEE Photon. Technol. Lett.*, vol. 11, pp. 931–933 (1999).

33. F. Heinrichsdorff, M. H. Mao, N. Kirstaedter, A. Krost, D. Bimberg, A. O. Kosogov, and P. Werner, "Room-temperature continuous-wave lasing from stacked InAs/GaAs quantum dots grown by metalorganic chemical-vapor-deposition," *Appl. Phys. Lett.*, vol. 71, pp. 22–24 (1997).

34. I. S. Ruddock and D. J. Bradley, "Bandwidth-Limited subpicosecond pulse generation in mode-locked cw dye lasers," *Appl. Phys. Lett.,* vol. 29, No. 5, pp 296-297 (1976).

35. R. L. Fork, B. I. Greene, and C. V. Shank, "Generation Of optical pulses shorter than 0.1 psec by colliding pulse mode-locking," *Appl. Phys. Lett.*, vol.38, pp. 671-672 (1981).

36. X. D. Huang, A. Stintz, H. Li, L. F. Lester, J. Cheng, and K. J. Malloy, "Passive mode-locking in 1.3 µm two-section InAs quantum dot lasers," *Appl. Phys. Lett.*, vol. 78, pp. 2825-2827 (2001).

37. O. B. Shchekin, J. Ahn, D. G. Deppe, "High temperature performance of self-organised quantum dot laser with stacked p-doped active region," *Electronics Letters*, vol. 38, no.14, pp.712-713 (2002).

38. K. Mukai, N. Ohtsuka, H. Shoji, and M. Sugawara, "Phonon bottleneck in self-

formed InxGa1-xAs/GaAs quantum dots by electroluminescence and time-resolved photoluminescence," *Phys. Rev. B*, vol. 54, pp. R5243-R5246 (1996).

39. P. Borri, S. Schneider, W. Langbein, and D. Bimberg, "Ultrafast carrier dynamics in InGaAs quantum dot materials and devices," *J. Opt. A*, vol. 8, pp. S33-S46 (2006).

40. D. B. Malins, A. Gomez-Iglesias, S. J. White, W. Sibbett, A. Miller, and E. U. Rafailov, "Ultrafast electroabsorption dynamics in an InAs quantum dot saturable absorber at 1.3 μm," *Appl. Phys. Lett.*, vol. 89, pp. 171111 (2006).

41. M. A. Cataluna, D. B. Malins, A. Gomez-Iglesias, W. Sibbett, A. Miller, and E. U. Rafailov, "Temperature dependence of electroabsorption dynamics in an InAs quantum-dot saturable absorber at 1.3 μm and its impact on mode-locked quantum-dot lasers," *Appl. Phys. Lett.*, vol. 97, pp. 121110 (2010).

42. P. J. Delfyett, H. Shi, S. Gee, C. P. J. Barty, G. Alphonse, and J. Connolly, "Intracavity spectral shaping in external cavity mode-locked semiconductor diode lasers," *IEEE J. Sel. Topics Quantum Electron.*, vol. 4, pp. 216-223 (1998).

43. F. Lelarge, B. Dagens, J. Renaudier, R. Brenot, A. Accard, F. Van Dijk, D. Make, O. Le Gouezigou, J. G. Provost, F. Poingt, J. Landreau, O. Drisse, E. Derouin, B. Rousseau, F. Pommereau, and G. H. Duan, "Recent advances on InAs/InP quantum dash based semiconductor lasers and optical amplifiers operating at 1.55 μm," *IEEE J. Sel. Top. Quantum Electron.*, vol. 13, pp.111-124 (2007).

44. M. G. Thompson, A. R. Rae, M. Xia, R. V. Penty, and I. H. White, "InGaAs quantum-dot mode-locked laser diodes," *IEEE J. Sel. Top. Quantum Electron.*, vol.15, pp.661-672 (2009).

45. E. A. Avrutin, and B. M. Russell, "Dynamics and spectra of monolithic mode-locked

laser diodes under external optical feedback," *IEEE J. Quantum Electron.*, vol. 45,

no. 11, pp.1456-1464 (2009).

Chapter 2

Cavity design of two-section passively mode-locked lasers

2.1 Introduction

Monolithic mode-locked lasers (MLLs) are promising candidates as optical interconnects for clock distribution at an inter-chip/intra-chip level as well as high bit-rate optical time division multiplexing, electro-optic sampling, and arbitrary waveform generation due to their compact size, low power consumption, and direct electrical pumping [1,2]. Some unique characteristics of quantum dot (QD) materials, such as ultra broad bandwidth, ultra fast gain dynamics, and easily saturated gain and absorption, make them an ideal choice for semiconductor monolithic MLLs.

For the QD system fabricated on a GaAs substrate, the most impressive results that clearly demonstrate complete mode-locking have been realized in the O-band (1260-1360 nm) that is suitable for metro networks [3-5]. Furthermore, QD lasers working around 1300nm can now be maturely grown on GaAs substrates. This represents a significant advantage compared to their quantum well (QW) counterparts, since QW lasers emitting at the same wavelength range have to be grown on InP substrates, with the associated degraded performance due to high nonradiative Auger recombination [6].

On the other hand, QD and quantum dash (QDash) MLLs made on InP substrates in the telecom optical band of 1.55-µm range have also been vigorously pursued. However, it is more challenging to achieve mode-locking in two-section devices using these

materials [7, 8]. In part, it is believed that this is caused by the higher threshold current density and waveguide internal loss in InP-based QDs and QDashes compared to the more mature InAs/GaAs QD material system [9,10]. To further improve the development of 1.55-µm passive QD/QDash MLLs, a simple analytical model is needed to provide cavity geometry guidelines that can improve the mode locking performance in two-section devices.

Besides, this analytic model is also beneficial for rapidly investigating the key mechanism limiting performance at high temperature operation. It highlights the usefulness in guiding the future design of temperature-stable MLLs that will be located close to the CPU cores and will need to maintain the performance in the vicinity of 100°C for optical interconnects applications.

In this chapter, an analytical model is derived in section 2.2 by extending the net-gain modulation phasor approach to account for the discrete distribution of the gain and saturable absorber sections in the cavity [11,12]. The new set of equations presented here includes the influence of the waveguide internal loss and the effect of separate as opposed to distributed gain and loss. Section 2.3 describes the wafer growth and processing procedure of the QDash MLL device. The optical characterization and gain/loss measurement through the segmented contact method are also reported [13,14]. In section 2.4, we theoretically predict and experimentally confirm the passive MLL geometries using the measured material gain and loss data. Compared to our previous delay differential equation model [15] and the work of Vladimirov and Turaev [16], the advantage of the proposed analytical model is the prediction of the functional mode-locking device layout through the use of measured static laser parameters *on the actual*

device. Thus, we can construct a simpler analytical model without knowing the material parameters such as the carrier lifetime or the gain/absorber recovery times because the limiting case of a sinusoidal modulated output is assumed. The theory is applied to the design of monolithic InAs/InP QDash passive MLLs emitting at 1.59-µm. Mode locking is achieved as predicted, and a repetition rate as high as 18.4 GHz is realized.

2.2 Net-gain modulation phasor approach: theory and modeling

As described in chapter 1, a frequently cited condition for passive mode-locking requires that the stability parameter, S, must be greater than 1:

$$S = \frac{E_{sat,g}}{E_{sat,abs}} = \frac{h\nu A / G_g}{h\nu A / G_a} = \frac{G_a}{G_g} > 1 \qquad (2.1)$$

where $E_{sat,abs}$ is the saturation energy of the absorber, $E_{sat,g}$ is the saturation energy for the gain section, h is Planck's constant, ν is the optical frequency, G_g is the differential gain in the gain section multiplied by the group velocity, G_a is the differential loss in the absorber multiplied by the group velocity and A is the optical mode cross-sectional area, which is equal in the absorber and gain sections of the monolithic semiconductor laser [17]. However, this requirement is not stringent and rarely used to guide semiconductor MLL cavity design. Using a net-gain modulation phasor approach, Lau and Paslaski derived a more useful guideline for obtaining passive mode-locking instead of self-pulsation in the region near lasing threshold where the two processes typically compete and the pulse width is typically the shortest [11,12]

This model, however, was based on the assumption that the gain and the saturable absorber are distributed *uniformly* in the optical cavity, not in separate electrically-

isolated sections as common done, and the internal loss was not considered. In the QDash material system, the gain and absorption per unit length are much smaller compared to those of a quantum well or bulk semiconductor system. Thus, we can approximate the actual lumped gain and absorber sections of the optical waveguide as an average gain and loss that are distributed uniformly. It is also important to include the internal loss effect in QDash material system due to the comparable value to the unsaturated absorption. Based on these approximations, we have extended Lau and Paslaski's model to a two-section MLL device geometry that includes a gain section of length L_g and an absorber section of length L_a, and have accounted for the internal loss, α_i, in the optical waveguide.

To understand the region of mode locking without self-pulsation, we employ the net-gain modulation phasor analysis [11,12]. In this approach, the photon intensity oscillation is represented by $s \cdot e^{iwt}$, where s is the real amplitude of the oscillation. $\omega = \Omega_{MLL}$ = the longitudinal mode spacing or mode-locking frequency. The net gain modulation represents the difference between the average gain and the average loss modulation in the gain and absorber media. Following Lau and Paslaski's model and accounting for the distribution of the gain and absorption in separate sections of the cavity, we write the modified net gain modulation equation for a two-section passive MLL as [12]:

$$g_{net} = \left\{ \frac{-G_g g_0 L_g}{i\omega + 1/T_g} - \frac{-G_a a_0 L_a}{i\omega + 1/T_a} \right\} \frac{s e^{i\omega t}}{L} = \hat{g}_{net} e^{i\omega t}$$

$$1/T_g = 1/\tau_g + G_g S_0 \qquad\qquad 1/T_a = 1/\tau_a + G_a S_0 \qquad\qquad (2.2)$$

$$G_g = v_g \frac{dg_0}{dn} \qquad\qquad G_a = v_g \frac{da_0}{dn}$$

g_{net} is a phasor quantity which is responsible for driving the optical modulation. In Eq. (2.2), g_0 is the modal gain in the gain section and a_0 is the unsaturated absorption in the absorber region. L is the cavity length and $L=L_a+L_g$; v_g and n are the group velocity and

the carrier density, respectively. $1/T_g$ is the carrier recombination rate in the gain section consisting of the sum of the spontaneous rate, $1/\tau_g$, and the stimulated rate $G_g S_0$. $1/T_a$ is the carrier removal rate in the absorber consisting of the sum of the spontaneous rate, $1/\tau_a$, and the stimulated rate, $G_a S_0$. τ_g and τ_a are the spontaneous carrier lifetimes in the gain and absorber regions, respectively, and should not be confused with the recovery times. The first quantity in { } in Eq. (2.2) is related to the average gain modulation, and the second quantity represents the average loss modulation.

The s in Eq. (2.2) is related to the modulation depth that is assumed to be 100% so that $s = S_0/2$. S_0 is the average photon density in the cavity:

$$S_0 = \frac{1}{\alpha_m v_g h v} \frac{\Gamma P}{W d L} \tag{2.3}$$

where α_m is the mirror loss, P is the peak optical power, hv is the photon energy, W is the lateral mode width, and Γ is the optical confinement factor.

The necessary conditions for mode-locking without self-pulsation are that the repetition rate should be much faster than the stimulated rates, i.e., $\omega = \Omega_{\mathrm{MLL}} = v_g/2L \gg G_{g/a} S_0$ and the stimulated rates are much greater than the spontaneous recombination rates in the gain and absorber section, i.e., $G_g S_0 \gg 1/\tau_g$ and $G_a S_0 \gg 1/\tau_a$ [12]. In this work, we further require that the real part of the net gain modulation must exceed the internal loss, α_i, of the waveguide:

$$\left(-G_g^2 g_0 \frac{L_g}{L} + G_a^2 a_0 \frac{L_a}{L} \right) \frac{S_0^2}{2\Omega_{MLL}^2} > \alpha_i \tag{2.4}$$

then:

$$\left(\frac{da_0}{dn} \right)^2 a_0 \frac{L_a}{L} - \left(\frac{dg_0}{dn} \right)^2 g_0 \frac{L_g}{L} > \frac{\alpha_i}{2} \left(\alpha_m v_g \frac{Wd}{\Gamma P} h v \right)^2 \tag{2.5}$$

Inequality (2.5) gives the necessary operating condition for a two-section passive MLL and highlights the interdependence of the material parameters and the device's two-section structure. To apply Eq. (2.5) to the design of an MLL cavity, we make approximations under two different conditions. First, we assume that the differential gain is much smaller than the differential absorption: $G_a >> G_g$ or, equivalently, that the gain section is biased under strong population inversion. In this case, Eq. (2.5) can be approximated by:

$$\left(\frac{da_0}{dn}\right)^2 \frac{a_0}{\alpha_i} > \frac{L}{2L_a}\left(\alpha_m \upsilon_g \frac{Wd}{\Gamma P}h\nu\right)^2 \tag{2.6}$$

Since it is difficult to measure the differential gain and absorption with respect to the carrier density in practice, dg_0/dn is replaced with dg_0/dJ according to the relationship [19]:

$$\frac{dg_0}{dn} = \frac{qd}{\eta_i\tau}\frac{dg_0}{dJ} \tag{2.7}$$

And Eq. (2.6) can be approximated by:

$$\left(\frac{dg_0}{dJ}\bigg|_{g_0=0}\right)^2 \frac{a_0}{\alpha_i} > \frac{L}{2L_a}\left(\eta_i\tau\frac{\alpha_m W\upsilon_g}{\Gamma P}\frac{h\nu}{q}\right)^2 \tag{2.8}$$

Here J is the current density, τ is the carrier lifetime, and η_i is the injection efficiency of the laser. We also conservatively approximate that $da_0/dn \approx dg_0/dn\big|_{g_0=0}$. The left-hand-side of Eq. (2.8) emphasizes that a high contrast between the unsaturated absorption, a_0, and the internal loss, α_i, is favorable for mode-locking. In addition, upon measuring the various devices and material parameters, we can use Eq. (2.8) to predict cavity designs (L_a and L_g) for two-section mode-locked lasers of a desired repetition rate using novel active region materials. This is the situation described below for the QDash

lasers. Alternatively, we can rearrange Eq. (2.8) to estimate the minimum required peak power level according to the following expression:

$$P > \sqrt{\frac{L\alpha_i}{2L_a a_0}} \left[\eta_i \tau \frac{\alpha_m W v_g}{\Gamma\left(dg_0/dJ\big|_{g_0=0}\right)} \frac{h\nu}{q} \right] \qquad (2.9)$$

Eq. (2.9) reinforces the idea that the internal loss is detrimental to mode-locking in a semiconductor laser by requiring a high power for the onset of operation.

Although it is possible to measure the variables in Eq. (2.8)-(2.9) for the *actual* mode-locked laser or test structures associated with it, the carrier lifetime is frequently difficult to obtain. Thus, a further assumption can be made to obtain a simpler analytical guideline. The second approximation assumes that the peak optical power is sufficiently large that the right-hand-side of Eq. (2.8) is negligible. In this case, the following condition analogous to that found in [11,12] is obtained:

$$\frac{a_0}{g_0} \frac{L_a}{L_g} > \left(\frac{\dfrac{dg_0}{dJ}}{\dfrac{dg_0}{dJ}\bigg|_{g_0=0}} \right)^2 \qquad (2.10)$$

From Eq. (2.10) it is observed that a longer absorber is desirable for realizing mode-locking, especially when the differential gain is not much smaller than the differential absorption. Similar to Eq. (2.1), Eq. (2.10) also suggests that the design strategy of a passive MLL is to minimize the ratio of the differential gain to differential absorption.

The threshold condition in the laser cavity, Eq. (2.11), is another constraint on the system and is applied to determine the modal gain, g_0.

$$g_0 L_g = a_0 L_a + (\alpha_m + \alpha_i)L \qquad (2.11)$$

Therefore, provided that the measured modal gain and loss data is also available from the segmented test structure that is integrated into the MLL, possible cavity designs can be explored using Eq. (2.10) before even fabricating them. These analytical guidelines have been successfully applied previously [18-20], but the range of designs and analysis is expanded in this dissertation verifying the broad applicability of the theory [21].

2.3 Wafer growth and fabrication

2.3.1 Material structure

The QDash active region investigated in this chapter was grown on an n^+-InP substrate (wafer #: ZLI258H) [22]. QDash materials are similar to QDs, but are elongated in one direction. Fig. 2.1 shows the structural diagram of the epitaxial layers, and an AFM image of the QDash is shown in Fig. 2.2. The dashes-in-a-well (DWELL) active region consists of 5 layers of InAs quantum dashes embedded in compressively-strained $Al_{0.20}Ga_{0.16}In_{0.64}As$ quantum wells separated by 30-nm undoped tensile-strained $Al_{0.28}Ga_{0.22}In_{0.50}As$ spacers. A lattice-matched 105-nm thick layer of undoped $Al_{0.30}Ga_{0.18}In_{0.52}As$ is added on each side of the active region. The p-cladding layer is step-doped AlInAs with a thickness of 1.5-µm to reduce free carrier loss. The n-cladding layer is 500-nm thick AlInAs. The laser structure is capped with a 100-nm heavily p-type doped InGaAs layer.
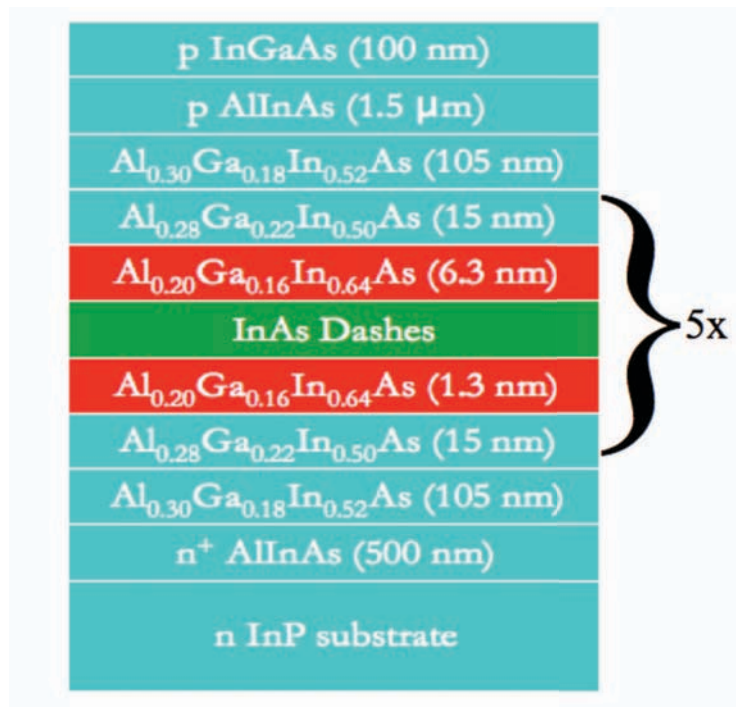
Fig. 2.1 The layer structure of the InAs QDash laser (ZLI258H).
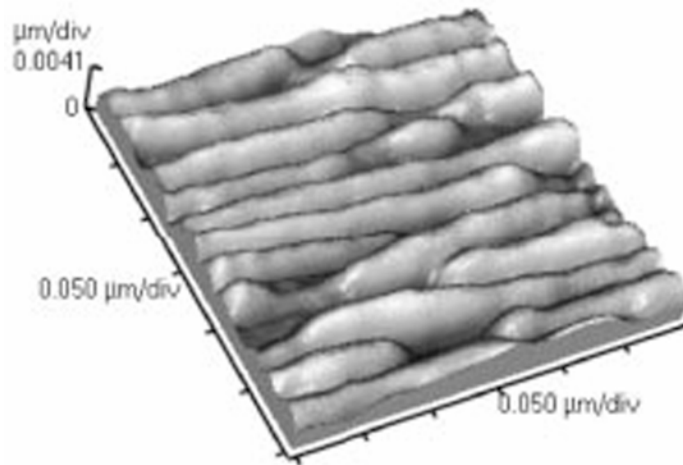
Fig. 2.2 AFM image of the QDash layer.

2.3.2 Device fabrication

For measuring the optical gain and absorption of the laser diode, the wafers are processed into multi-section devices following standard ridge waveguide processing. The wafer was cleaned with a 1:30 ammonium hydroxide solution to remove any native oxide that may have formed between growth and processing. Following the native oxide etch, the wafer underwent photolithography to pattern a 4-μm wide ridge waveguide on the p-side of the substrate. The ridge-waveguide-mask consisted of several patterns to set the footprint for multiple devices with varying dimensions. This would allow for future experiments with devices of various gain and absorber lengths. After patterning, the ridge was etched in an inductively coupled plasma (ICP) machine using BCl_3 as the etchant. To confine the spreading of the injected current and improve the optical field confinement, the ridge was etched to just 0.1-μm above the active region of the device. Then liquid Benzocyclobutene (BCB) was spun onto the wafer and it was baked at 250°C. Once cured, the wafer was placed in a reactive ion etch (RIE) machine employing Oxygen and CHF_3 to remove the BCB until the surface of the ridge was clearly visible. The BCB dielectric processing was applied for planarization and to electrically isolate the p-type metal and the etched upper cladding layer. Next the wafer underwent the second photolithography step to create the pattern for the p-metal contact. The p-type metal consisting of 500-Å titanium (Ti), 500-Å platinum (Pt), and 3000-Å gold (Au) was evaporated on to the wafer. A third photolithography step was then performed to create the pattern needed for ion implantation. The wafer was processed using proton implantation to electrically isolate each 500-μm section with an isolation resistance of >10 MΩ. Then the wafer was lapped and polished to produce a final thickness around

150-µm. This ensured high quality cleaved facets and sufficient thermal heat sinking. The backside of the wafer was then placed into the metal evaporator and the n-type metal consisting of Ge/Au/Ni/Au was deposited on to the backside. After n-metal deposition, the wafer was annealed at 380°C. A higher temperature was not used because this would result in the cracking of the BCB. The processing flowchart is illustrated in Fig. 2.3. Such a device can be cleaved and tested with a fiber coupling system. By changing the wire-bonding configuration, different section-length devices can also be created as shown in Fig. 2.4.
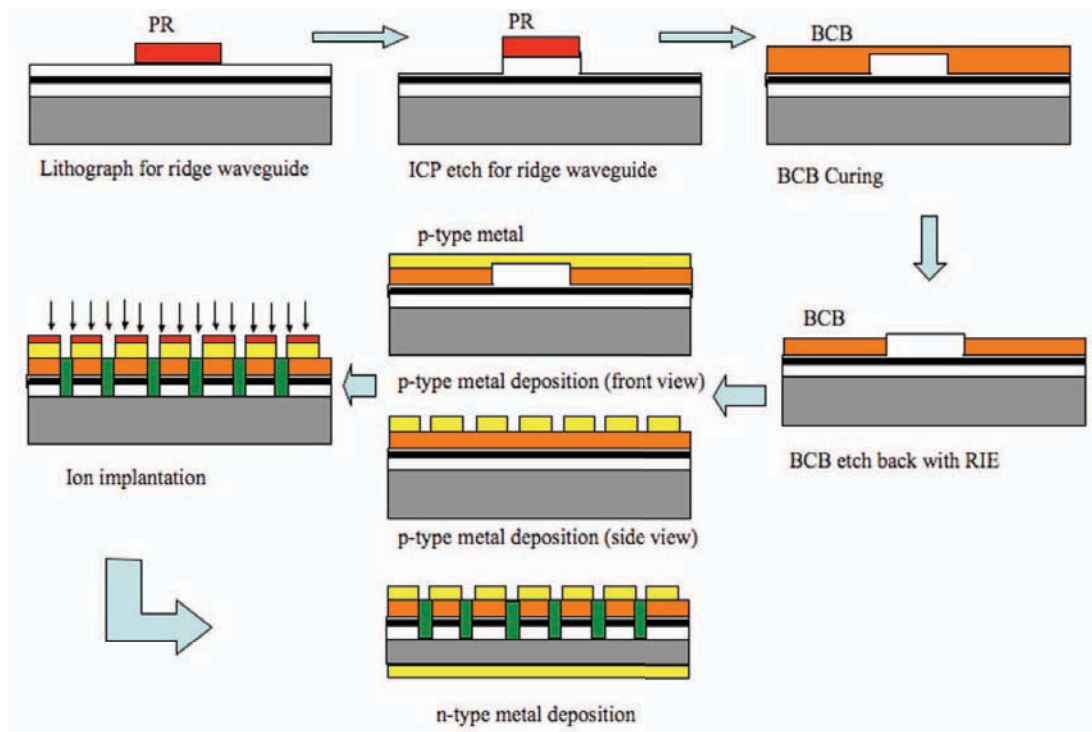
Fig. 2.3 Processing flowchart of the segmented contact devices [23].
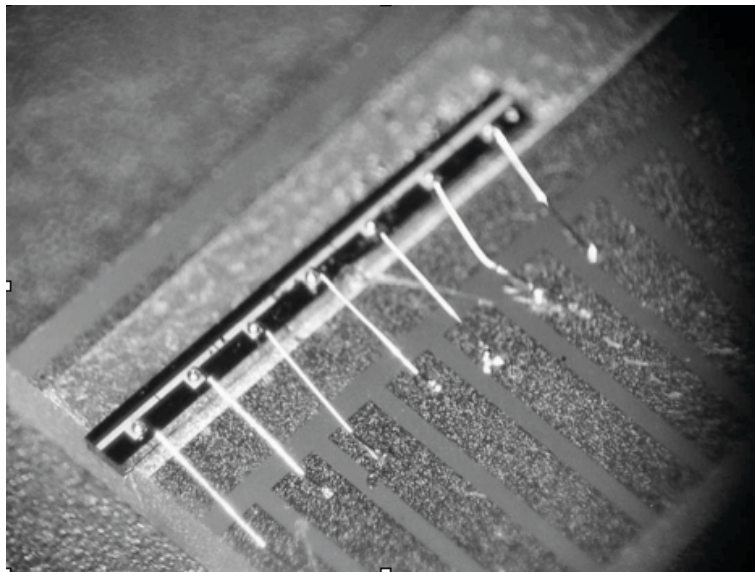
Fig. 2.4 A multi-section device with 7 electrically-isolated sections that can be reconfigured to form different mode-locked laser layouts. Each anode is wire-bonded to a chip carrier shown on the lower right where the reconfiguration is realized.

2.4 The modal gain and loss measurement and MLL device preparation

The optical cavity shares a common 4-µm wide ridge waveguide with 0.5-mm segmented anode contacts that have approximately 10 MΩ electrical isolation between them. First, this layout is used to measure the modal gain and loss characteristics of the InAs QDash active region using an improved segmented contact method [13]. Second, the MLL is built by reconfiguring this same linear array of diodes [4].

2.4.1 The modal gain and loss characterization

The device was mounted p-side up on an AlN submount on a copper heat sink. A thermoelectric cooler (TEC) was used to control the heat sink temperature at 25°C. The sections were wire-bonded and connected to a switch mechanism, with the exception of the absorption section. A reverse bias of -5 V was applied to the absorption section to minimize reflection from the back facet. A schematic diagram of the multi-section device structure is shown in Fig. 2.5.

The test setup includes two main blocks, an electrical-pumping block, and a signal-detecting block. For the current-pumping block, the CW-pumping setup is used to determine the characteristics of the device under actual working conditions. For the signal-detecting block, a fiber-coupling system is utilized for fast alignment and data collection. Fig. 2.6 shows the fiber-coupling setup with an optical spectrum analyzer (OSA) and CW-pumping block [13]. In the CW operation, each section of the device has a dedicated current source and the bias current is monitored with a multi-meter. In the fiber-coupling system, the light emitted from the device is collected into a polarization-maintaining fiber (PMF) by means of a coupling lens. An isolator is inserted to prevent

the back reflection to the laser chip. The inline fiber-polarizer is connected to the PMF to select the TE mode or TM mode emission by switching the direction of the key on the FC connector. In this chapter, all data are based on TE mode emission. An OSA measures the amplified spontaneous emission (ASE) spectrum. After collecting all required ASE spectrum data, the modal gain and total loss can be calculated through Eq. (5) and (7) in ref. [13].
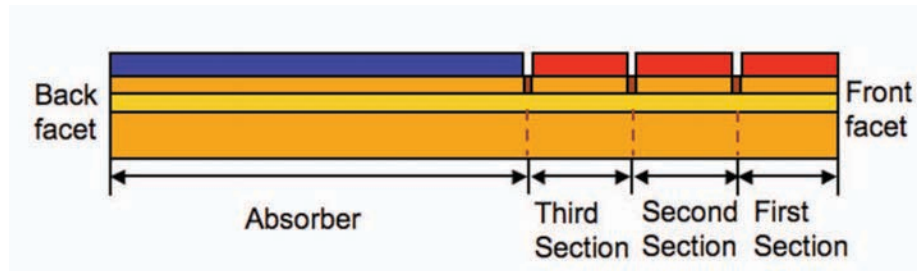
Fig. 2.5 Schematic diagram of the multi-section device structure.
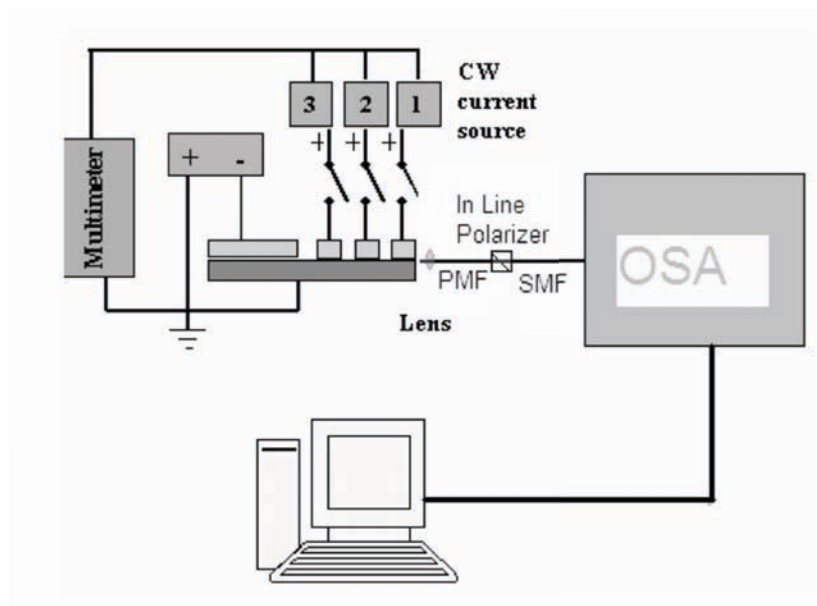
Fig. 2.6 Test setup of the modal gain and absorption measurement.

Fig. 2.7 and 2.8 show the modal gain and total loss data as a function of the emission wavelength, respectively. The notable features include: 1) the gain and loss are relatively modest and comparable to quantum dot active region values and 2) the long-wavelength limit of the total loss measurement gives an estimate of the internal loss (about 14 cm^{-1}) that is generally more reliable than that derived from efficiency measurements of different cavity length lasers [13,17].
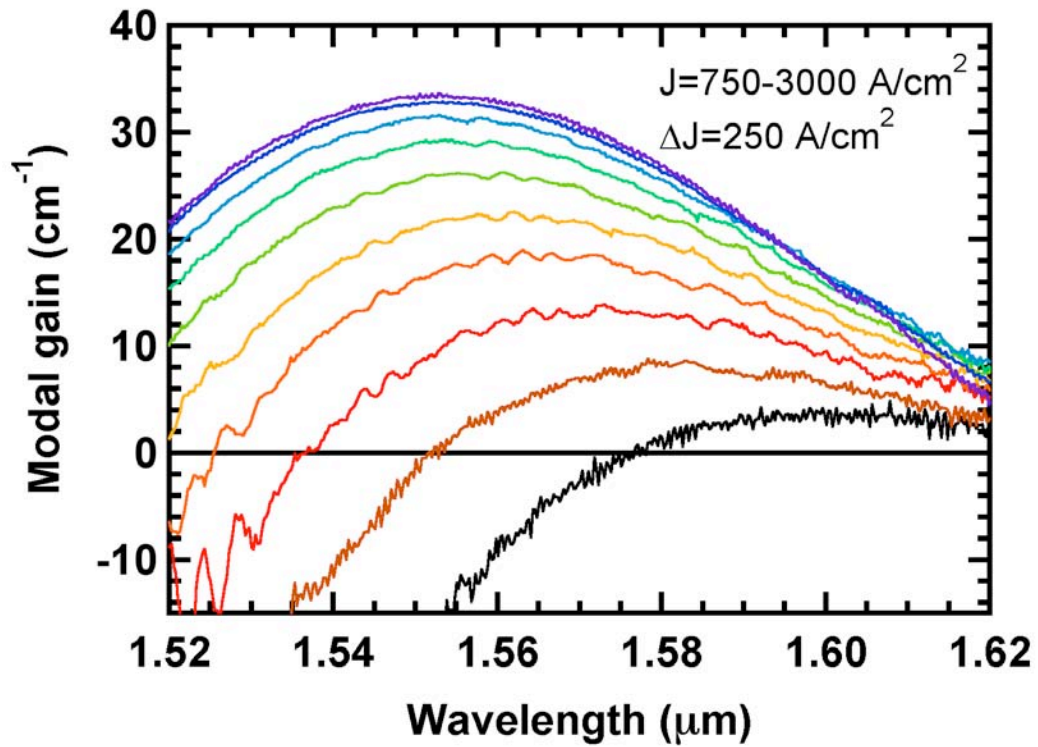
Fig. 2.7 The room-temperature modal gain measured using the segmented contact method.
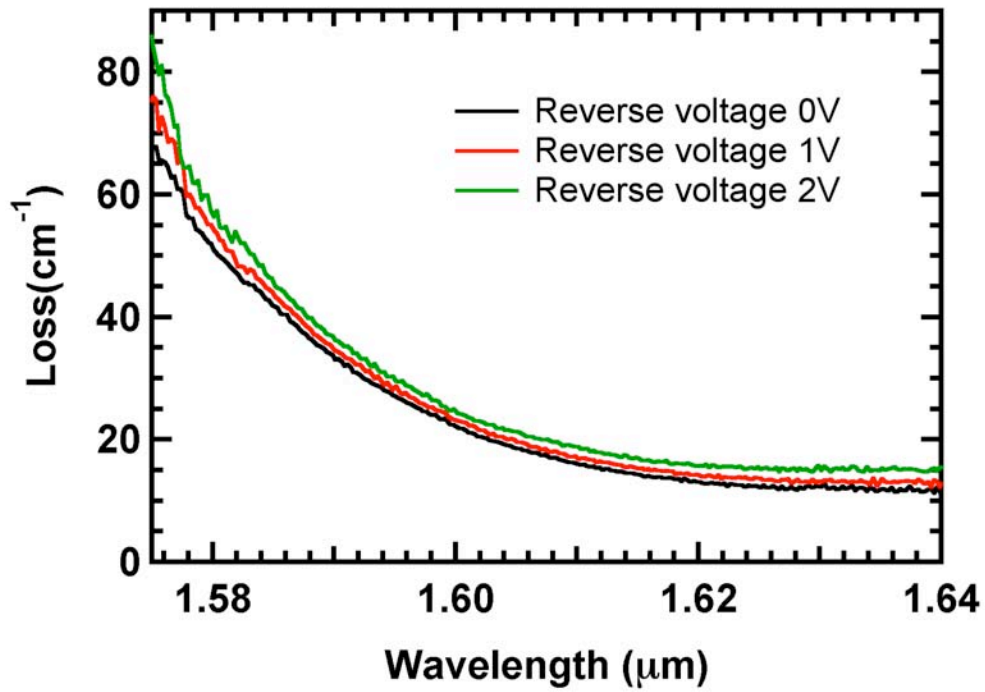
Fig. 2.8 The room-temperature total loss measured using the segmented contact method.
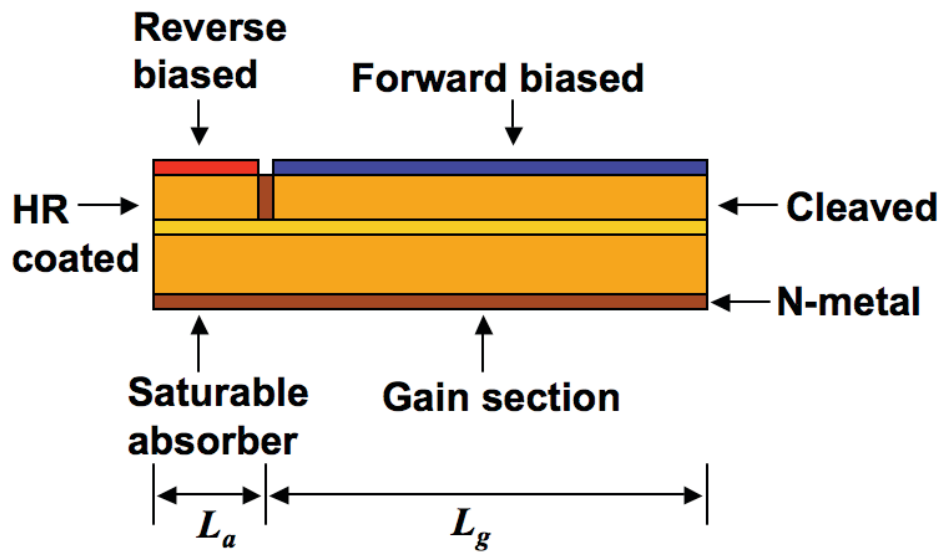
Fig. 2.9 The side view of the two-section passive QDash MLL.

42

2.4.2 MLL device preparation

The segmented device is cleaved and configured into an MLL by wire bonding to form a two-section device with separate gain and saturable absorber regions as depicted in Fig. 2.9. A highly reflective coating (95% reflectivity) is applied to the mirror facet next to the absorber, and the other facet is cleaved and uncoated (32% reflectivity). All the lasers examined in this chapter operate at a wavelength of 1.59 µm, which is noticeably longer than the peak gain wavelengths observed in Fig. 2.7. As explained in Fig. 2.10, which plots a qualitative comparison of the left- and right-hand sides of Eq. (2.11), this result is due primarily to the rapid rise of the loss with decreasing wavelength as seen experimentally in Fig. 2.8.

Fig. 2.11 presents the modal gain at a wavelength of 1.59-µm as a function of pump current density and derived from Fig. 2.7. The differential gain with respect to current density can be obtained from this figure. It is observed that the modal gain starts to saturate at 21 cm^{-1} for a pump current density over 2.5 kA/cm^2 and with that, consequently, the differential gain decreases rapidly to near zero in this region. As shown in Fig. 2.11, a unique property of the QDash two-section MLL that we exploit compared to a single-section device is the abrupt gain saturation characteristic of the nanostructure compared to the traditional QW materials. Thus from Eq. (2.10), QDashes have a significant advantage in achieving stable mode-locking compared to QW-based MLLs.

Based on Eq. (2.10), it is a reasonable assumption that the device will more easily mode-lock when the current density in the gain section is over 2.5 kA/cm^2. Conversely, at a modal gain value equal to zero, dg_0/dJ is 0.018 cm/A, and the unsaturated absorption at 1 V reverse voltage and 1.59-µm is 17.5 cm^{-1}. The latter is calculated by deducting the

internal loss of 14 cm^{-1} from the total loss value at the relevant wavelength. After obtaining the parameters of the MLL cavity, possible geometries for the 1.59-μm InAs/InP passive QDash MLL can be predicted and the robustness of Eq. (2.10) can be evaluated.
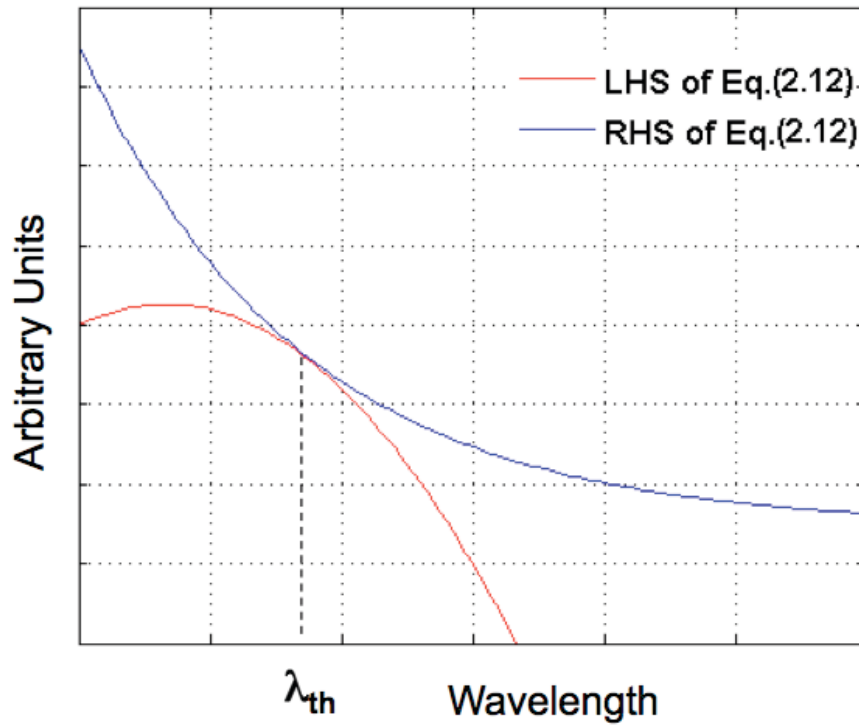
Fig. 2.10 Qualitative comparison of the left- and right-hand sides of Eq. (2.12) and the determination of the threshold wavelength.
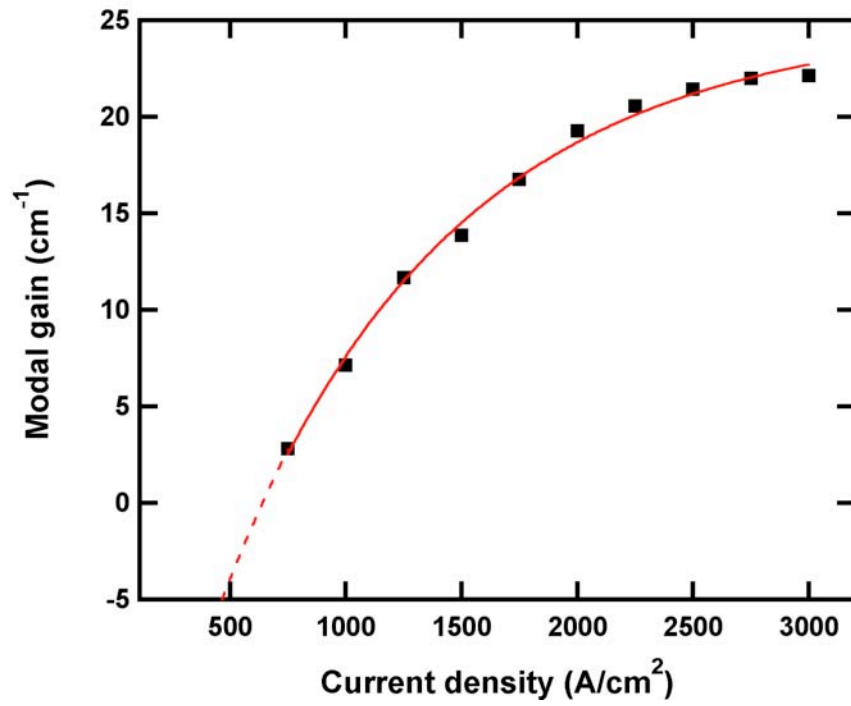
Fig. 2.11 The modal gain vs. pump current density at the wavelength of 1.59-μm.

2.5 MLL device design and characterization

According to the model from section 2.2, we examined InAs QDash passive MLLs with a total cavity length of 2.3-mm, 3.5-mm, and 4-mm, respectively. For the 2.3-mm cavity length with an absorber of 0.3-mm, the gain section must provide a modal gain, g_0, of 21.8 cm^{-1} at 1.59-μm according to the threshold condition. This value is near to the maximum modal gain value with a corresponding current density of 2750 A/cm^2. The differential gain is 0.0008 cm/A, which is much smaller than the differential loss value. After calculation, the 2.3-mm and 3.5-mm devices satisfy the condition stated in Eq. (2.10), and it is noteworthy that the 2.3-mm device has a ratio of over 60 comparing the left- and right-hand sides of Eq. (2.10). In contrast, the 4-mm cavity length MLL does not satisfy Eq. (2.10). The 2.3-mm and 3.5-mm QDash MLLs are predicted to work under mode-locking operation without self-pulsation and the 4-mm device should not mode-lock at all. The device parameter values and the mode-locking analysis results are summarized in Tables 2.1 and 2.2. A 4-mm cavity length device with a 0.5-mm absorber and a 3.5-mm gain section is abbreviated as $A_{0.5}G_{3.5}$.

According to Eq. (2.9), the minimum peak power required can be estimated as well. Using a carrier lifetime of 170 ps, injection efficiency of 81%, and an optical confinement factor equal to 0.096 [24], the estimated value for the minimum peak power is about 0.6 W for the 3.5-mm QDash MLL. This is a high estimate because of the conservatively low value that is used for the differential absorption, but is reasonable considering typical peak operating powers in QD MLLs [3].

Table 2.1 Parameter values for the mode-locked laser simulation

	$A_{0.5}G_{3.5}$	$A_{0.5}G_{3.0}$	$A_{0.3}G_{2.0}$
α_m (cm^{-1})	1.48	1.7	2.58
a_0 at 1.59-µm (cm^{-1})	17.5 (Vr=1V)	17.5 (Vr=1V)	18 (Vr=2V)
dg_0/dJ (cm/A)	0.0073	0.0021	0.0008
dg_0/dJ at g_0=0 (cm/A)	0.018	0.018	0.018

Table 2.2 Mode-locking analysis according to Eq. (2.1) and (2.11)

Eq. (2.1) satisfied	Yes	Yes	Yes
Eq. (2.10) satisfied	No	Yes	Strong
Mode-locking operation?	No	Yes	Yes

The figures below show data for the 2.3-mm and 3.5-mm cavity length passive QDash MLLs. Fig. 2.12 is the Light-Current (LI) curve of the laser for various absorber biases of the 2.3-mm device. The maximum slope efficiency is 0.05 W/A with 0 V applied to the absorber. Fig. 2.13 demonstrates the optical spectrum under 170-mA DC bias on the gain section and -2 V applied to the absorber. The peak lasing wavelength is around 1.59-µm as described above. Fig. 2.14 confirms that the mode-locked repetition rate is 18.4 GHz for the 2.3-mm device and shows the first two harmonics without any undesirable self-pulsation. Fig. 2.15 corroborates that the fundamental mode-locked repetition rate is 12.3 GHz for the 3.5-mm device and shows that at least three harmonics are observed, again without self-pulsation. Both diagrams show at least two harmonics in the RF spectrum, which gives us confidence that the devices of 2.3-mm and 3.5-mm length are mode-locked as was established in [15,17]. The RF spectral analysis is relied upon to characterize the mode-locking because it is relatively difficult to acquire a second

harmonic generation autocorrelator with the required sensitivity at 1.59 µm wavelength. From the measurement results of the RF spectrum (not shown), we confirm that the 4-mm device does not mode-lock, which substantiates our prediction from the cavity design guidelines derived above and described in Table 2.2.
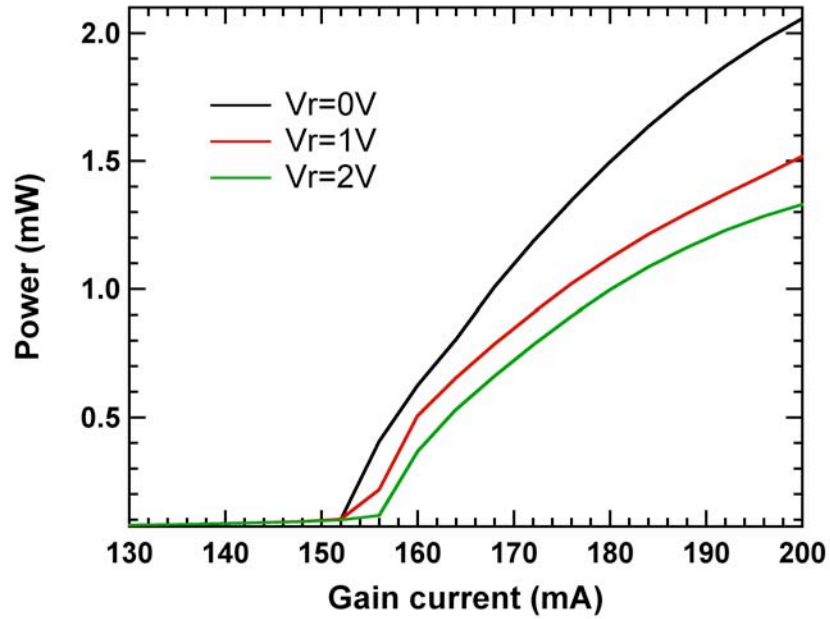
Fig. 2.12 L-I curve with reverse voltage from 0V to 2V of the 2.3-mm passive MLL.
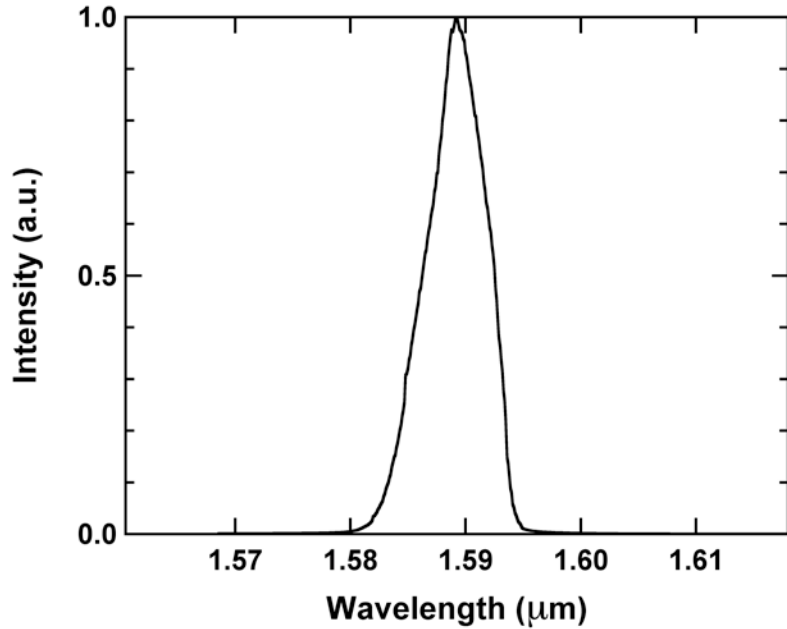
Fig. 2.13 Optical spectrum with a DC gain current of 170-mA on the 2-mm gain section

and a reverse voltage of 2V on the 0.3-mm absorber.
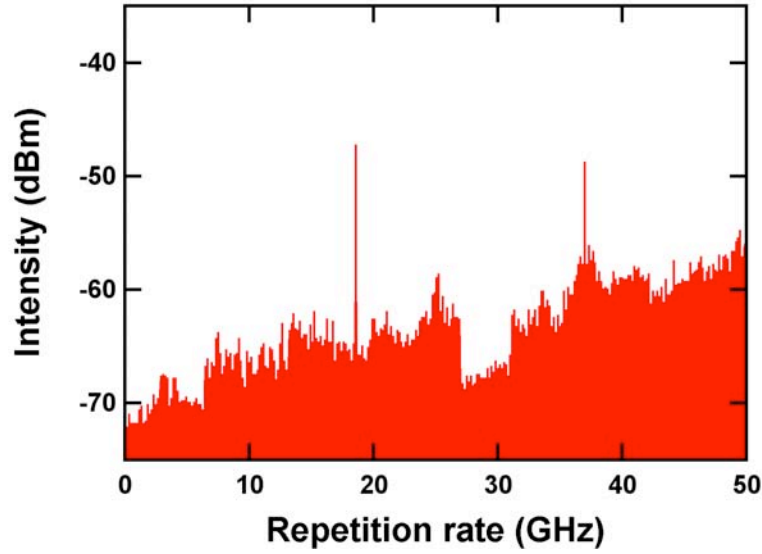
Fig. 2.14 The full span of the RF spectrum at 170mA and 2V reverse voltage of the 2.3-mm two-section passive QDash MLL device. The fundamental repetition frequency is 18.4 GHz. The RF spectrum clearly shows the first two harmonic components.
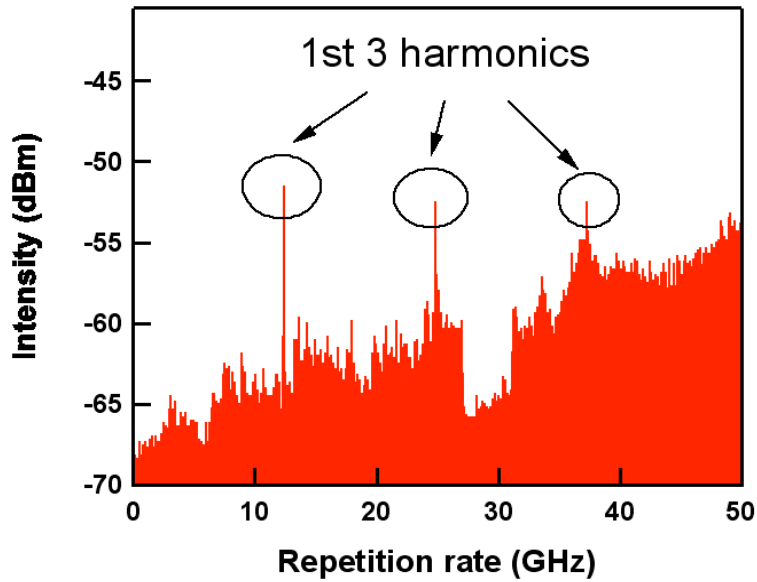
Fig. 2.15 The full span of the RF spectrum at 400mA and 1V reverse voltage of the 3.5-mm two-section passive QDash MLL device. The fundamental repetition frequency is 12.3 GHz. The RF spectrum clearly shows the first three harmonic components.

2.6 Conclusion

Valuable guidelines for mode-locking in two-section passive MLLs that have separate gain and saturable absorber regions and significant internal loss have been derived through the net-gain modulation phasor approach and applied to a variety of cavity designs for long-wavelength QDash MLLs. It has been shown that the new set of equations can be used to predict functional device layouts using measured modal gain and loss characteristics that are obtained through the segmented contact method on the *actual* device. After the modal gain and total loss measurement, the MLL was built by reconfiguring this same linear array of diodes. Eq. (2.10) was found to be most useful when designing the two-section passive MLL cavities since it does not include the peak power, carrier lifetime and waveguide internal loss. From Table 2.2, it has been confirmed that Eq. (2.1) is not particularly instructive for designing two-section semiconductor MLLs. The experimental results corroborated the theoretical predictions, which should be an invaluable tool for future realization of long-wavelength passive QDash MLLs that are generally difficult to achieve [21]. Furthermore, based on this analytic model we have also shown that the deterioration of performance with increasing temperature is caused mainly by the associated degradation in the differential gain with increasing temperature. This model will be useful in designing the next generation QD MLL capable of stable operation from 20°C to 100°C for optical interconnects applications [25].

References:

1. D. A. B. Miller, "Device requirements for optical interconnects to silicon chips," *IEEE Proc.,* vol. 97, no. 7, pp. 1166-1185 (2009).

2. G. A. Keeler, B. E. Nelson, D. Agarwal, C. Debaes, N. C. Helman, A. Bhatnagar, and D. A. B. Miller, "The benefits of ultrashort optical pulses in optically interconnected systems," *IEEE J. Sel. Top. Quantum Electron*., vol. 9, pp. 477-485 (2003).

3. Y.-C. Xin, Y. Li, V. Kovanis, A. L. Gray, L. Zhang, and L. F. Lester, "Reconfigurable quantum dot monolithic multi-section passive mode-locked lasers," *Opt. Express,* vol. 15, pp. 7623-7633 (2007).

4. E. U. Rafailov, M. A. Cataluna, W. Sibbett, "Mode-locked quantum-dot lasers," *Nature Photonics*, vol. 1, pp. 395-401 (2007).

5. M. G. Thompson, A. R. Rae, M. Xia, R. V. Penty, and I. H. White, "InGaAs quantum-dot mode-locked laser diodes," *IEEE J. Sel. Top. Quantum Electron*., vol. 15, pp. 661-672 (2009).

6. L. C. Chiu and A. Yariv, "Auger recombination in quantum well InGaAsP Heterostructure lasers," *IEEE J. Quantum Electron.*, vol. 18, pp. 1406-1409 (1982).

7. M. J.R. Heck, E. A.J.M. Bente, B. Smalbrugge, Y. S. Oei, M. K. Smit, S. Anantathanasarn, and R. Nötzel, "Observation of Q-switching and mode-locking in two-section InAs/InP (100) quantum dot lasers around 1.55 μm," *Opt. Express*, vol. 15, pp. 16292–16301 (2007).

8. F. Lelarge, B. Dagens, J. Renaudier, R. Brenot, A. Accard, F. Van Dijk, D. Make, O. Le Gouezigou, J. G. Provost, F. Poingt, J. Landreau, O. Drisse, E. Derouin, B. Rousseau, F. Pommereau, and G. H. Duan, "Recent advances on InAs/InP quantum

dash based semiconductor lasers and optical amplifiers operating at 1.55 μm," *IEEE J. Sel. Top. Quantum Electron.*, vol. 13, pp. 111-124 (2007).

9. D. Zhou, R. Piron, M. Dontabactouny, O. Dehaese, F. Grillot, T. Batte, K. Tavernier, J. Even, and S. Loualiche, "Low threshold current density of InAs quantum dash laser on InP (100) through optimizing double cap technique," *Appl. Phys. Lett.*, vol. 94, pp. 081107 (2009).

10. G. T. Liu, A. Stintz, H. Li, K.J. Malloy and L. F. Lester, "Extremely Low Room-Temperature Threshold Current Density Diode Lasers Using InAs Dots in an $In_{0.15}Ga_{0.85}As$ Quantum Well," *Electron. Lett.*, vol. 35, p. 1163-65 (1999).

11. K. Y. Lau and J. Palaski, "Condition for short pulse generation in ultrahigh frequency mode-locking of semiconductor-Lasers," *IEEE Photon. Technol. Lett.*, vol. 3, pp. 974-976 (1991).

12. J. Palaski and K. Y. Lau, "Parameter ranges for ultrahigh frequency mode-locking of semiconductor lasers," *Appl. Phys. Lett.*, vol. 59, pp. 7-9 (1991).

13. Y.-C. Xin, Y. Li, A. Martinez, T. J. Rotter, H. Su, L. Zhang, A. L. Gray, S. Luong, K. Sun, Z. Zou, J. Zilko, P. M. Varangis, and L. F. Lester, "Optical gain and absorption of quantum dots measured using an alternative segmented contact method," *IEEE J. Quantum Electron.*, vol. 42, pp. 725-732 (2006).

14. P. Blood, G. M. Lewis, P. M. Smowton, H. Summers, J. Thomson, and J. Lutti, "Characterization of semiconductor laser gain media by the segmented contact method," *IEEE J. Sel. Top. Quantum Electron.*, vol. 9, pp. 1275-1282 (2003).

15. N. G. Usechak, Y.-C. Xin, C.-Y. Lin, L. F. Lester, D. J. Kane, and V. Kovanis, "Modeling and direct electric-field measurements of passively mode-locked quantum-

dot lasers," *IEEE J. Sel. Top. Quantum Electron*., vol. 15, pp. 653-660 (2009).

16. A. G. Vladimirov and D. Turaev, "Model for passive mode locking in semiconductor lasers," *Phys. Rev. A*, vol. 72, pp. 033808-1-033808-13 (2005).

17. P. Vasilev, *Mode-locking Diode Lasers, Ultrafast diode lasers Fundamentals and applications,* (Artech House, Boston 1995), Chap. 4.

18. Y.-C. Xin, C.-Y. Lin, Y. Li, H. P. Bae, H. B. Yuen, M. A. Wistey, J. S. Harris, S. R. Bank, and L. F. Lester, "Monolithic 1.55 μm GaInNAsSb quantum well passively modelocked lasers," *Electron. Lett.*, vol. 44, pp. 581-582 (2008).

19. C.-Y. Lin, Y.-C. Xin, N. A. Naderi, F. L. Chiragh, and L. F. Lester, "Monolithic 1.58-micron InAs/InP quantum dash passively mode-locked lasers," *Proc. SPIE* ,vol. 7211, pp. 721118 (2009).

20. F. Grillot, C.-Y. Lin, N.A. Naderi, M. Pochet, and L. F. Lester, "Optical feedback instabilities in a monolithic InAs/GaAs quantum dot passively mode-locked laser," *Appl. Phys. Lett*., vol. 94, pp. 153503 (2009).

21. C.-Y. Lin, Y.-C. Xin, Y. Li, F. L. Chiragh, and L. F. Lester, "Cavity design and characteristics of monolithic long-wavelength InAs/InP quantum dash passively mode-locked lasers," Opt. Express, vol. 17, no. 22, pp. 19739–19748 (2009).

22. R.-H Wang, A. Stintz, P. M. Varangis, T. C. Newell, H. Li, K. J. Malloy, L. F. Lester, "Room-temperature operation of InAs quantum-dash lasers on InP (001)," *IEEE Photon. Technol. Lett.,* vol. 13**,** pp. 767-769 (2001).

23. Y.-C. Xin, "Quantum dot multi-section light emitters," PhD dissertation, University of New Mexico, (2006).

24. N. Naderi, M. Pochet, F. Grillot, N. Terry, V. Kovanis, and L. F. Lester, "Modeling

the injection-locked behavior of a quantum dash semiconductor laser," *IEEE J. Sel. Top. Quantum Electron.*, vol. 15, pp. 563-571 (2009).

25. M. T. Crowley, N. Patel, D. Murrell, M. Breivik, C.-Y. Lin, Y. Li and L. F. Lester, "Modeling the temperature performance of monolithic mode-locked quantum dot lasers," *IEEE Lester Eastman Conference on High Performance Devices*, (2010).

Chapter 3

Compact optical generation of microwave signals using a quantum dot mode-locked laser

3.1 Introduction

Due to the global interest in higher frequency bandwidths, producing compact RF signal sources on a chip is a key research topic for applications such as the wireless communication field, software-defined radio, radar, and satellite communication systems. Monolithic passively mode-locked lasers (MLLs) are promising candidates for microwave generation [1-3] because of their compact size, low power consumption, direct electrical pumping, and high electrical-to-optical-to-electrical (E/O/E) conversion efficiency. Several unique advantages of quantum dot (QD) materials, such as their ultra-broad bandwidth, feedback resistance, ultra-fast gain dynamics, and easily saturated gain and absorption, make them an ideal choice for monolithic semiconductor MLLs [4-7]. These characteristics give QD MLLs the advantage of pulse stability over a wider power range than their quantum well (QW) counterparts. Previous semiconductor active regions such as quantum wells could produce the same optical gain and absorption functions, but frequently required separate optimization of the optical materials in the MLL cavity. The QD MLL can easily use the *same* epitaxial layer structure in both the absorber and gain sections [8-10].

Furthermore, The QD MLL chip can be extended to a multi-section layout that brings the reconfigurable function for diverse wave/repetition rate generation applications [11,12]. Fig. 3.1 shows the top-view schematic diagram of the multi-section QD MLL. The absorber positions that can be used to excite higher-order harmonics are labeled. More importantly, a compact, reconfigurable chip-scale RF frequency generator can be realized by this multi-section QD MLL layout as will be described in detail in this chapter [12]. In this special device format, the reconfigurable RF frequency generator could potentially self-heal, which is useful for future satellite communication applications [13,14]. The self-healing mechanism would be realized through a software-designed control system that could salvage or bypass degraded or damaged components.
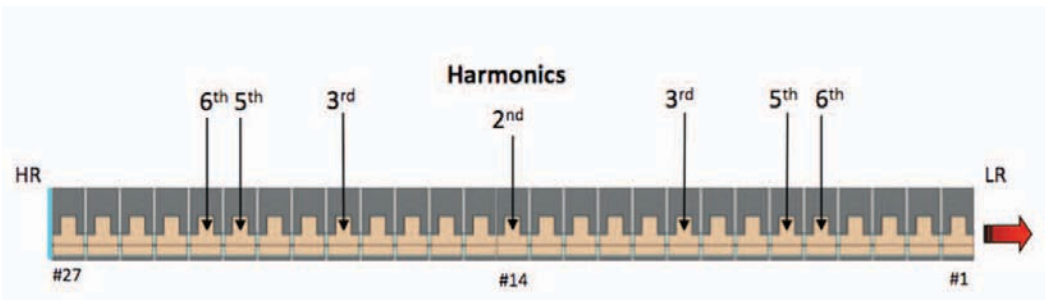
Fig. 3.1 The top-view schematic diagram of the multi-section QD MLL that has 27 electrically-isolated anodes of equal length. The absorber positions that potentially excite higher-order harmonics are labeled.

Conventionally, optical generation of microwave signals can be achieved by using two different laser sources applied to a photodetector or a photomixer made from low-temperature-grown GaAs [15]. The beat signal with a required frequency equivalent to the spacing of the two wavelengths is extracted from the output of the photodetector. This approach is called optical heterodyning or photomixing. The advantage of this technique

is the wide tunability of the output frequency from near DC to the THz range. However, the drawback is the relatively low conversion efficiency and frequency stability issue. Several groups have contributed towards improving the conversion efficiency and maintaining high stability in heterodyned systems [16-20]. In this previous research, optical injection locking or an optical phase-locked loop was implemented to reduce the phase noise and maintain high stability [16, 17]. However in this case, a high-quality microwave reference signal is also required. Thus, it is hard to apply this technique to a wireless communication system in which no reference signal is available for the local oscillator. To avoid using a reference signal, the beat signal at the output of a photodetector is generated by a single laser source that has either a single wavelength with dual longitudinal modes [18, 19] or two wavelengths operating in single longitudinal mode for each wavelength [20].

In this chapter, we combine the optical pulse generation of a two-section passive MLL with the high-speed characteristics of the quantum dot saturable absorber (SA) to produce a microwave signal directly from the same laser diode. From the RF point of view, the SA behaves as a p-i-n photodetector. When an optical pulse train passes through the SA, an electrical pulse is directly generated at the same repetition rate as the optical pulses using *only DC bias*. This compact RF signal generator can then be integrated with a reconfigurable antenna that accesses the various frequencies available from the pulsed source. Fig. 3.2 shows an example of this hybrid integration, which has been described in ref. 2.

In order to validate the QD MLL as a candidate for a compact RF generator, we focus on the characterization and conversion efficiency of the microwave signal

generation through the SA of a two-section passive QDMLL first. The antenna design and hybrid integrated transmitting module will then be discussed. This chapter is organized as follows. Section 2 is devoted to the laser structure and the RF generation mechanism. The experimental setup and RF signal characterization are presented in Section 3. In Section 4, the results and discussion on the conversion efficiency of the passive quantum dot mode-locked laser is presented. The hybrid integrated transmitting module is characterized in Section 5.   Finally, the key findings and future work are summarized in Section 6.
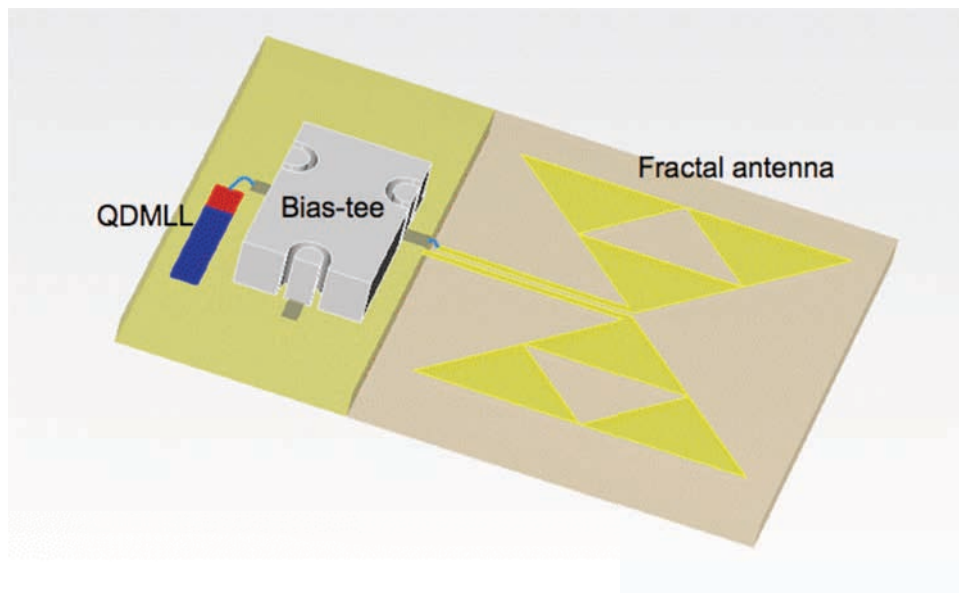
Fig. 3.2 The integration of the QDMLL with a reconfigurable bowtie antenna. First, high frequency electrical pulse signals are generated from the saturable absorber of the QDMLL. These signals are next routed by a bias-tee and a coplanar waveguide to a reconfigurable bowtie antenna. This integrated unit can then be used as a cellular block in more complex arrays that are controlled, for example, by field programmable gate arrays.

3.2 Device structure and RF generation mechanism

The laser epitaxial structure of this device is a multi-stack "Dots-in-a-WELL" (DWELL) structure that is composed of an optimized six-layer QD active region grown by solid-source molecular beam epitaxy on a (001) GaAs substrate (wafer #: ZLG792F-AH) [11]. The p- and n-type AlGaAs cladding layers have 20% Al content, and graded interfaces are used between the clads and the GaAs waveguide layer surrounding the DWELL structure. The 3.5-µm wide optical ridge-waveguide devices are fabricated following standard dry-etch, planarization, and metallization processing. In this work, the two-section QD passive MLLs are made with a total cavity length of 4.1-mm and a SA length of 0.8-mm. A highly reflective (HR) coating ($R_1 \approx 95\%$) is applied to the mirror facet next to the SA and the other facet is cleaved ($R_2 \approx 32\%$). Fig. 3.3 shows a schematic diagram of a two-section passive MLL.

Typically, the electrical pulse train can be generated using a low-temperature (LT) metal-semiconductor-metal (MSM) detector that converts the optically generated pulse from MLL to an RF output signal [21]. However, an alternative approach that we favor for optically generating the RF frequencies is to bypass the LT-MSM detector entirely and use the transient photocurrent produced in the SA of the passive QD MLL as the microwave signal source [2]. This device layout is simpler and has the potential to convert the ultrafast optical signal to electrical pulses more efficiently. As a picosecond optical pulse goes into the SA, the leading edge of the optical pulse is absorbed and creates free carriers. The resulting electrons and holes are swept to the metal contacts as the photocurrent due to the built-in electrical field. This process has the potential to be very fast since absorbers composed of quantum dots have demonstrated sub-picosecond

recovery times [4,8]. Most likely the speed of the electrical impulse from the absorber

section will be limited by electrical parasitics that can be reduced by decreasing the

bonding pad capacitance or the length of the absorber itself. Normally, decreasing the

length of the absorber would diminish the optical-to-electrical conversion efficiency as in

any waveguide-based photodetector. However, in the passive MLL geometry, the ability

to apply HR coatings to both mirror facets is a significant advantage for realizing

simultaneous high-speed and high efficiency. In our first example presented here, only

one laser mirror is HR-coated for simplicity.
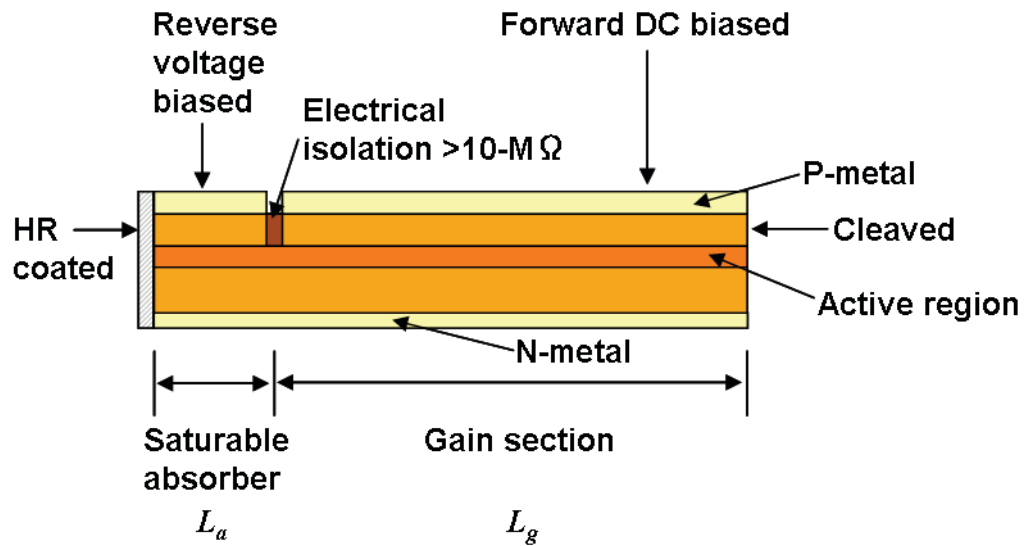
Fig. 3.3 A schematic diagram of the two-section passive MLL (side-view).

3.3 Device characterization

This section describes the basic output characteristics of the QDMLL and the operating parameters of the devices that are necessary for evaluating the DC to RF differential efficiency as shown in Section 4. Fig. 3.4 shows the total loss data as a function of the emission wavelength using an improved segmented contact method [22]. From Fig. 3.4, the internal loss of the optical waveguide is found to be 2 cm^{-1}. Fig. 3.5 is the light-current (LI) curve of the laser for various absorber biases of the 4.1-mm device. The maximum slope efficiency is 0.27 W/A with 0 V applied to the absorber. The inset of Fig. 3.5 demonstrates the single-section laser diode case for comparison. To realize this layout, the anodes of the gain and absorber section were tied together through wire bonding and then pumped uniformly. The differential quantum efficiency of the laser diode can be determined through this layout. The optical spectrum under 200 mA DC bias on the gain section and 0 V applied to the absorber is shown in Fig. 3.6. The peak lasing wavelength is at 1.21-μm and the mode-locked 3-dB spectral bandwidth is about 2.8 nm with a typical pulse width on the order of 10 ps and an RMS timing jitter of 1-2 ps calculated from the offset range of 30 kHz to 30 MHz [23]. Under the condition of complete mode-locking, which was confirmed by optical pulse measurement from a background-free Femtochrome autocorrelator, the measured current from the SA is the average RF photocurrent. The RF power spectrum was measured using the setup shown in Fig. 3.7 using high-speed RF probing. The series connection of a bias-tee and an on-wafer RF probe was used to apply the reverse voltage on the SA and to extract the microwave signal from the QDMLL simultaneously. Fig. 3.8 shows that the average RF photocurrent is on the order of 40 mA when up to 200 mA of DC current is injected into

the gain section. The maximum DC current for this study is limited to 200 mA to avoid deleterious heating of the device.   Fig. 3.9 also demonstrates an RF power of -2 dBm under 200 mA DC bias on the gain section and -1 V applied to the absorber. Thus, these RF current pulses can generate a reasonable amount of power that can be transmitted by a reconfigurable bowtie antenna for microwave applications [2]. In general, more power can be directed to the fundamental harmonic by increasing the current bias of the device above 200 mA because this situation expands the pulse width of the QD MLL which favors the baseline frequency.

Another primary advantage of the QD MLL is the expanded range of stable mode-locking [11] that permits wider bias operation over which to extract RF signals from the device. The stable bias condition for mode-locking was investigated, and the operating regime was mapped out using the gain current and SA reverse voltage as control parameters as seen in Fig. 3.10. Compared to the QW MLL used for RF generation, the monolithic passive QD MLL clearly demonstrates a mode-locking operation over a wider range of gain currents and absorber voltages [24].
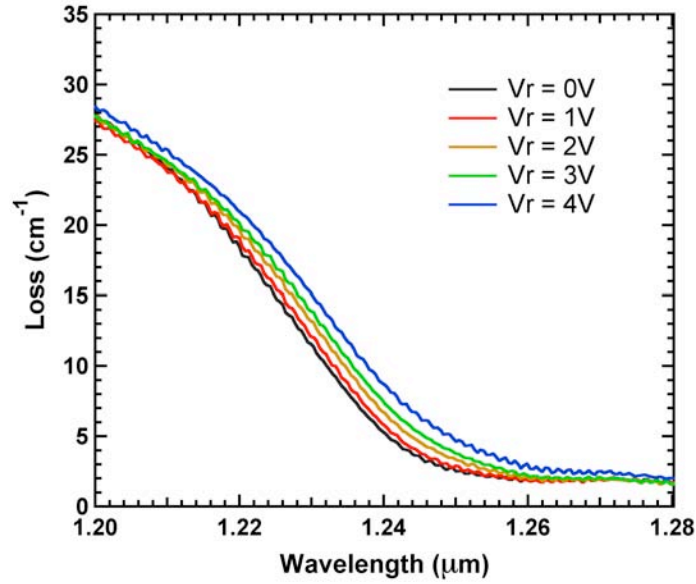
Fig. 3.4 The room-temperature total loss spectra of the QDMLL device as measured by

the multi-section technique.
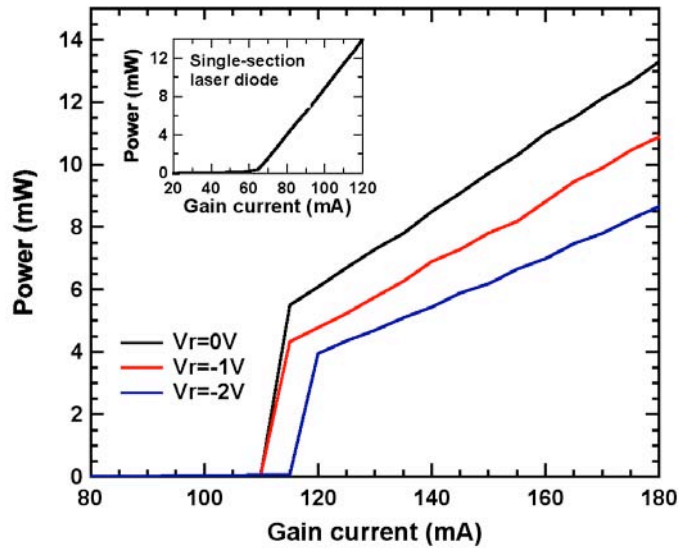
Fig. 3.5 The Light-Current curve of the laser for various absorber biases from 0V

to -2V. The inset shows a single-section, uniformly pumped case.
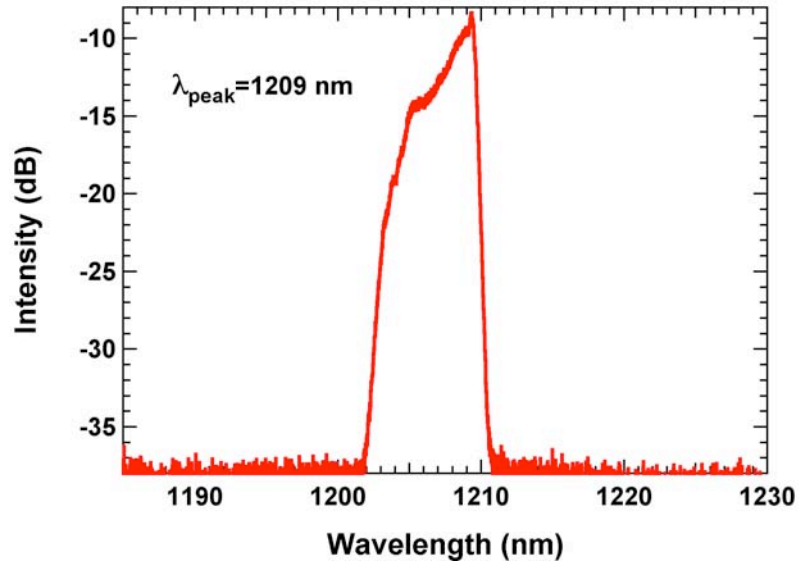
Fig. 3.6 The optical spectrum of the QDMLL device under 2000 mA DC bias on the gain

section and 0 V applied to the absorber.
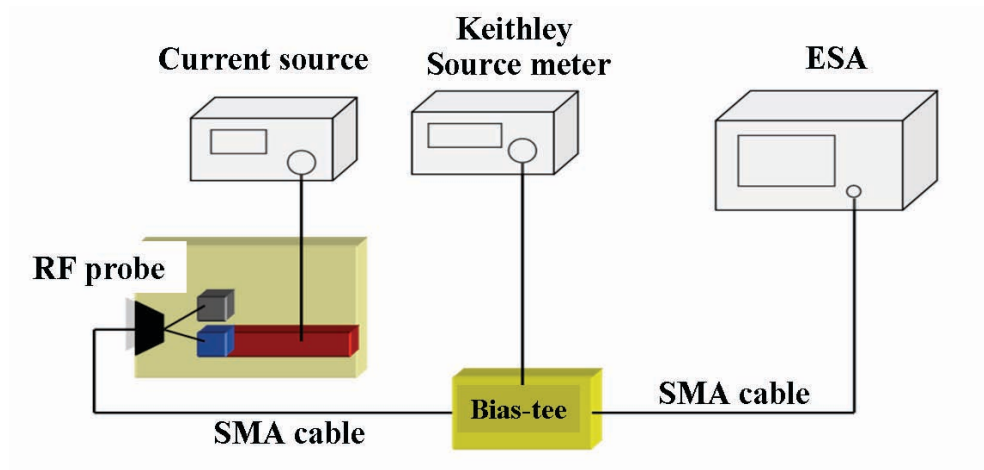
Fig. 3.7 The apparatus of the RF signal measurement.
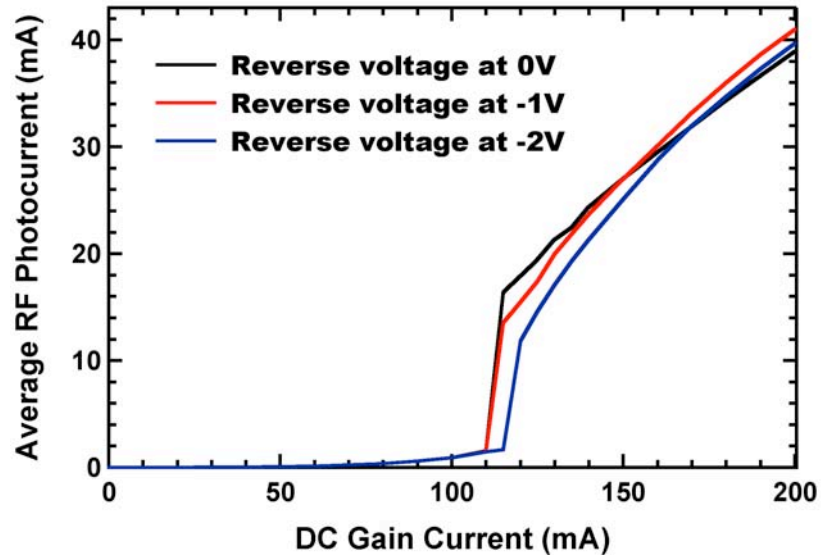
Fig. 3.8 The average RF photocurrent generated in the saturable absorber of the QDMLL

as a function of the DC current applied to the gain section of the laser for various

absorber biases.
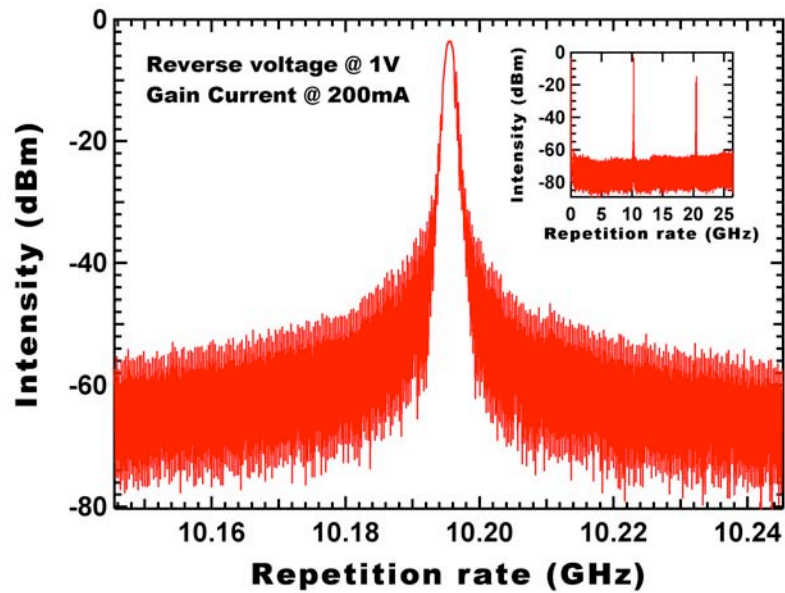
Fig. 3.9 The RF power spectrum of the electric pulse signal directly extracted from the

saturable absorber. The resolution bandwidth: 1MHz
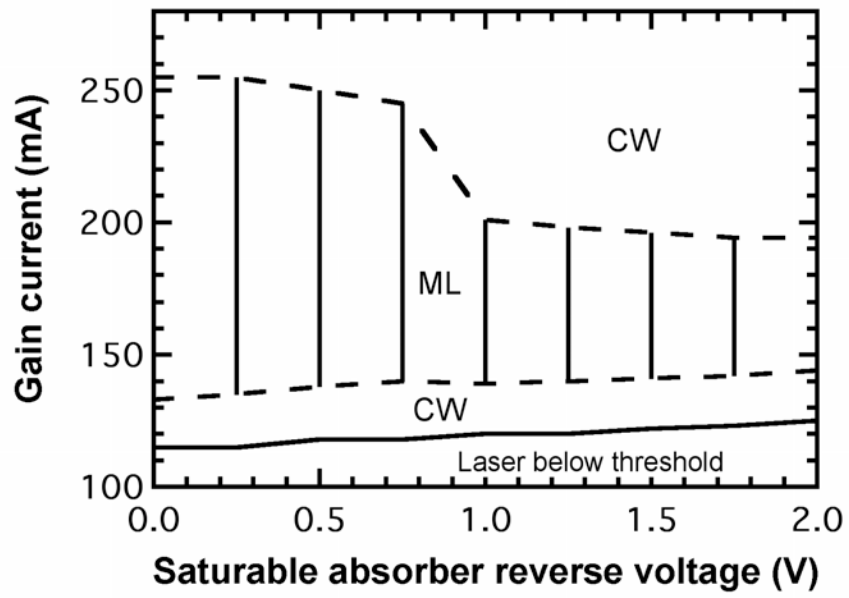
Fig. 3.10 Operating regime map for 4.1-mm passive QDMLL device. CW: continuous

wave

3.4 Result and discussion on the conversion efficiency of the passive quantum dot mode-locked laser

3.4.1 Derivation of the conversion efficiency of the passively quantum dot mode-locked laser

The design strategy for microwave signal generation from the QDMLL is different from the approach for short optical pulse generation. Since optical power output is not desirable for maximizing the RF output from the absorber, different coating concerns and bias conditions are necessary to maximize the electrical pulse output while maintaining the mode-locking operation. As derived below, lowering the mirror loss, α_m, by implementing HR coatings improves the conversion of DC power to RF output power. Another change is that the reverse bias and the length of the absorber should be increased as much as possible at the expense of optical output power since these approaches directly benefit the RF power generation.

The DC to RF differential efficiency, η_{DCRF}, or "conversion efficiency" is found by measuring the change in the average RF photocurrent as a function of the DC gain current above threshold. η_{DCRF} is about 33% as calculated from Fig. 3.8 under the optimum bias condition of -2 V applied to the absorber. This value compares favorably with that demonstrated by the optical heterodyning approach that is commonly used to produce microwave signals. The typical power conversion efficiency of the optical heterodyning is around 2% at the millimeter-wave region [15].

Another important parameter related to the conversion efficiency is the extraction efficiency, η_E, of the SA. Since the epitaxial layer structure is normally designed for the

efficient operation of the laser, which seeks to maximize the *injection* efficiency, the extraction efficiency of the reverse-biased absorber is not necessarily optimized. Unlike the conversion efficiency, the extraction efficiency is not directly measurable in the mode-locked laser. In order to derive an expression for η_E so that it can be calculated from other measurements, the differential quantum efficiency, η_d, which can be determined from a uniformly-pumped laser diode, is found first. (This uniformly-pumped case is experimentally realized by tying the anodes of the SA and gain sections together.) η_d, is defined as:

$$\eta_d = \frac{q}{h\nu} \times \frac{\Delta P}{\Delta I} \tag{3.1}$$

where q is the electronic charge, h is the Planck's constant, ν is the optical frequency, and $\Delta P/\Delta I$ is the slope above the threshold from the LI curve as found in the inset of Fig. 4. The injection efficiency of the laser diode, η_i, is then calculated using η_d and the loss from the waveguide and mirror facets according to the following relation:

$$\eta_i = \eta_d \cdot \frac{\alpha_i + \alpha_m}{\alpha_m} \tag{3.2}$$

where α_i is the internal loss of the waveguide which can be derived from the loss measurement, α_m is the mirror loss of the laser device, $\alpha_m = \frac{1}{2L}\ln\left(\frac{1}{R_1 R_2}\right)$, and L is the total cavity length. For our QD diode laser material, η_i is 0.63 calculated from all the parameters given above.

After all the basic device parameters are calculated from the single-section case, the various two-section bias conditions that produce mode-locking need to be analyzed. The convention here is to quote the bias current on the gain section and the reverse voltage on

the absorber section of the MLL. For the two-section laser, the differential quantum efficiency is measured at a fixed reverse voltage on the absorber. For instance, the differential quantum efficiency of the QD MLL under -1V reverse voltage bias to the SA, η_{d_1V} is denoted as:

$$\eta_{d\_MLL} = \eta_{d\_1V} = \frac{q}{h\nu} \times \frac{\Delta P_{1V}}{\Delta I_{1V}} \tag{3.3}$$

Next, the expression for the injection efficiency, Eq. (3.2), has to be modified to take into account the optical loss induced by the SA of the MLL:

$$\eta_i = \eta_{d\_1V} \times \frac{\alpha_i + \alpha_m + \alpha_{ave\_abs} \times \dfrac{L_a}{L}}{\alpha_m} \tag{3.4}$$

where L_a is the length of the SA and α_{ave_abs} is the time-averaged loss of the SA. Since the injection efficiency is the same for the uniformly-pumped laser and the MLL, re-arranging Eq. (3.4) allows the calculation of the time-averaged loss according to the following expression:

$$\alpha_{ave\_abs} = \frac{L}{L_a}\left[\alpha_m\left(\frac{\eta_i}{\eta_{d\_MLL}} - 1\right) - \alpha_i\right] \tag{3.5}$$

Next, from the definition of the DC to RF differential efficiency above, we can express η_{DCRF} mathematically as the following equation:

$$\eta_{DCRF} = \eta_i \times \eta_E \times \frac{\alpha_{ave\_abs} \times \dfrac{L_a}{L}}{(\alpha_i + \alpha_m) + \alpha_{ave\_abs} \times \dfrac{L_a}{L}} \tag{3.6}$$

70

The ratio on the right-hand-side of Eq. (3.6) represents the fraction of the optical power that is converted into electron-hole-pairs (EHPs) in the absorber. η_E is then the fraction of EHPs in the absorber that are collected at the external electrodes of the device as photocurrent. Finally, after rearranging Eq. (3.6), the extraction efficiency of the SA can be described by the following relation:

$$\eta_E = \frac{\eta_{DCRF}}{\eta_i \alpha_{ave,abs}} \left(\frac{\alpha_i L}{L_a} + \frac{\alpha_m L}{L_a} + \alpha_{ave,abs} \right) \tag{3.7}$$

3.4.2 Experimental results

The device parameters and the conversion efficiency analysis results are summarized in Table 3.1 for different reverse voltages applied to the SA. For reverse voltages greater than 2V, the mode-locking starts to degrade due to excessive absorption. According to the experimental data and equations derived above, the average η_E of the SA is about 80% as calculated from Eq. (3.7). The extraction efficiency is not noticeably voltage dependent indicating that the carriers are nearly or at velocity saturation in the SA for all biases. The time-averaged loss of the SA rises from 20 to 33 cm^{-1}, depending upon the reverse voltage of the SA, which is consistent with the Stark shift of the absorption edge as a function of increasing electric field across the quantum dots. The time-averaged loss values are also generally consistent with the measured 1209 nm absorption data shown in Fig. 3. The values at 1209 nm are chosen for comparison because this is the peak lasing of the QDMLL as presented in Fig. 5. The time-averaged loss result for the 2V reverse voltage case is somewhat larger than that reported in Fig. 3, which is probably due to device heating that decreases the energy gap as the absorber collects a larger current density for increasing reverse bias. It is noted that the overall trend in the conversion

efficiency, η_{DCRF}, mirrors that of the time-averaged loss with reverse bias on the SA. This result is to be expected since the ratio on the right-hand-side of Eq. (3.6) maximizes at about 65% for a reverse voltage of 2V. In other words, 65% of the optical power is going into the absorber at this bias. Increasing the number of QD stacks in the active region could potentially increase the power collected by the SA. However, this approach requires increasing the active region thickness, which could cause more EHP recombination that would lower the extraction efficiency. Increasing the width of the active layer could also undesirably broaden the pulse width of the QDMLL because of a longer carrier transit time across the absorber.

Table 3.1 Device parameters and the conversion efficiency result

Reverse voltage on SA	0V	1V	2V
$\eta_d\,(\%)$	13	11	9.3
$\alpha_{ave\_abs}\,(1/cm)$	20	25	33
$\eta_{DCRF}\,(\%)$	25	32	33
$\eta_E\,(\%)$	75	86	79

It is noted that the extraction efficiency actually exceeds the injection efficiency of 63%, which is probably due to the choice of 20% Al content in the AlGaAs cladding layers and the graded interfaces. The heterojunction offsets between the core and clad layers are probably not large enough for good carrier confinement and optimal injection efficiency in the laser, but this smaller energy offset is obviously beneficial to the transport of carriers in the absorber. In the future, alternative passive QDMLL layouts will be investigated with different QD stack numbers and cladding composition to optimize the conversion efficiency.

3.5 Hybrid integrated transmitting module

After characterizing the power conversion efficiency and the photocurrent generated from the absorber of the laser device, the two-section passive QD MLL has been shown to be a potential candidate for a compact, efficient RF signal generator. In this section, we will integrate the laser chip with a rectangular microstrip antenna to make a transmitting module to confirm its suitability for RF applications.

3.5.1 Antenna design

Among numerous choices of antennas, the rectangular microstrip antenna is chosen. A microstrip antenna plays a key role in modern communications due to its low profile, cost efficiency and simplicity in design [25]. Since the temperature controller is required under the laser chip, the integrated antenna sits on a large ground plane. Therefore, the patch-type-antenna is more realizable than coplanar antennas. In Fig. 3.11, the proposed antenna is designed to couple to the 10 GHz fundamental repetition rate of the 4.1-mm long QD MLL. The designed antenna is fabricated on a semi-insulating (SI) GaAs substrate with a thickness of 450 µm. The detailed fabrication process is described in ref. [2]. The size of the rectangular patch is designed to be 5.1 mm wide and 4.45 mm long. The biasing line for the absorber is also shown in Fig. 3.11. This microstrip antenna is designed to be matched at 10 GHz. The simulation is performed using the CST Microwave Studio based on the finite integral technique [26]. As shown in Fig. 3.12, the measured return loss is well matched to the simulation result.
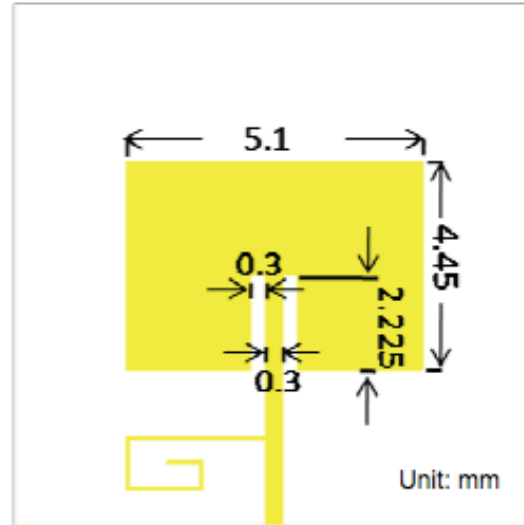
Fig. 3.11 Designed rectangular microstrip antenna with a biasing line.
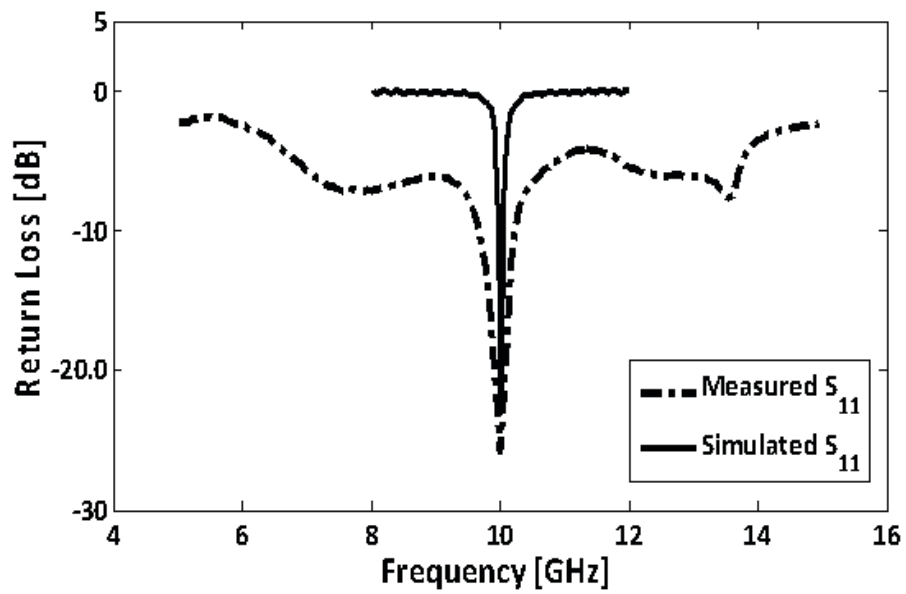
Fig. 3.12 Return loss of the designed microstrip antenna.

3.5.2 Radiation measurement of the hybrid transmitting module

To verify the function of a QDMLL as a RF signal generator, the integration with a rectangular patch antenna system was investigated. The hybrid integration of these two components results in the compact RF transmitter shown in Fig. 3.13. Fig. 3.14 depicts the radiation measurement setup, consisting of the current and voltage source for biasing the gain and absorber section, respectively, and an RF spectrum analyzer to characterize the radiation signal gathered from an X-band horn antenna. The optical generation of microwave signal from the absorber is delivered to the fabricated antenna via wire bonding and radiated out. Then, the radiation signal out of the microstrip antenna is scanned by an X-band horn antenna and measured by the RF spectrum analyzer. The RF spectrum shown in Fig. 10 experimentally validates the radiation function of this hybrid integrated transmitting module.
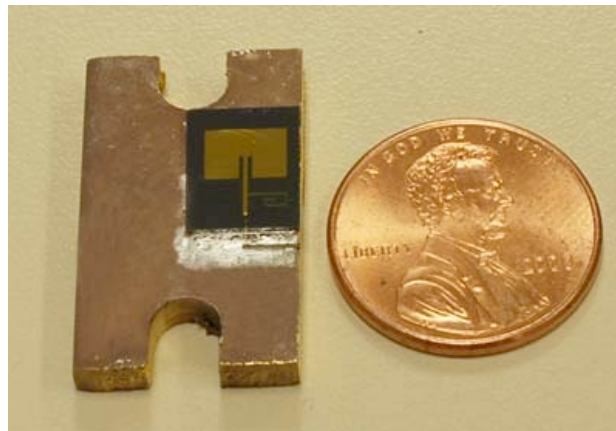
Fig. 3.13 Photo of the hybrid-integrated RF transmitting module.
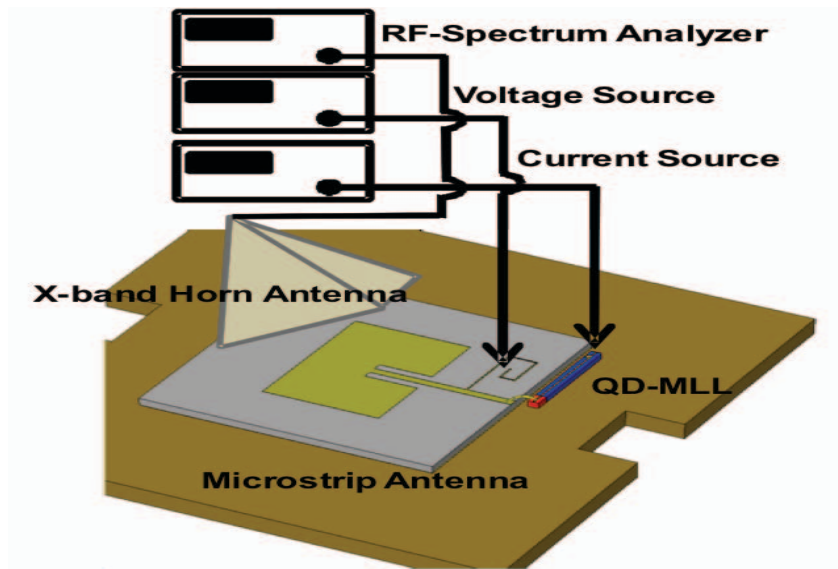
Fig. 3.14 Radiation measurement setup of the hybrid transmitting module.
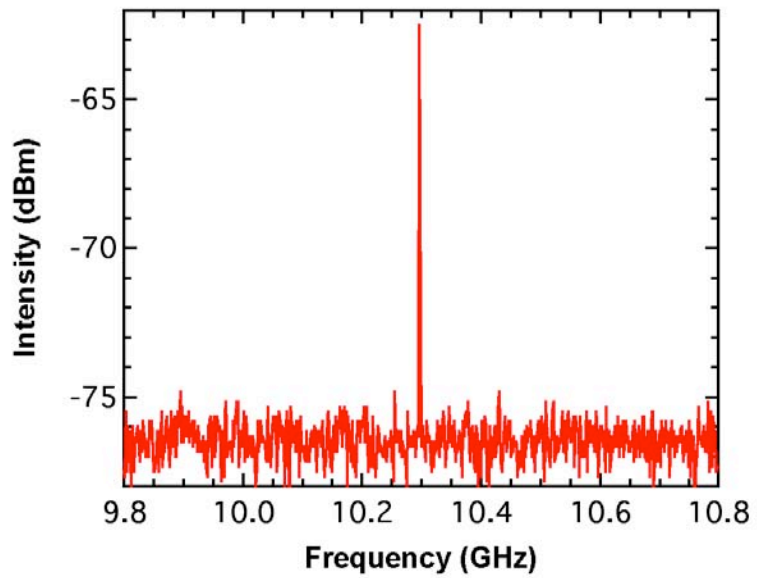
Fig. 3.15 Radiation RF spectrum of the hybrid-integrated transmitting module.

3.6 Summary and future work

Compared to the conventional optical heterodyning method, the larger conversion efficiency and easier frequency stabilization of the generated RF frequency from a monolithic passive QDMLL is presented. The optical generation of microwave signals from the passive QDMLL decreases the uncorrelated phase noise and temperature fluctuations that are undesirable effects for wireless communication applications. 33% DC to RF conversion efficiency and 86% extraction efficiency of the SA are reported. The tradeoffs in optimizing the laser injection efficiency, absorber extraction efficiency, and the power collected by the absorber were discussed. The extraction-injection efficiency product could be improved through choices of different alloy composition in the cladding layer and QD stacks in the active region. Various laser structures will be tested in the future. The QD MLL device clearly demonstrates a wider ML operating region compared to the QW MLL used for the RF signal source.

On the other hand, phase noise is also a critical issue for wireless application. The QD laser diode should have less phase noise compared to a QW system because of less spontaneous emission noise in the cavity [23]. In the next chapter, we will investigate the timing stability issue in a passive QD MLL and present the external stabilization method to further improve the noise performance of the laser device.

The idea of the hybrid integrated transmitting module can be extended for the beam steering application. Depending on the forward or reverse voltage applied to the absorber, the phase difference of the photocurrent signal can be adjusted. Some preliminary results have been shown with a QD MLL-integrated antenna array in ref. 27. The measured angle difference of the maximum radiation intensity is around 10 degrees. In the future, a

larger angle tuning can be expected with a multi-section QD MLL layout that has more flexibility to locate and change the absorber's location and lengths, respectively. With all the advantages shown above, the monolithic passive QDMLL will be a promising candidate of the compact, efficient RF signal source in wireless and satellite communication applications.

References:

1. A. J.C. Vieira, P. R. Herczfeld, A. Rosen, M. Ermold, E. E. Funk, W. D. Jemison, and K. J. Williams, "A mode-locked microchip laser optical transmitter for fiber radio," *IEEE Trans. Microw. Theory Tech.*, vol. 49, no. 10, pp. 1882–1887, (2001).

2. J. H. Kim, C. G. Christodoulu, Z. Ku, C.-Y. Lin, Y.-C. Xin, N. A. Naderi, and L. F. Lester, "Hybrid Integration of a Bowtie Slot Antenna and a Quantum Dot Mode-Locked Laser," *IEEE Antennas and Wireless Propagation Letters*, vol. 8, pp. 1337-1340 (2009).

3. D. J. Derickson, R. J. Helkey, A. Mar, J. G. Wasserbauer, and J. E. Bowers, "Microwave and millimetre-wave signal generation using modelocked semiconductor lasers with intrawaveguide saturable absorbers," *Proc. of IEEE Int. Symp. on Microwave Theory and Techniques*, vol. 2, pp. 753–756, (1992).

4. E. U. Rafailov, M. A. Cataluna, W. Sibbett, "Mode-locked quantum-dot lasers," *Nature Photonics*, vol. 1, no. 7, pp. 395-401, (2007).

5. M. G. Thompson, A. R. Rae, M. Xia, R. V. Penty, and I. H. White, "InGaAs quantum-dot mode-locked laser diodes," *IEEE J. Sel. Top. Quantum Electron.*, vol. 15, no. 3, pp. 661-672, (2009).

6. F. Grillot, C.-Y. Lin, N. A. Naderi, M. Pochet, and L. F. Lester, "Optical feedback instabilities in a monolithic InAs/GaAs quantum dot passively mode-locked laser," *Appl. Phys. Lett*., vol. 94, no. 15, p. 153503, (2009).

7. H. Su, A. L. Gray, R. Wang, T. C. Newell, K. J. Malloy, and L. F. Lester, "High external feedback resistance of laterally loss-coupled distributed feedback quantum dot semiconductor lasers," *IEEE Photon. Technol. Lett.*, vol. 15, no.11, pp. 1504-

1506, (2003).

8. D. B. Malins, A. Gomez-Iglesias, S. J. White, W. Sibbett, A. Miller, and E. U. Rafailov, "Ultrafast electroabsorption dynamics in an InAs quantum dot saturable absorber at 1.3 µm," *Appl. Phys. Lett.*, vol. 89, no. 17, p. 171111, (2006).

9. X. D. Huang, A. Stintz, H. Li, A. Rice, G. T. Liu, L. F. Lester, J. Cheng, and K. J. Malloy, "Bistable operation of a two-section 1.3-µm InAs quantum dot laser - absorption *saturation* and the quantum confined Stark effect," *IEEE J. of Quantum Electron.*, vol. 37, no. 3, pp. 414-417, Mar. 2001.

10. X. D. Huang, A. Stintz, H. Li, L. F. Lester, J. Cheng, and K. J. Malloy, "Passive mode-locking in 1.3 µm two-section InAs quantum dot lasers," *Appl. Phys. Lett.*, vol. 78, no. 19, p. 2825, May 2001.

11. Y.-C. Xin, Y. Li, V. Kovanis, A. L. Gray, L. Zhang, and L. F. Lester, "Reconfigurable quantum dot monolithic multi-section passive mode-locked lasers," *Opt. Express,* vol. 15, pp. 7623-7633 (2007).

12. Y. Li, F. L. Chiragh, Y.-C. Xin, C.-Y. Lin, J. H. Kim, C. G. Christodoulou, and L. F. Lester, "Harmonic mode-locking using the double interval technique in quantum dot lasers," *Opt. Express,* vol. 18, pp. 14637-14643 (2010).

13. B. K. Henderson and J. C. Lyke, "The Science and Technology of Responsive Space and Its Implications on Risk," *High Frontier Journal*, vol. 6, no. 3, (2010).

14. L. F. Lester, C.-Y. Lin, Y. Li, J. H. Kim, and C. G. Christodoulou, "Reconfigurable, Multi-Section Quantum Dot Mode-Locked Lasers," in *Conference on Lasers and Electro-Optics (CLEO)*, paper CMII1, (2010).

15. E. R. Brown, F. W. Smith, and K. A. McIntosh, "Coherent millimeter-wave

generation by heterodyne conversion in low-temperature-grown GaAs photoconductors," *J. Appl. Phys.*, vol. 73, no. 3, pp.1480-1484, (1993).

16. J. Genest, M. Chamberland, P. Tremblay, M. Tetu, "Microwave signals generated by optical heterodyne between injection-locked semiconductor lasers," *IEEE J. Quantum Electron.*, vol. 33, no. 6, pp. 989-998, (1997).

17. Z. F. Fan and M. Dagenais, "Optical generation of a megahertz-linewidth microwave signal using semiconductor lasers and a discriminator-aided phase-locked loop," *IEEE Trans. Microw. Theory Tech.*, vol. 45, no. 8, pp. 1296–1300, (1997).

18. M. Hyodo, M. Tani, S. Matsuura, N. Onodera, and K. Sakai, "Generation of millimeter-wave radiation using a dual-longitudinal-mode microchip laser," *Electron. Lett.*, vol. 32, no. 17, pp. 1589–1591, (1996).

19. M. Tani, O. Morikawa, S. Matsuura and M. Hangyo, "Generation of terahertz radiation by photomixing with dual- and multiple-mode lasers," *Semicond. Sci. Technol.*, vol. 20, pp. 151-163, (2005).

20. X. F. Chen, Z. Deng, and J. P. Yao, "Photonic generation of microwave signal using a dual-wavelength single-longitudinal-mode fiber ring laser," *IEEE Trans. Microw. Theory Tech.*, vol. 54, no. 2, pp. 804–809, (2006).

21. L. F. Lester, K. C. Hwang, P. Ho, J. Mazurowski, J. Ballingall, J. Sutliff, S. Gupta, J. Whitaker, and S. R. Williamson, "Ultra-Fast Long-Wavelength Photodetectors Fabricated on Low-Temperature InGaAs on GaAs," *IEEE Photon. Technol. Lett.*, vol. 5, no. 5, pp. 511-514, (1993).

22. Y.-C. Xin, Y. Li, A. Martinez, T. J. Rotter, H. Su, L. Zhang, A. L. Gray, S. Luong, K. Sun, Z. Zou, J. Zilko, P. M. Varangis, and L. F. Lester, "Optical gain and absorption

of quantum dots measured using an alternative segmented contact method," *IEEE J. Quantum Electron.*, vol. 42, no. 7, pp.   725-732, (2006).

23. L. Zhang, L.-S. Cheng, A. L. Gray, H. Huang, S. Kutty, H. Li, J. Nagyvary, F. Nabulsi, L. Olona, E. Pease, Q. Sun, C. Wiggins, J. C. Zilko, Z. Zou, and P. M. Varangis, "High-power low-jitter quantum-dot passively mode-locked lasers," *Proc. SPIE,* vol. 6115, p. 611502, (2006).

24. M. Passerini, M. Sorel and P.J.R. Laybourn, "Optimisation and regime characterisation of monolithic semiconductor mode-locked lasers and colliding-pulse mode-locked lasers at microwave and millimeter-wave frequency," *IEE Proc.-Optoelectron.*, vol. 151, no. 6, pp. 508-512, (2004).

25. D. Pozar, "An update on microstrip antenna theory and design including some novel feeding techniques," *IEEE Antennas and Propagation Society Newsletter*, vol. 28, no. 5, pp. 4-9, (1986).

26. "CST Microwave Studio" Computer Simulation Technology, Fram- ingham, MA, 2006 [Online]. Available: www.cst.com

27. J. H. Kim, C.-Y. Lin, N. Naderi, Y. Li, C. G. Christodoulou, and L. F. Lester, "Beam steering of a linearly tapered slot antenna array integrated with quantum dot mode-locked lasers," *IEEE Photonics society annual meeting*, 2010.

Chapter 4

Microwave characterization and stabilization of timing jitter in a quantum dot passively mode-locked laser via external optical feedback

4.1 Introduction

We have discussed the cavity design of a passive MLL in chapter 2 and the optical generation of microwave signal from the saturable absorber of a monolithic passive MLL in chapter 3. For the device design strategy and application fields mentioned above, the timing stability issue is a critical topic for the potential applications of monolithic passive MLLs such as the compact pulse source in optical time division multiplexing (OTDM) [1]. The operational principle of OTDM is achieved by splitting an input optical pulse train operating at a slow rate into multiple paths, each with a different delay. These delayed signals are then recombined into one output at an effectively higher data-rate. The delay between each path determines the final bit rate. Therefore, any arbitrarily high bit rate can be achieved by controlling the number of paths that the input signal is split over and the delay difference between each path. A schematic of the OTDM architecture is illustrated in Fig. 4.1. It starts with a *1:N* splitter that splits the input pulse signal into *N* channels. Each of these channels is delayed by a multiple of a path-length difference, ΔL, or equivalent to a time of $T_{NB} = 1/(NB)$ where B is the bit-rate of the input signal. The channels are then recombined into a high bit rate composite channel using an *N*:1

combiner [1]. For example, if the data source operates at 5 Gb/s and eight paths are used, the bit-rate of the photonic link will be 40 Gb/s using this OTDM technique. One limitation of this approach is that the input signal must be pulsed and the duration of the individual pulses must be significantly less than the final bit-period T_{NB}. And the pulse-to-pulse timing jitter should be small enough to prevent the ambiguity between neighboring pulses.
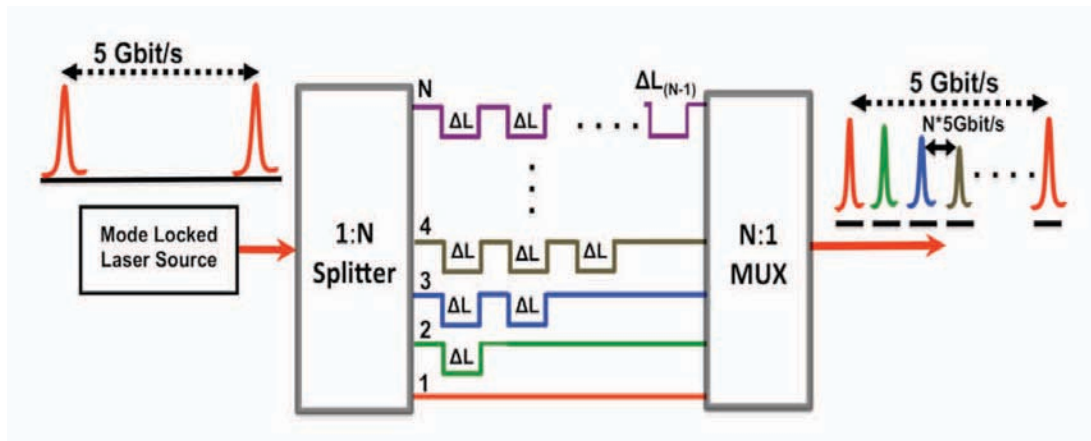
Fig. 4.1 Optical Time-Division Multiplexing scheme. The device takes in short optical pulses operating at 5Gb/s (left) and multiplexes them to 5N Gbit/s (right) by splitting the original pulses into N separate channels and then recombining them after they go through bit-rate determined delays ΔL [1].

To realize the multi-gigahertz repetition rates and low timing jitter required by these applications, different semiconductor mode-locking architectures have been introduced in chapter 1 including active, passive, and hybrid mode-locking mechanisms. Among different MLL configurations, monolithic two-section passive MLLs offer several advantages including compact size, simple fabrication, DC bias only, and the ability for hybrid integration to silicon substrates. Compared to active mode-locking, however, the

noise performance issue is the drawback of passive MLLs due to the lack of an external reference source. Since timing fluctuations in the optical pulse train play an important role in determining the laser and system performance, reducing the phase noise and stabilizing the MLL have attracted numerous theoretical and experimental studies. Several methods have been proposed to reduce the RF phase noise in active and passive MLLs with high repetition rate. Methods such as injection locking, introduction of an intracavity etalon, and intracavity active phase modulation have been implemented in harmonically/actively mode-locked semiconductor lasers [2-4]. For passive MLLs, phase noise reduction has been observed through the injection locking method or external optical feedback [5-9]. In the optical injection locking case, an external tunable laser is used as the master laser source to lock the frequency comb of the MLL. Thus, the timing jitter is reduced due to a stabilized phase-locking relationship between the cavity modes of the laser device. However, the injection technique needs an extremely precise injection power and wavelength to obtain the widest phase-locked comb with high visibility. Previously, it was found that increasing the injected power decreases the optical bandwidth, while lowering the injection power reduces the visibility of the phase-locked comb [2]. Moreover, the existence of the external tunable laser makes the whole system bulky and expensive. External optical feedback is the other option for stabilizing the timing fluctuation in a passive MLL. It owns several advantages such as simple implementation in design and a cost-effective fiber-based feedback arm [8]. Thus, it is the main stabilization technique that will be studied in this chapter. The operational principle and experimental setup will be described in detail later. In this chapter, the noise performance of a packaged passive QD MLL subjected to stably-resonant and nearly-

exact resonant external optical feedback and steady temperature control is investigated. In the stably-resonant case, an RF linewidth of 170 Hz is achieved at an operation temperature of 17°C. The nearly-exact resonant case exhibits significant linewidth rebroadening as the feedback level is increased, which agrees well with previously published theory [10].

After introducing the methods to improve the noise performance, it is also crucial that the jitter characterization in a passive MLL be studied more thoroughly. Since the timing-jitter fluctuations in a passive MLL constitute a nonstationary process, the phase noise does not scale with harmonic number. Thus, it will be shown that the commonly-used model for calculating the integrated rms jitter proposed by von der Linde [11], which assumes a stationary process only, is not suitable for a passive MLL unless the offset frequency is above the corner frequency. For the pulse-to-pulse timing jitter calculation, we present an alternative all-microwave technique based on previously published theory by Eliyahu et al. [12] and compare this different RF measurement approach to the work reported by Kefelian et al. [13].

This chapter is organized as follows. Section 2 is devoted to a brief comparison of jitter and RF linewidth performance in quantum well and QD MLLs. The external optical feedback mechanism in the passive QD MLL is also introduced. Device structure and fabrication are presented in Section 3. In Section 4, the experimental setup and results are discussed for the QD MLL. The laser stability is experimentally shown to bifurcate under the resonant feedback situations leading to either a reduction or an enhancement of the noise within the laser's cavity. Section 5 is devoted to the introduction of noise performance characterization in a passive MLL, including the integrated root mean

square (rms) timing jitter and the pulse-to-pulse rms timing jitter. Following that, we experimentally characterize the pulse-to-pulse rms timing jitter using the analytical model by Eliyahu *et al.* [15] and make comparisons with prior research. Timing jitter reduction is achieved by using a controlled external feedback arm to stabilize the QD MLL. The jitter value reduces from 295 fs/cycle to 32 fs/cycle under external optical feedback. Finally, the key findings of this phase of the dissertation research are summarized in Section 6.

4.2 RF linewidth and jitter performance in semiconductor mode-locked lasers

In the characterization of a passive MLL, the integrated rms timing jitter is generally given in terms of the integrated single-sideband phase noise (SSB-PN) spectral density measured from the transient photocurrent through an electrical spectrum analyzer (ESA) [11]. Since it is hard to find a high performance photodetector and ESA to measure the SSB-PN spectral density at a very high repetition rate (>50 GHz), the RF linewidth at the first harmonic can provide a simpler, alternative way to characterize the timing stability [13]. Furthermore, the integrated rms timing jitter above the corner frequency has been found theoretically and previously demonstrated experimentally by the dissertation author to vary with the square root of the RF linewidth [8, 13]. Fig. 4.2 shows this jitter-linewidth relation for a passive MLL in the free-running case and the inset demonstrates the integrated SSB-PN spectral density, $L(f)$, at the fourth harmonic over the offset frequency range of 30 KHz to 30 MHz [13].
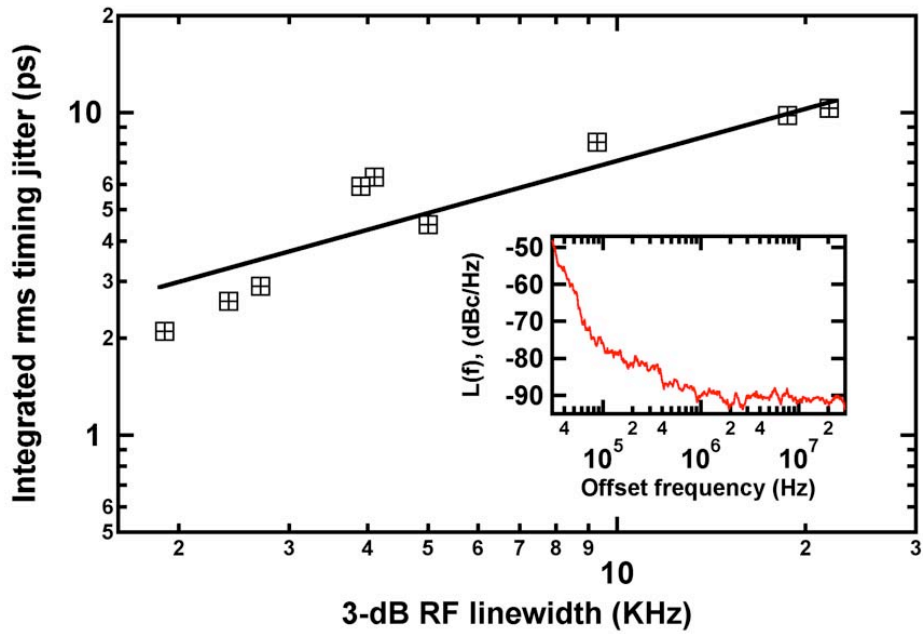
Fig. 4.2 A log-log plot of the integrated rms timing jitter as a function of the RF linewidth for a passive QD MLL in the free-running case. The slope of the solid line follows a square-root dependence. Inset: SSB-PN spectral density, $L(f)$, at the fourth harmonic over the offset frequency range of 30 KHz to 30 MHz [13].

In a passive MLL, a pulse circulates in the optical cavity with a dynamic broadening in the gain section and a pulse trimming effect in the saturable absorber (SA). As noted by Yvind et al. [14], the minimization of pulse reshaping is the key to improve the noise behavior and, consequently, the RF linewidth in these lasers. To date, low noise performance from a monolithic passive QW MLL has been achieved through special design and optimization of the active structure. In these laser devices, the optical confinement factor that refers to the overlap of the optical field with the active material is designed to be low, allowing improved timing stability and noise performance. With a low optical confinement factor, the device demonstrates a small coupled amplified

spontaneous emission noise in the laser cavity that results in a narrow RF linewidth performance. For instance, a 3-dB RF linewidth of 30 kHz has been achieved in a single InGaAsP quantum well MLL device that owns a small optical confinement factor of 1% [15]. Recently, the passive QD MLL device has demonstrated a superior noise performance with an RF linewidth of 500 Hz from the University of Cambridge group [16]. From the aspect of material property, the QD structure owns a high gain saturation energy that indicates a low pulse broadening effect in the gain section. In addition, QD materials also show low internal loss [17], reduced threshold current density, lower associated spontaneous emission [18], and low linewidth enhancement factor [19]. All these unique properties in the QD lead to improved noise performance and a demonstrated narrower RF linewidth compared to QW MLLs.

For further improvement, external optical feedback can be implemented to lower the phase noise in the laser device. For instance it has been theoretically shown that even small external reflections have to be considered in determining the mode-locking dynamics [10]. On one hand, under the non-resonant case, which is reached when the optical lengths of the cavities are arbitrary, the operation of the laser gets unstable beyond a certain level of optical feedback with at least two pulses competing with each other [10]. Such severe instabilities lead to a sharp increase of the noise as pointed out in [20]. On the other hand, under the resonant case, which is obtained when the optical length of the external cavity is about a multiple of that of the solitary laser, an RF linewidth reduction can be expected over a wide bias current and external reflectance range as compared to the non-resonant situation [10].

4.3 Device structure and fabrication

The QD structure investigated in this chapter was grown by elemental source molecular beam epitaxy on an n^+-doped (100) GaAs substrate (wafer #: ZLG414). The active region consists of six "Dots-in-a-Well" (DWELL) layers. In each layer, an equivalent coverage of 2.4 monolayer InAs QDs is confined approximately in the middle of a 10 nm $In_{0.15}Ga_{0.85}As$ QW [17]. The epitaxial structure and waveguide design are described in Fig. 4.3. The 3-µm-wide ridge-waveguide devices were processed under the similar steps described in section 3 of chapter 2. The two-section passive QD MLLs were made with a total cavity length of 7.8-mm and a saturable absorber (SA) length of 1.1-mm. The nominal repetition rate of the QD MLL is 5.11 GHz. A highly reflective coating ($R \approx 95\%$) was applied to the mirror facet next to the SA to create self-colliding pulse effects in the SA for pulse narrowing, and the output facet was cleaved ($R \approx 32\%$). The devices were p-side-up mounted on AlN heatsink carriers. These chip-on-carriers were then packaged with a polarization-maintaining lensed fiber pigtail as shown in Fig. 4.4 (ZLG414C-D-1.1, #0003). The function of the packaged module is to reduce environmental noise and enhance mechanical stability. The fiber-coupled light-current (L-I) curve under -1 V reverse voltage bias condition at $20^{\circ}C$ is displayed in Fig. 4.5. The abrupt jump in optical power just above the threshold current is due to the nonlinear behavior of the SA. The inset is the optical spectrum showing the peak lasing wavelength at 1.33-µm under a gain current of 280-mA and an SA reverse voltage of -1 V. The typical average powers emitted by these devices under mode-locking conditions at the end of the fiber pigtail are 1.5-2.5 mW. The pulse durations are on the order of 10 ps.

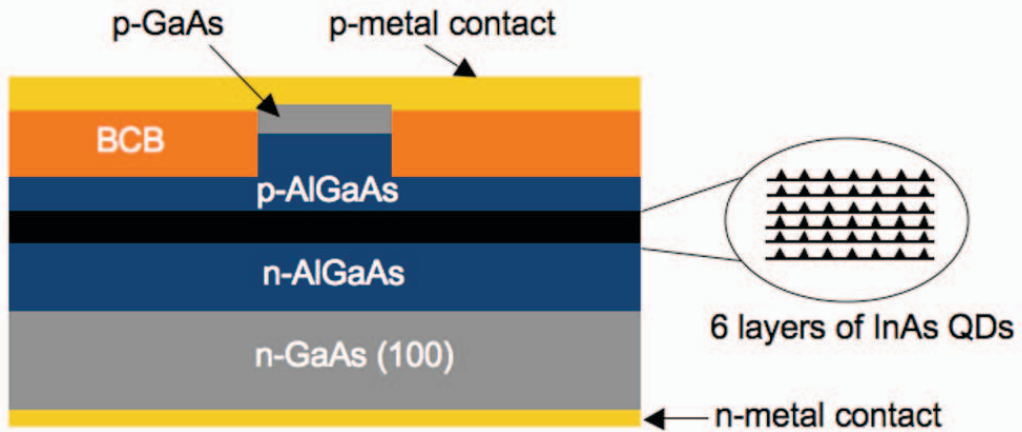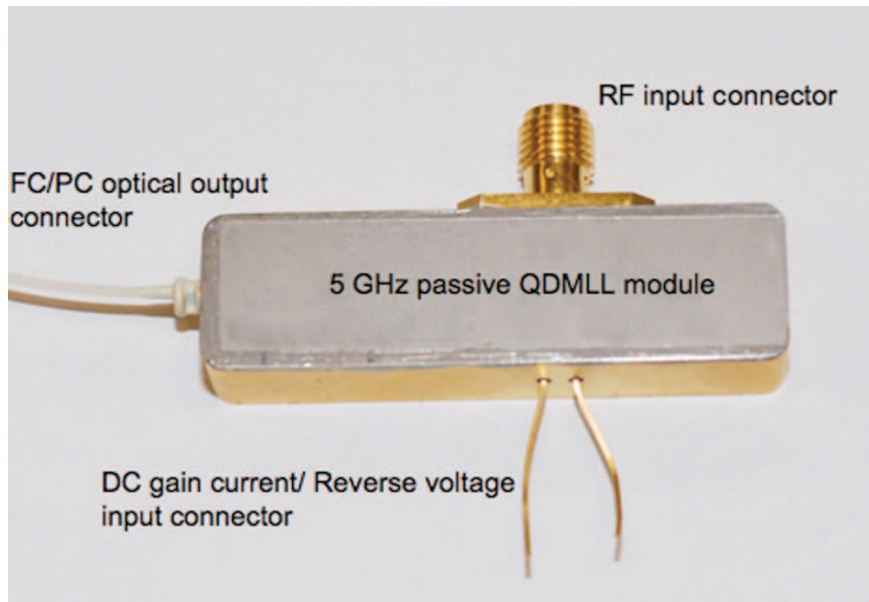Fig. 4.3 Schematic of the epitaxial layer structure of the InAs QD laser.

Fig. 4.4 Picture of the passive QD MLL packaged module. The RF connector shown on

the top of the package was not used for this experiment (ZLG414C-D-1.1).
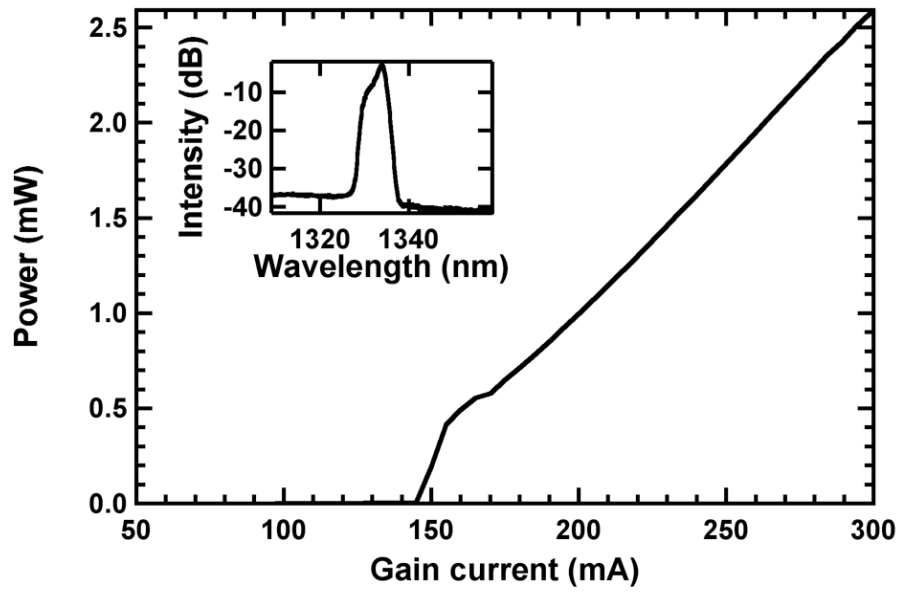
Fig. 4.5 L-I characteristic measured at 20^oC for an absorber bias of -1 V. The inset shows

the optical spectrum under 280-mA gain current and -1 V reverse voltage.

4.4 Optical Feedback experimental setup and results

4.4.1 Experimental setup

The passive QD MLL module with thermoelectric cooler (TEC) was investigated under external optical feedback using the experimental setup shown in Fig. 4.6. The emitted light that is coupled from the laser chip through a lensed fiber pigtail is injected into port 1 of a 50/50 optical fiber coupler. The optical feedback is created from a high-reflectivity (R> 95%) coating applied to the fiber at the end of port 2. The feedback power level is controlled via a variable attenuator and its value is measured by the power meter in port 4. The optical delay line (General Photonics VDL-001) that has a step-controlled fine delay stage (resolution: 0.1-mm) is introduced to change the external fiber loop length. In order to maximize the feedback effect, a polarization controller is used to make the feedback beam polarization identical to that of the emitted wave.   The effect of the optical feedback is analyzed in port 3 through a 45 GHz bandwidth photodiode coupled to an ESA. An optical isolator is used to prevent any unwanted reflection from the ESA. The quantity of injected feedback into the laser is defined as the ratio $\Gamma = P_1/P_0$ where P_1 is the power returned to the facet and P_0 the emitted one. The amount of reflected light that effectively returns into the laser can then be expressed as follows:

$$\Gamma(\text{dB}) = P_r(\text{dBm}) - P_0(\text{dBm}) + C_{dB} \tag{4.1}$$

where P_r is the optical power measured at port 4, C_{dB} is the optical coupling loss of the device to the fiber which was estimated to be about -5dB and kept constant during the whole experiment. The feedback experiment is studied under the long external cavity condition that assumes that $f_r\tau \gg 1$, where f_r is the relaxation oscillation frequency of the

free-running laser (a few GHz) and τ is the external round trip time of several hundred nanoseconds.

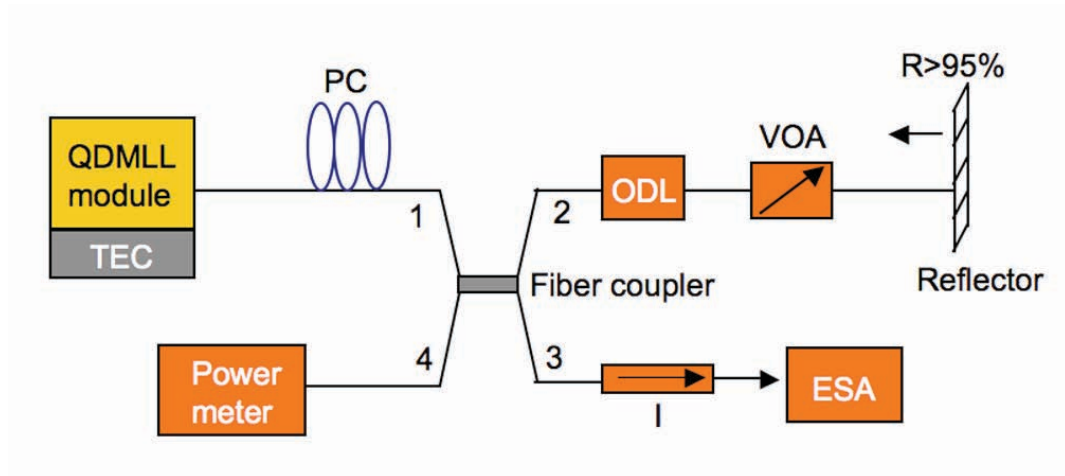Fig. 4.6 Schematic drawing of the experimental setup. PC: polarization controller; ODL: optical delay line; VOA: variable otpical attenuator; I: isolator; ESA: electrical spectrum analyzer.

4.4.2 Discussion of stably-resonant and nearly-exact resonant cases

All measurements were operated with a controlled TEC to adjust and maintain the substrate temperature. As shown in Fig. 4.7, the variation in the RF linewidth was first analyzed over a broad range of optical delays in the feedback loop and a temperature of 20°C. The experimental results demonstrate a similar trend to those observed in QW MLLs under optical external feedback [21]. The noise enhancement as seen in the RF linewidth has been predicted by Avrutin in a two-section monolithic MLL [Fig. 9 of ref. 10] and is indentified as the nearly-exact resonant feedback case. The periodicity can be viewed approximately as 1.5-mm (delay time: ~200 ps), which corresponds to the mode-locking frequency of ~5 GHz.

In terms of the optical delay, the stably-resonant and nearly-exact resonant cases are both in the same general vicinity where the ratio of the optical length of the external cavity to the optical length of the solitary laser, L_{ext}/L, is about an integer. The technologically important regime where the RF linewidth is substantially reduced is called the stably-resonant condition. For this case, we have extended our previous study [8] by including a controlled, adjustable temperature and a packaged module that lessens environmental noise and increases mechanical stability. Fig. 4.8 shows the evolution of the RF spectrum over temperature for the stably-resonant feedback case (optical delay set at 2.7 mm) under 280-mA DC bias on the gain section and -1 V applied to the absorber. The RF linewidth of this laser module is 8 kHz in the free-running case at 20°C. By fixing the fiber loop length through the optical delay line to the resonant case and tuning the TEC to lower temperature, the 3-dB RF linewidth is improved from 3.5 kHz at 35°C down to 170 Hz at 17°C under feedback. The measurement is limited to 17°C because of

the temperature-induced misalignment between the device and lensed fiber inside the sealed package. The small RF linewidth can be explained by the relatively low threshold of a QD laser and the correspondingly lower amount of spontaneous emission noise coupled into the laser's optical modes. This noise also decreases with temperature and thereby lowers the phase noise and so the RF linewidth. The data for the minimum RF linewidth of 170 Hz, which is realized at a feedback level as low as -42 dB, is shown in Fig. 4.8. Lorentzian curve-fitting of the ESA data using a frequency span of 100 kHz and a resolution bandwidth of 100 Hz is used to calculate the value.
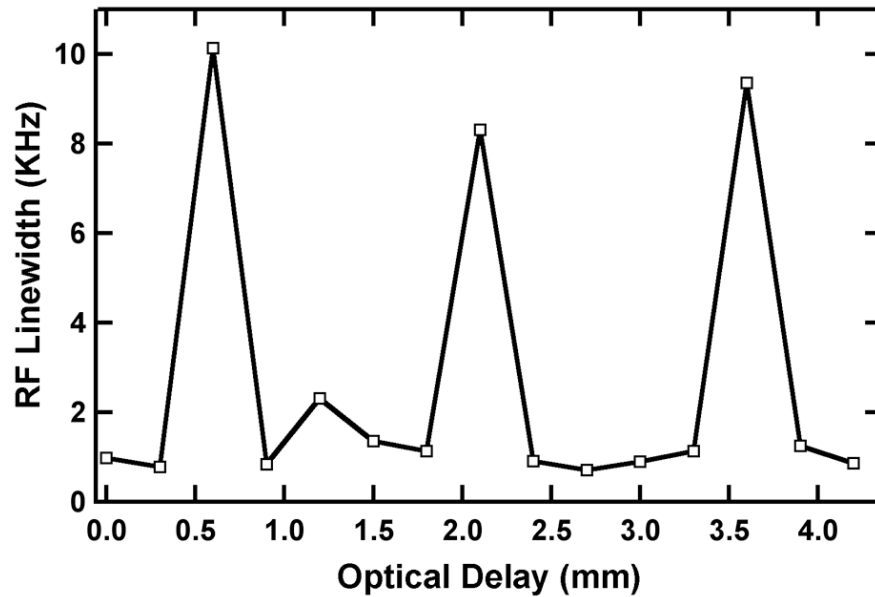
Fig. 4.7 RF linewidth variation under feedback ratio of -44 dB as a function of optical delay line change at 20°C, showing a periodicity of roughly 1.5 mm corresponding to the laser round trip time of 200 ps. Bias condition of QD MLL: 280 mA gain current and -1 V reverse voltage.
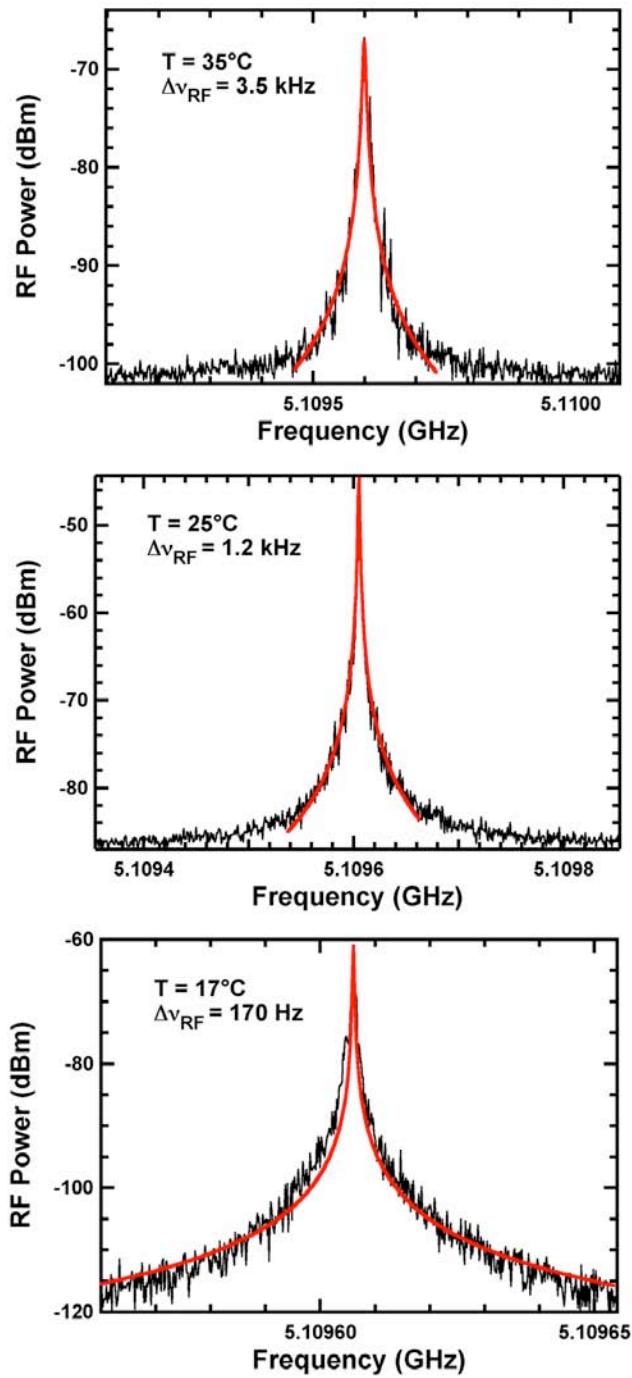
Fig. 4.8 Evolution of the RF linewidth for three different temperatures under the stably-resonant feedback condition. Bias condition: 280 mA gain current and -1 V reverse voltage.

For the nearly-exact resonant feedback condition, for which the optical delay is 0.6-mm, 2.1-mm or 3.6-mm, an increase in RF linewidth is observed as shown in Fig. 4.7. It is stressed that since the step-size of the optical delay line is 0.1-mm, the experimental resolution on the peak location has to be considered. Although this means the delay step is in increments of 13 ps, the nearly-exact resonant condition has been identified clearly by the abrupt step in the center frequency shift as described in [8, 21]. In order to verify previously published simulations [10], the variation in the RF linewidth versus the optical feedback ratio is found for the optical delay fixed to 3.6-mm. The same bias conditions as described above are used, and the results are depicted in Fig. 4.9 at a temperature of 20$^\text{o}$C. At a small to moderate feedback strength (Γ < -38 dB), the MLL behaves stably and shows a relatively low RF linewidth compared to the free-running case. As the feedback ratio is increased beyond -38 dB, the RF linewidth becomes much broader than the free-running case. This behavior matches the simulation result [Fig. 10 of ref. 10] that demonstrates an increase in phase noise with a small external reflectance on the order of 10^{-4} (Γ = -40 dB). We also observe the same trend at different QD MLL bias conditions for this nearly-exact resonant case. The maximum feedback ratio strength was limited to -30 dB in this experiment. This rebroadening phenomenon could be a precursor to the coherence collapse regime [22]. The coherence collapse regime remains independent of the external cavity length and the feedback phase provided that the long external cavity situation is valid ($f_r\tau$ >> 1). Numerous papers describe the coherence collapse regime as coexisting chaotic attractors [23] whereas others explain it as an important source of noise [24, 25]. Also it is stressed that the onset of the coherence collapse is strongly linked to the linewidth enhancement factor (LEF) [26, 27], and the influence of such a

parameter on the QD MLL laser dynamics is under investigation. For instance, it has been numerically shown that the LEF is a decisive parameter under the resonant case [10]. Thus, a low LEF should produce a broader stably-resonant operation and should also increase the critical external reflectance related to the occurrence of the coherence collapse regime. The low LEF encountered in long-cavity QD lasers could explain the relative wide region with respect to the feedback strength of stable resonant operation that is observed in the QD MLL presented here.
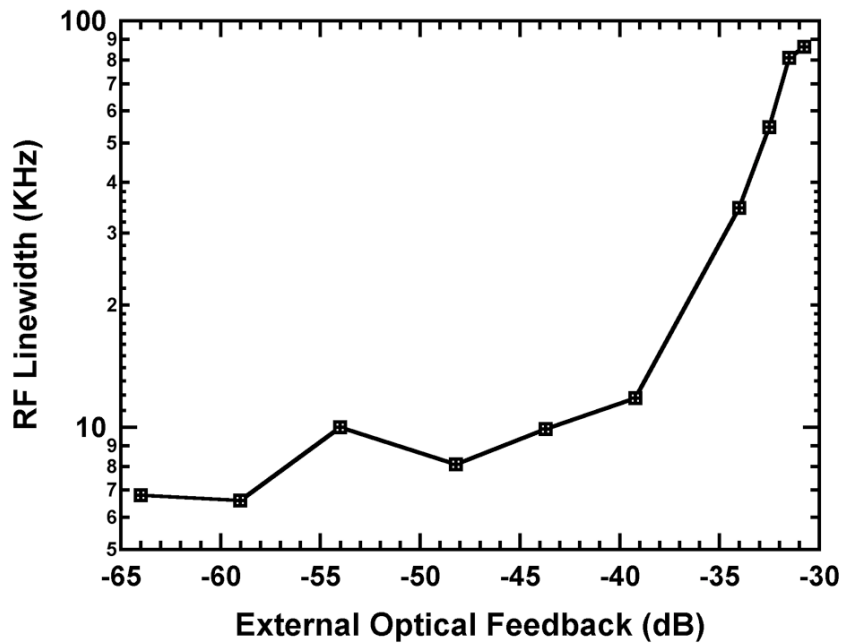

Fig. 4.9 RF linewidth as a function of the external feedback ratio at a bias of 280 mA gain current and -1 V on the absorber at 20°C under nearly-exact resonant case.

4.5 Pulse-to-Pulse rms timing jitter characterization in a passive quantum dot mode-locked laser

Because of the intrinsic phase noise properties of a passive MLL (nonstationary process) [12, 28], it is more straightforward to investigate the noise performance based on the pulse-to-pulse timing fluctuations. In this section, we will discuss the noise performance characterization in a passive MLL, including the integrated rms timing jitter and the pulse-to-pulse rms timing jitter, σ_{pp}. Following that, we experimentally characterize σ_{pp} using the analytical model by Eliyahu *et al.* [12] and make comparisons with prior research. Timing jitter reduction is also achieved by using a controlled external feedback arm that has been described in previous section to stabilize the QD MLL.

4.5.1 Device optical characterization

The laser epitaxial structure of the MLL device is a multi-stack "Dots-in-a-WELL" structure that is composed of an optimized six-stack InAs QD active region on a <100>-oriented GaAs substrate that is similar to the one in previous section. After the same processing steps described in chapter 2, these chip-on-carriers were then packaged into an industry-standard 14-pin butterfly package integrated with a thermoelectric cooler and a polarization-maintaining lensed fiber pigtail as shown in Fig. 4.10 (ZLG414G-AH-6). The function of the butterfly-packaged module is to reduce environmental noise and enhance mechanical stability. Fig. 4.11 shows the fiber-coupled L-I curve under various reverse voltage bias conditions at 20°C. The inset is the optical spectrum showing the peak lasing wavelength at 1313 nm under a gain current of 100 mA and an SA reverse voltage of -7 V. The typical average powers emitted by these devices under mode-locking

conditions at the end of the fiber pigtail are 1-2.5 mW. The pulse durations shown in Fig. 4.12 are typically about 10 ps and were measured by a Tektronix DSA 8200 oscilloscope with a 140 GHz optical sampling head. Fig. 4.13(a) demonstrates the full-span RF spectrum with 9 detected harmonics under a 90 mA DC bias on the gain section and -7 V applied to the absorber. The optimum 3-dB RF linewidth of the free-running laser at the fundamental harmonic shown in Fig. 4.13(b) is 46.2 kHz at the same bias condition. The RF linewidth is confirmed with a Lorentzian curve fit on the electrical spectrum analyzer output with a resolution bandwidth of 1 kHz.
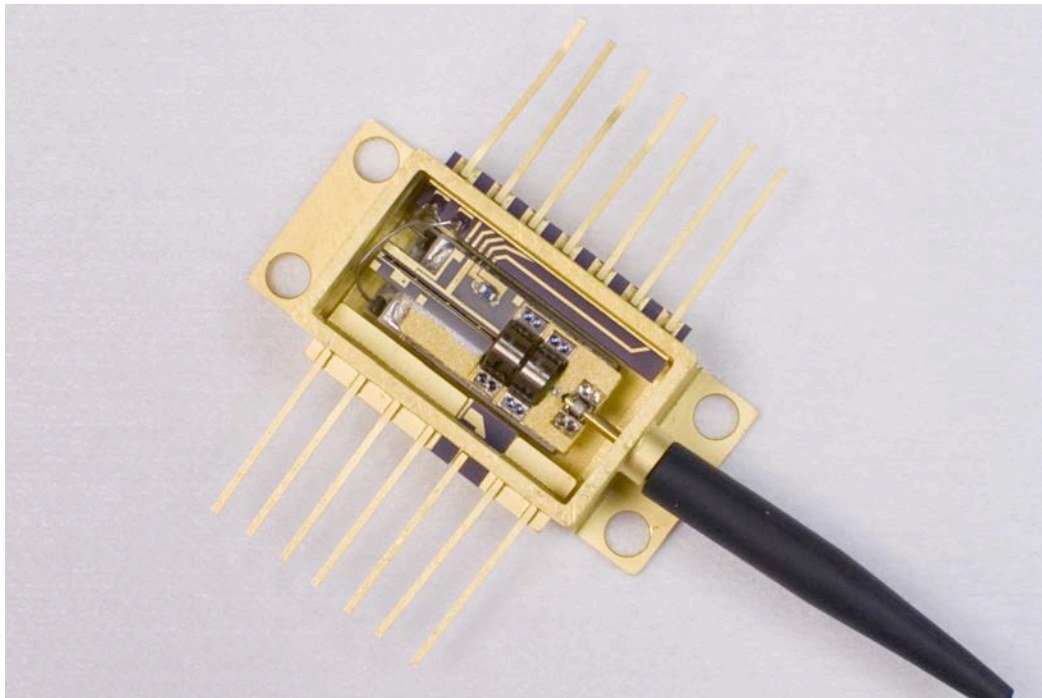
Fig. 4.10 Picture of the passive QD MLL butterfly-packaged module (ZLG414G-AH-6).
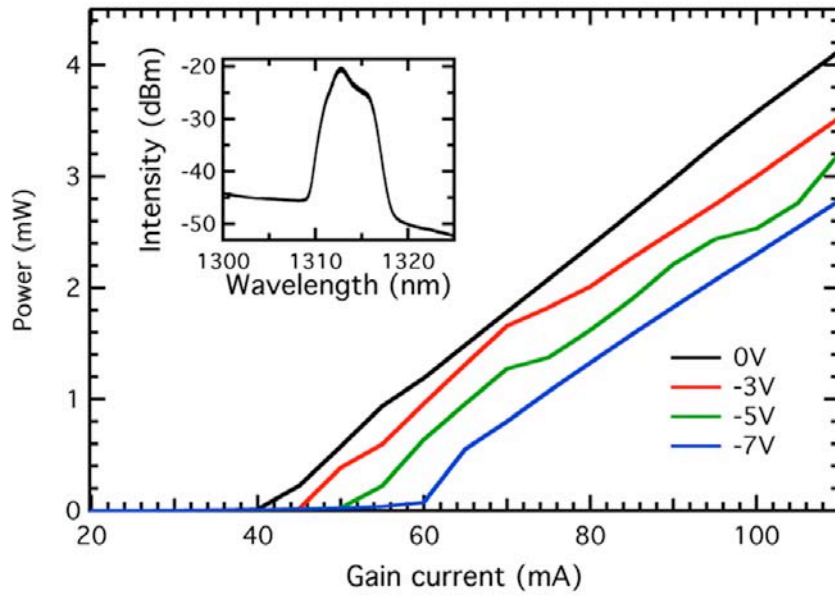
Fig. 4.11 Light current characteristics measured at 20^0C under various absorber bias voltages. The figure in the inset shows the optical spectrum under 280-mA gain current and -1 V reverse voltage.
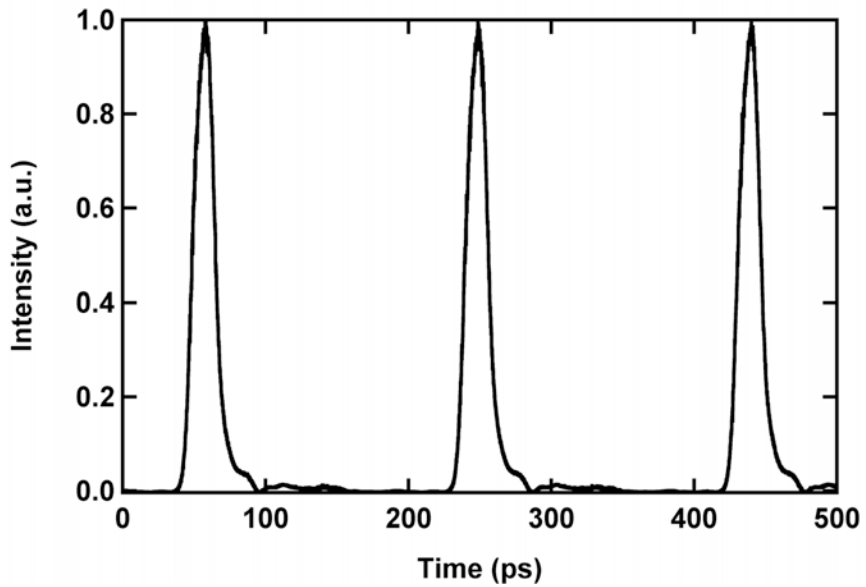
Fig. 4.12 Pulsewidth of 10.9-ps under 75-mA gain current and -7 V reverse voltage through high speed sampling oscilloscope measurement.
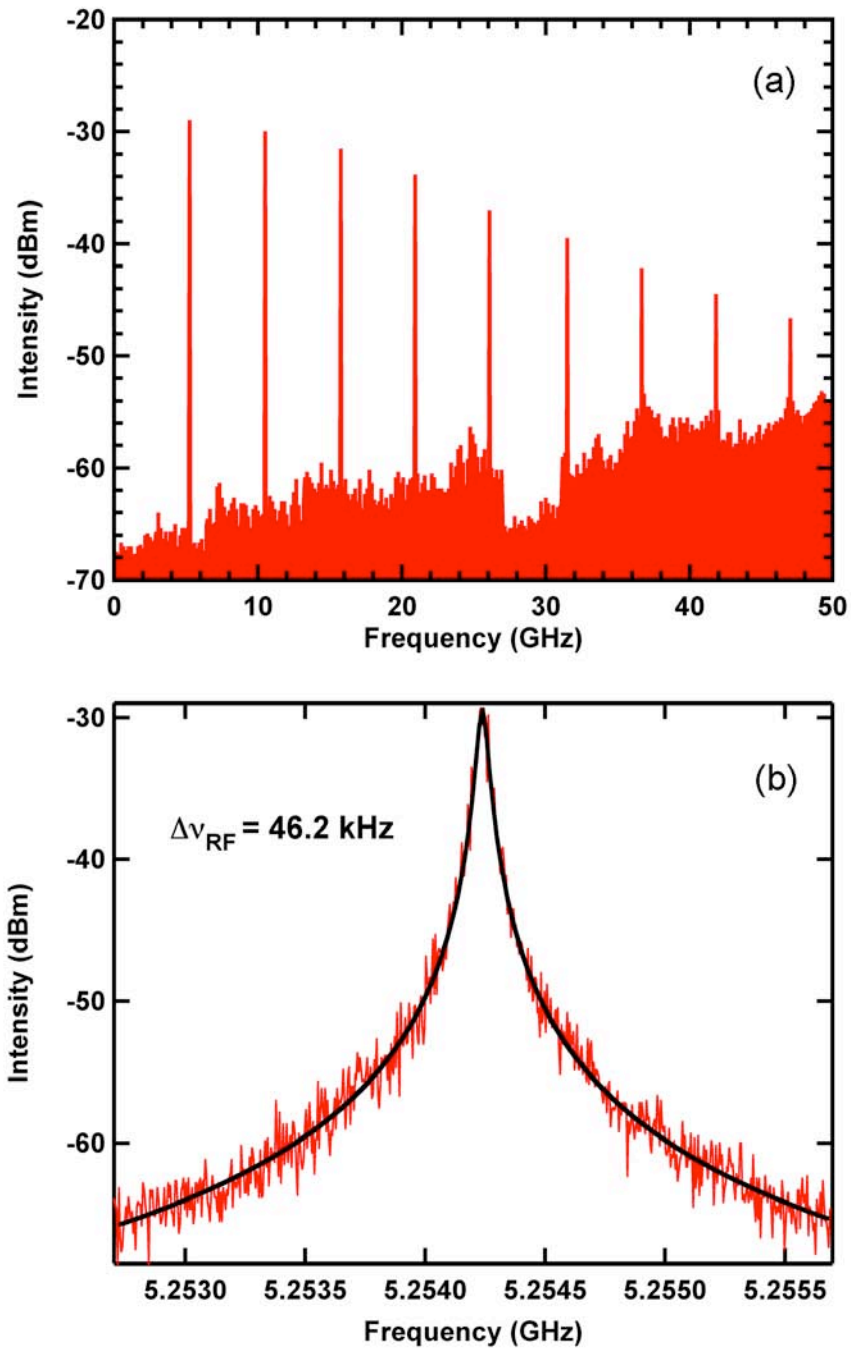
Fig. 4.13 RF spectrum under 100 mA gain current and -7 V reverse voltage. (a) the full-span condition. (b) 3-dB RF linewidth of 46.2 kHz.

4.5.2 Noise performance characterization

Conventionally, the noise characterization of an MLL by von der Linde's method uses timing jitter as the figure-of-merit [11]. In particular, the rms timing jitter is calculated by integrating the single-sideband phase noise spectral density, $L(f)$, from an ESA using the following expression.

$$\sigma = \frac{1}{2\pi n f_R} \sqrt{2 \int_{f_{\min}}^{f_{\max}} L(f) df} \qquad (4.2)$$

where n is the number of the harmonic at which the phase noise is measured, f_R is the repetition frequency, and $f_{\min}$ and $f_{\max}$ determine the offset frequency range over which the $L(f)$ is integrated. Fig. 4.14(a) displays the SSB-PN spectral density for different harmonics of the 5.25 GHz passive QD MLL device in the free-running case. The relatively low repetition rate of this monolithic passive MLL makes the characterization of a relatively large number of harmonics possible in a standard 50 GHz ESA.

However, although this technique is suitable for noise characterization in an active MLL that naturally has an external reference source, it should be applied carefully to a passive MLL. Since the timing-jitter fluctuation in a passively mode-locked laser is a nonstationary process, the phase noise does not scale with harmonic number until beyond the corner frequency as clearly seen in Fig. 4.14(b). Consequently, it is only appropriate to use von der Linde's method for offset frequencies above the corner frequency where the phase noise trace shows the typical roll-off with a slope of −20 dBc/Hz per decade. From the phase noise data in Fig. 4.14(b), we see that a meaningful lower bound to the integration range would be about 1-2 MHz for this particular device.
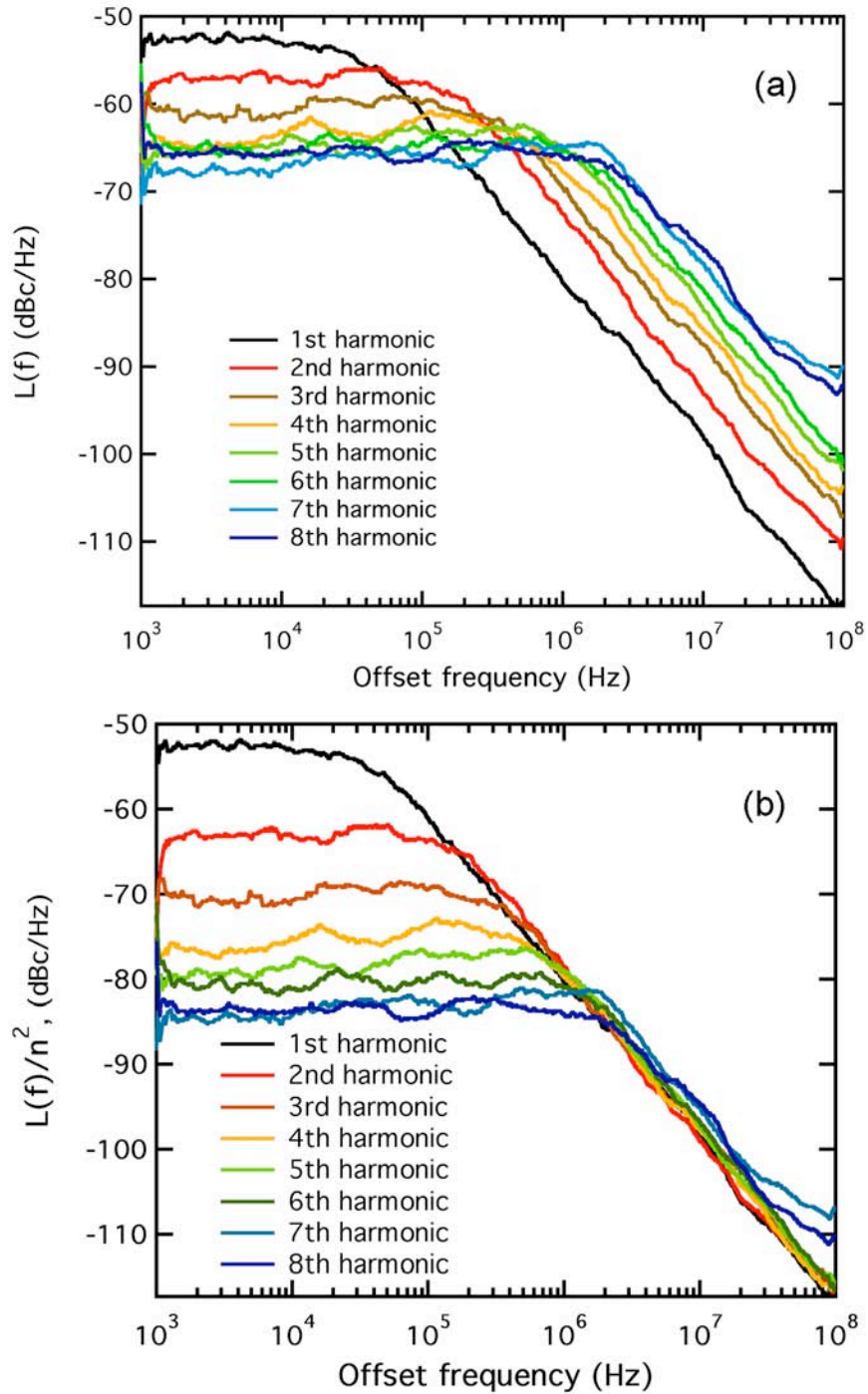
Fig. 4.14 (a) SSB-PN spectral density for different harmonics under 100 mA gain current and − 7 V reverse voltage in the free-running case. (b) SSB-PN spectra density normalized to n^2

Past research has quoted the integrated rms timing jitter over a variety of different frequency ranges, which can be confusing for comparing devices [29, 30]. For example, in ref. [29], the offset frequency range used to characterize the jitter performance is from 16 to 320 MHz while the offset frequency is 1 to 20 MHz in ref. [30]. Thus, it is more straightforward to investigate the noise performance based on the pulse-to-pulse timing fluctuations since the integration range does not have to be specified. The relevant theory for determining the pulse-to-pulse jitter is described next.

Due to the absence of a restoring external force, the timing of each pulse in a passive MLL depends on that of the previous one, and its fluctuation results from the sum of many assumed independent processes. Thus, the timing-jitter noise can be described by diffusion theory for Gaussian processes whenever fluctuations of timing jitter between successive neighboring pulses are uncorrelated. An analytical model has been derived by Eliyahu *et al*. [12], and the power spectrum in a passive MLL is expressed as the following equation:

$$P_I(\omega) = |F(\omega)|^2 \frac{\sinh(\omega^2 DT/2)}{\cosh(\omega^2 DT/2) - \cos(\omega T)} \tag{4.3}$$

where $F(w)$ is the amplitude term of the pulse, w is the frequency, T is the pulse repetition period, and D is the diffusion constant which can be described as:

$$D = \left\langle (\delta T_n - \delta T_{n\pm1})^2 \right\rangle / T \tag{4.4}$$

Equation (4.4) represents the timing-jitter fluctuations between successive neighboring pulses and can be rearranged to find the pulse-to-pulse rms timing jitter, σ_{pp}:

$$\sigma_{pp} = \sqrt{DT} \tag{4.5}$$

The analytical model above provides an appropriate method to characterize the noise performance in a passive MLL that obeys a nonstationary process. Thanks to the relatively low repetition rate of our QD MLL device, there are more harmonics available experimentally to examine this analytical model and to extract the average D and σ_{pp} values through curve fitting [31]. Table 4.1 lists the fitting results that were extracted from the experimental data shown in Fig. 4.14(a). The experimental results are in good agreement with the analytical model. In the free-running case, an average D of $4.59*10^{-16}$ (sec) and an average σ_{pp} of 295 (fs/cycle) were obtained with the pulse period T equal to 190 ps.

Following the same assumption of the noise properties in a semiconductor passive MLL [28], another analytical derivation presented by Kefelian *et al.* [13] explores the RF linewidth of the first harmonic of the photocurrent to characterize the timing stability of a passive MLL. In this approach, the pulse-to-pulse rms timing jitter can be described as follows:

$$\sigma_{pp\_K} = T\sqrt{\frac{\Delta\nu_{RF}NT}{2\pi}} \qquad (4.6)$$

where $\Delta\nu_{RF}$ is the 3-dB RF linewidth and N is the number of periods between the two compared pulses. According to (4.6), using the optimum 3-dB RF linewidth of the free-running QD MLL at the fundamental harmonic, 46.2 kHz, corresponds to a pulse-to-pulse rms timing jitter of 225 fs/cycle. This model provides a way to characterize the noise performance in a passive MLL, especially for those devices with a high repetition rate, where it is difficult to measure the SSB-PN spectral density at higher-order harmonics as mentioned in section 4.2. From our experimental pulse-to-pulse timing jitter

calculations, the analytical models of Eliyahu and Kefelian agree with each other reasonably well.

Table 4.1 Timing jitter characterization in the free-running case

Harmonic #	D (sec)	σ_{pp} (fs/cycle)
1	$4.01 \ 10^{-16}$	276
2	$4.01 \ 10^{-16}$	276
3	$4.50 \ 10^{-16}$	292
4	$4.98 \ 10^{-16}$	307
5	$5.14 \ 10^{-16}$	312
6	$4.87 \ 10^{-16}$	304
7	$4.56 \ 10^{-16}$	294
8	$4.67 \ 10^{-16}$	298

4.5.3 Optical feedback stabilization

For further noise performance improvement, external optical feedback can be implemented to lower the phase noise in a passive MLL. This method provides a simple, compact, and cost-effective fiber-based loop compared to the injection locking technique which needs an external CW tunable laser. Under the stably-resonant feedback case, which is obtained when the optical length of the external cavity is about a multiple of that of the solitary laser, an RF linewidth and timing jitter reduction can be expected.

The passive QD MLL butterfly package with TEC was investigated under external optical feedback using the experimental setup described in section 4.4. The total fiber length of the feedback arm is approximately 18 meters. Fig. 4.15 shows a photograph of the experimental setup including an external enclosure that helps to reduce the environmental noise during the measurement. All measurements were operated with the TEC at 20°C. Under the optimum feedback condition (Γ = -33 dB), the RF linewidth was reduced from 46 kHz to 1.1 kHz as shown in Fig. 4.16, while simultaneously introducing a comb of adjacent modes separated by 5.7 MHz as shown in the inset. Most importantly, as seen from Eq. (4.6), the reduction of RF linewidth decreases the pulse-to-pulse rms timing jitter. Thus, the 42-fold RF linewidth reduction under optical feedback should decrease σ_{pp} by a factor of ~ 6.5. Using Eq. (4.6), the RF linewidth under the optimum feedback case, 1.1 kHz, corresponds to a pulse-to-pulse timing jitter of 35 (fs/cyle). This result can be compared to the Eliyahu model calculations using the same approach as for the free-running analysis.
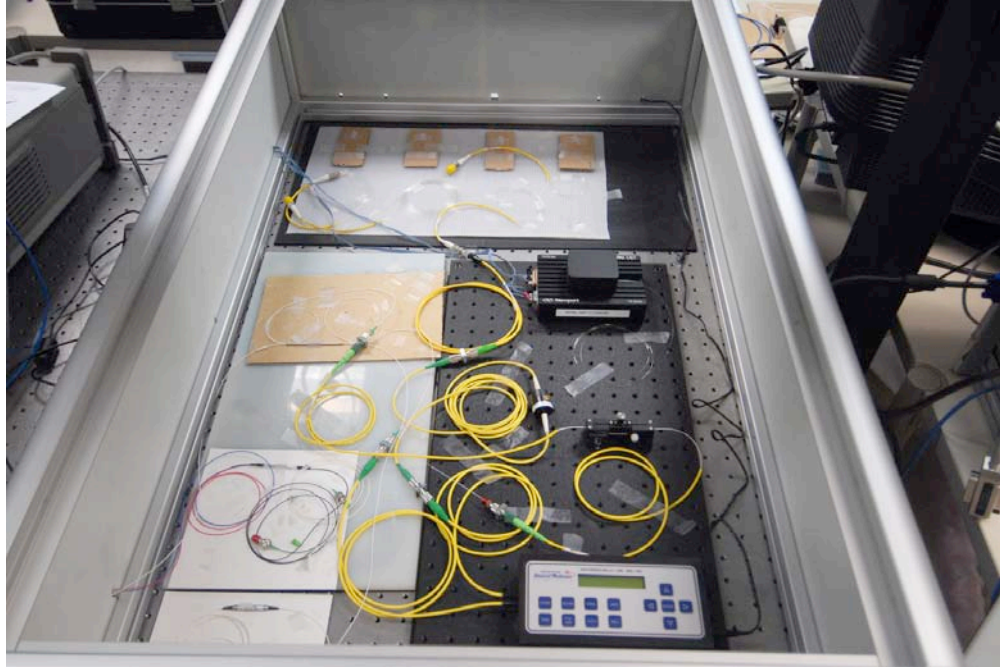
Fig. 4.15 Photograph of feedback experiment setup within a vibration- and RF-isolated enclosure.
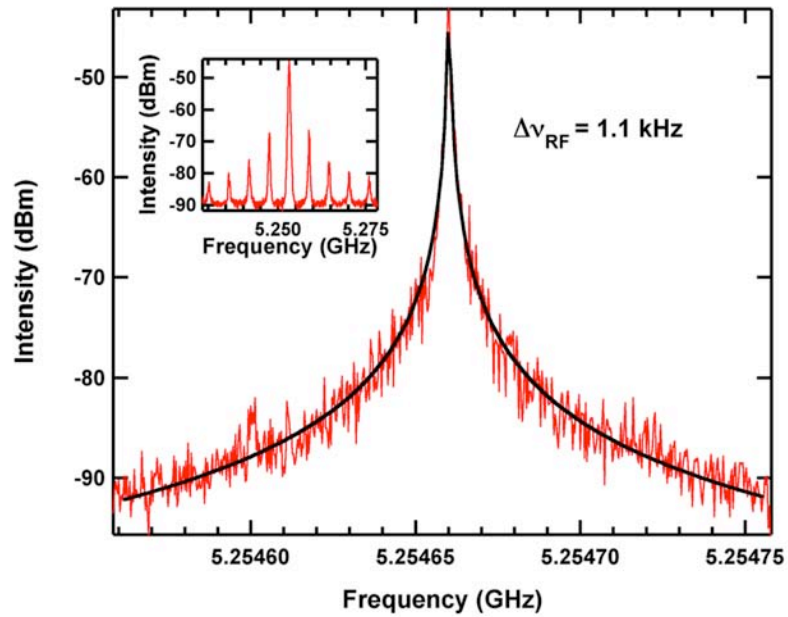

Fig. 4.16 RF linewidth of 1.1 kHz under optimum feedback condition (Γ=-33dB). Inset: RF spectrum with mode-comb separated by 5.7 MHz.

After the RF linewidth characterization, the SSB-PN spectral density at different harmonics was measured under the external feedback effect as shown in Fig. 4.17. Due to the limited dynamic range of the phase noise measurement under feedback, the SSB-PN spectrum at the 5th harmonic is the maximum number that can be evaluated in this measurement. With the same approach used in the free-running case, we can extract the values of the diffusion constant, D, and the pulse-to-pulse timing jitter, σ_{pp}, at different harmonics under optical feedback. Table 4.2 lists the fitting results that were found from the experimental data shown in Fig. 4.17. In the external optical feedback case, an average D of $5.53*10^{-18}$ (sec) and an average σ_{pp} of 32 (fs/cycle) are obtained. Again, this jitter value agrees well with the one derived from Eq. (4.6).

Conventionally, the rms pulse-to-pulse timing jitter can be measured directly by optical cross-correlation using the second harmonic generation in a nonlinear crystal. However, this measurement needs a particular nonlinear crystal, precise mountings, stable optical alignment, accurate temperature control, and long mechanical scanning. Furthermore, when the timing fluctuation is much smaller than the autocorrelation width, the measurement error becomes very large [32, 33]. Compared to the optical cross-correlation method, the all-microwave technique based on Eliyahu's theory provides a simpler way to characterize the average pulse-to-pulse timing jitter thanks to the family of phase noise spectra at different harmonics.
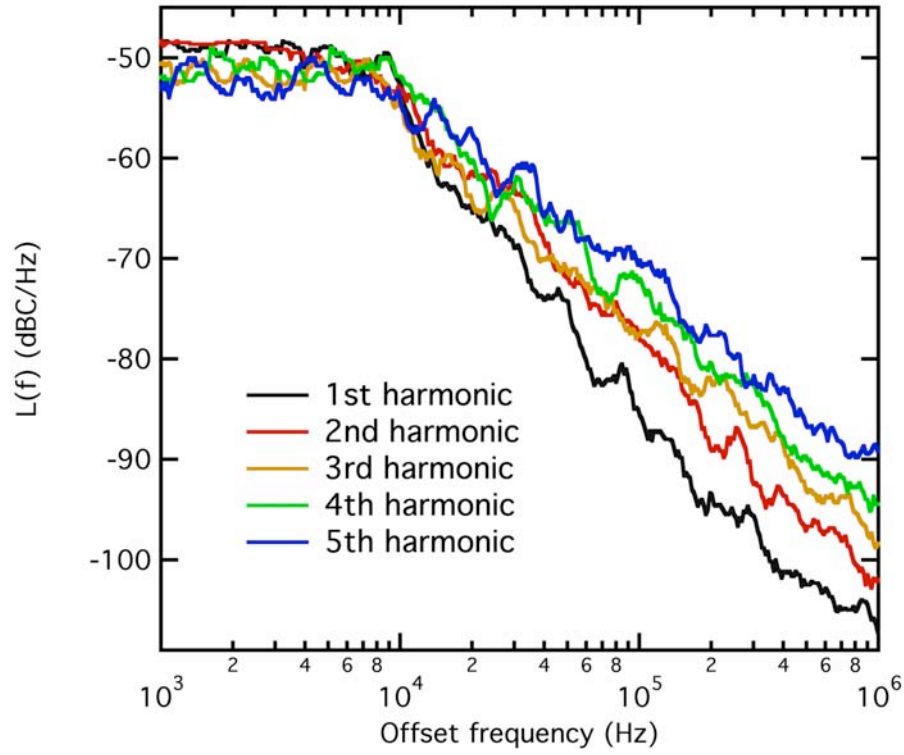
Fig. 4.17 SSB-PN spectra density from different harmonics under 100 mA gain current
and −7 V reverse voltage at the optimum feedback case.

Table 4.2 Timing jitter characterization in the optical feedback case

Harmonic #	D (sec)	σ_{pp} (fs/cycle)
1	$4.97 \ 10^{-18}$	30.8
2	$6.83 \ 10^{-18}$	36.1
3	$6.52 \ 10^{-18}$	35.2
4	$4.35 \ 10^{-18}$	28.8
5	$4.97 \ 10^{-18}$	30.8

4.6 Summary and future work

The effect of external optical feedback for the stably-resonant and nearly-exact resonant (rebroadening) cases on a passive QD MLL module has been studied in this chapter. The experimental results agree well with previously published theory. Under stably-resonant feedback, the RF linewidth is reduced to 170 Hz due to the environmentally-isolated package design and steady temperature control. The unique properties of QDs including a low threshold, a small linewidth enhancement factor, and low spontaneous emission noise are also contributing factors to the reported performance. Wider temperature characterization could be investigated in the future by enhancing the coupling efficiency between the laser device and the lensed fiber pigtail when changing temperature. The RF linewidth rebroadening phenomenon in the nearly-exact resonant feedback case represents a precursor to the coherence collapse regime. A stronger feedback ratio is needed for examining the complete evolution of coherence collapse in the future. For a more advanced compact architecture, the monolithic QD MLL can be hybrid-integrated to a silicon chip that has optical waveguide delay lines as the feedback arm for the MLL device [34]. However, it might be a challenging topic to improve the coupling efficiency between the laser and silicon chip.

Furthermore, the timing jitter performance of a 5.25-GHz passive QD MLL was investigated at different harmonics in the RF spectrum. The relatively low repetition rate of the laser device enables SSB-PN spectra to be measured up to the 8th harmonic in the free-running configuration, and up to the 5th harmonic under feedback. An all-microwave technique has been used to determine the pulse-to-pulse rms timing jitter. Compared to the conventional optical cross-correlation technique, it provides an alternative and simple

method to characterize the timing stability in a passive MLL. To the best of our knowledge, the previously published, diffusion-based model by Eliyahu *et al.* has been validated in the passive QD MLL device for the first time. The experimental findings also demonstrated a good agreement for both analytical approaches from Eliyahu *et al.* and Kefelian *et al.* [12, 13]. As measured by the Eliyahu model, the pulse-to-pulse timing jitter was reduced by nearly an order of magnitude through external optical feedback effect. Thus, the QD MLL packaged module with a simple implementation of an optical feedback arm offers an attractive method for OTDM intra-chip/on-chip communications.

References:

1. A. A. Aboketaf, A. W. Elshaari, and S. F. Preble, "Optical time division multiplexer on silicon chip," *Opt. Express*, vol. 18, pp. 13529–13535 (2010).

2. F. Quinlan, S. Gee, and P. J. Delfyett, "Greater than 20-dB supermode noise suppression and timing jitter reduction via cw injection of a harmonically mode-locked laser," *IEEE Photon. Technol. Lett.*, vol. 19, no. 16, pp. 1221-1223 (2007).

3. S. Gee, F. Quinlan, S. Ozharar, and P. J. Delfyett, "Simultaneous optical comb frequency stabilization and super-mode noise suppression of harmonically mode-locked semiconductor ring laser using an intracavity etalon," *IEEE Photon. Technol. Lett.*, vol. 17, no. 1, pp. 199-201 (2005).

4. S. Ozharar, I. Ozdur, F. Quinlan, and P. J. Delfyett, "Jitter reduction by intracavity active phase modulation in a mode-locked semiconductor laser," *Opt. Lett.*, , vol. 34, no. 5, pp. 677–679 (2009).

5. T. Habruseva, S. O'Donoghue, N. Rebrova, D. A. Reid, L. P. Barry, D. Rachinskii, G. Huyet, and S. P. Hegarty, "Quantum-dot mode-locked lasers with dual-mode optical injection," *IEEE Photon. Technol. Lett.*, vol. 22, no. 6, pp. 359-361 (2010).

6. A. Akrout, A. Shen, A. Enard, G.-H. Duan, F. Lelarge, and A. Ramdane, "Low phase noise all-optical oscillator using quantum dash modelocked laser," *Electron. Lett.*, vol. 46, no. 1, pp. 73-74 (2010).

7. K. Merghem, R. Rosales, S. Azouigui, A. Akrout, A. Martinez, F. Lelarge, G.-H. Duan, G. Aubin, and A. Ramdane, "Low noise performance of passively mode locked quantum-dash-based lasers under external optical feedback," *Appl. Phys. Lett.*, vol. 95,

no. 13, p. 131111 (2009).

8. C.-Y. Lin, F. Grillot, N. A. Naderi, Y. Li, and L. F. Lester, "rf linewidth reduction in a quantum dot passively mode-locked laser subject to external optical feedback," *Appl. Phys. Lett.*, vol. 96, no. 5, p. 051118 (2010).

9. K. Merghem, R. Rosales, S. Azouigui, A. Akrout, A. Martinez, F. Van Dijk, G. Aubin, and A. Ramdane, "Coherence collapse in monolithic quantum-dash-based passive mode-locked lasers," *Proc. SPIE*, vol. 7720, p. 772018 (2010).

10. E. A. Avrutin, and B. M. Russell, "Dynamics and spectra of monolithic mode-locked laser diodes under external optical feedback," *IEEE J. Quantum Electron.*, vol. 45, no. 11, pp. 1456-1464 (2009).

11. D. von der Linde, "Characterization of the noise in continuously operating mode-locked lasers," *Appl. Phys. B*, vol. 39, pp. 201–217 (1986).

12. D. Eliyahu, R. A. Salvatore, and A. Yariv, ''Noise characterization of pulse train generated by actively mode-locked lasers,'' *J. Opt. Soc. Am. B*, vol. 13, no. 7, pp. 1619–1626 (1996).

13. F. Kefelian, S. O'Donoghue, M. T. Todaro, J. G. McInerney, and G. Huyet, "RF linewidth in monolithic passively mode-locked semiconductor laser," *IEEE Photon. Technol. Lett.*, vol. 20, no. 16, pp. 1405-1407 (2008).

14. K. Yvind, D. Larsson, J. Mørk, J. M. Hvam, M. Thompson, R. Penty, and I. H. White, "Low-noise monolithic mode-locked semiconductor lasers through low-dimensional structures," *Proc. SPIE*, vol. 6909, pp. 69090A1–69090A9 (2008).

15. K. Merghem, A. Akrout, A. Martinez, G. Moreau, J. P. Tourrenc, F. Lelarge, F. Van Dijk, G. H. Duan, G. Aubin, and A. Ramdane, "Short pulse generation using a

passively mode locked single InGaAsP/InP quantum well laser," *Opt. Express*, vol. 16, no. 14, pp. 10675–10683 (2008).

16. G. Carpintero, M. G. Thompson, R. V. Penty, and I. H. White, "Low noise performance of passively mode-locked 10-GHz quantum-dot laser diode," *IEEE Photon. Technol. Lett.*, vol. 21, no. 6, pp. 389-391 (2009).

17. Y.-C. Xin, Y. Li, A. Martinez, T. J. Rotter, H. Su, L. Zhang, A. L. Gray, S. Luong, K. Sun, Z. Zou, J. Zilko, P. M. Varangis, and L. F. Lester, "Optical gain and absorption of quantum dots measured using an alternative segmented contact method," *IEEE J. Quantum Electron.*, vol. 42, no. 7, pp. 725-732 (2006).

18. E. U. Rafailov, M. A. Cataluna, and W. Sibbett, "Mode-locked quantum-dot lasers," *Nat. Photonics*, vol. 1, no. 7, pp. 395-401 (2007).

19. F. Grillot, B. Dagens, J. G. Provost, H. Su, and L. F. Lester, "Gain compression and above-threshold linewidth enhancement factor in 1.3 μm InAs-GaAs quantum dot lasers," *IEEE Journal of Quantum Electronics*, vol. 44, no. 10, pp. 946-951 (2008).

20. F. Grillot, C.-Y. Lin, N. A. Naderi, M. Pochet, and L. F. Lester, "Optical feedback instabilities in a monolithic InAs/GaAs quantum dot passively mode-locked laser," *Appl. Phys. Lett.*, vol. 94, no. 15, p. 153503 (2009).

21. O. Solgaard, and K. Y. Lau, "Optical feedback stabilization of the intensity oscillations in ultrahigh-frequency passively modelocked monolithic quantum-well lasers," *IEEE Photon. Technol. Lett.*, vol. 5, no. 11, pp. 1264-1267 (1993).

22. D. Lenstra, B. H. Verbeek, and A. J. Den Boef, "Coherence collapse in single-mode semiconductor lasers due to optical feedback," *IEEE J. Quantum Electron.*, vol. 21, no. 6, pp. 674-679 (1985).

23. J. Mork, B. Tromborg, and J. Mark, "Chaos in semiconductor lasers with optical feedback: theory and experiment," *IEEE J. Quantum Electron.*, vol. 28, no. 1, pp. 93–108 (1992).

24. J. Mork, B. Tromborg, and P. L. Christiansen, "Bistability and low-frequency fluctuations in semiconductor lasers with optical feedback: a theoretical analysis," *IEEE J. Quantum Electron.*, vol. 24, no. 2, pp. 123–133 (1988).

25. B. Tromborg, and J. Mork, "Nonlinear injection locking dynamics and the onset of coherence collapse in external cavity lasers," *IEEE J. Quantum Electron.*, vol. 26, no. 4, pp. 642–654 (1990).

26. J. S. Cohen, and D. Lenstra, "The critical amount of optical feedback for coherence collapse in semiconductor lasers," *IEEE J. Quantum Electron.*, vol. 27, no. 1, pp. 10-12 (1991).

27. F. Grillot, N. A. Naderi, M. Pochet, C.-Y. Lin, P. Besnard, and L. F. Lester, "Tuning of the critical feedback level in 1.55-μm quantum dash semiconductor laser diodes," *IET Optoelectron.,* vol. 3, no. 6, pp. 242-247 (2009).

28. H. A. Haus and A. Mecozzi, "Noise of mode-locked lasers," *IEEE J. Quantum Electron.*, vol. 29, no. 3, pp. 983–996 (1993).

29. M. G. Thompson, D. Larsson, A. Rae, K. Yvind, R. V. Penty, I. H. White, J. Hvam, A. R. Kovsh, S. Mikhrin, D. Livshits, and I. Krestnikov, "Monolithic hybrid and passive mode-locked 40 GHz quantum dot laser diodes," in *Proc. Eur. Conf. Opt. Commun. (ECOC)*, pp. 1–2 (2006).

30. J. P. Tourrenc, A. Akrout, K. Merghem, A. Martinez, F. Lelarge, A. Shen, G. H.

Duan, and A. Ramdane, "Experimental investigation of the timing jitter in self-pulsating quantum-dash lasers operating at 1.55 μm," *Opt. Express*, vol. 16, pp. 17706–17713 (2008).

31. C.-Y. Lin, F. Grillot, Y. Li, R. Raghunathan, and L. F. Lester, "Characterization of timing jitter in a 5 GHz quantum dot passively mode-locked laser," *Opt. Exp.*, vol. 18, pp. 21932–21937 (2010).

32. M. T. Todaro, J. P. Tourrenc, S. P. Hegarty, C. Kelleher, B. Corbett, G. Huyet, and J. G. McInerney, "Simultaneous achievement of narrow pulsewidth and low pulse-to-pulse timing jitter in 1.3　mm passively mode-locked quantum-dot lasers," *Opt. Lett*., vol. 31, no. 21, pp. 3107–3109 (2006).

33. J. P. Tourrenc, S. O'Donoghue, M. T. Todaro, S. P. Hegarty, M. B. Flynn, G. Huyet, J. G. McInerney, L. O'Faolain, and T. F. Krauss, "Cross-correlation timing jitter measurement of high power passively mode- locked two-section quantum-dot lasers," *IEEE Photon. Technol. Lett*., vol. 18, no. 21, pp. 2317-2319, (2006).

34. A. W. Elshaari, A. Aboketaf, and S. F. Preble, "Controlled storage of light in silicon cavities," *Opt. Exp.*, vol. 18, pp. 3014–3022 (2010).

Chapter 5

Conclusions and Future Work

5.1 Summary

In this dissertation, the microwave techniques for designing the cavity layout and improving the timing jitter characterization in a passive QD MLL were studied. The optical generation of microwave signals from a monolithic QD MLL device was also reported and combined with a patch antenna as a hybrid-integrated RF transmitting module.

Firstly, by extending the net-gain modulation phasor approach to account for the discrete distribution of the gain and saturable absorber sections in the cavity, a convenient model was derived and experimentally verified for the cavity design of two-section passive QDash MLLs. A new set of equations was used to predict functional device layouts using the measured modal gain and loss characteristics as input. It was shown to be a valuable tool for realizing the cavity design of monolithic long-wavelength InAs/InP QDash passively mode-locked lasers.

In chapter 3, microwave signal generation from the saturable absorber of a monolithic passive QD MLL was presented. We observed a differential efficiency of 33% that measures the optical to RF power conversion. Furthermore, the hybrid integration of the laser chip with a patch antenna was also investigated to verify the function of a QD MLL as an RF signal generator. Our findings confirmed that QD MLLs

are suitable candidates for the optical generation of RF signals in a compact, efficient semiconductor device and are promising RF microwave sources for hybrid integration with a rectangular patch antenna.

Finally, the stabilization techniques to reduce the phase noise in a passive MLL were presented. The optical external feedback method has been studied in detail owning to the compact, cost-effective fiber-based feedback arm. It has been shown that under the stably-resonant feedback case with relatively low feedback strength and constant temperature control, the RF linewidth narrows to a value as low as 170 Hz. Following that, the timing jitter characterization in a passive MLL was also examined. The pulse-to-pulse rms timing jitter of a 5.25 GHz two-section passive QD MLL was characterized through an all-microwave technique. The experimental phase noise spectra at different harmonics were in good agreement with previous diffusion-based theory. This theory was validated for a semiconductor QD MLL device for the first time. This measurement technique provides a simple way to characterize the noise performance of a passively mode-locked laser. Furthermore, the average pulse-to-pulse rms timing jitter was reduced from 295 fs/cycle to 32 fs/cycle via external optical feedback.

5.2 Future investigations

For the clock distribution application, the monolithic passive MLL will be located close to the CPU cores and will need to tolerate temperatures in the vicinity of $100°$C. The analytical model derived in chapter 2 will be a valuable tool to underpin the key mechanism limiting performance at high temperature environment and to highlight its usefulness in guiding the future design of temperature-stable passive MLLs [1].

The architecture of the hybrid-integrated RF transmitting module can be further extended for the beam steering application [2]. The schematic drawing of a QDMLL-integrated-phased antenna array is illustrated in Fig. 5.1. Depending on the forward or reverse voltage applied to the absorber, the phase difference of the photocurrent signal can be achieved. The measured angle difference of the maximum radiation intensity is around 10 degrees [2]. In the future, a larger angle tuning can be expected with a multi-section QD MLL layout that has more flexibility to locate and change the absorber's location and length, respectively.

For more advanced architectures of a compact OTDM system, the monolithic QD MLL can be hybrid-integrated to a feedback arm that is built from silicon-based optical waveguide [3]. Thus, the compact laser chip with external stabilization mechanism can be achieved at a chip-size scale. However, it might be a challenging topic to improve the coupling efficiency between the laser and silicon chip in the future. With this novel idea and the optical time division multiplexer on a silicon chip [4], the compact OTDM system with high bandwidth links could provide a simpler and more power-efficient scheme compared to the wavelength division multiplexing system.
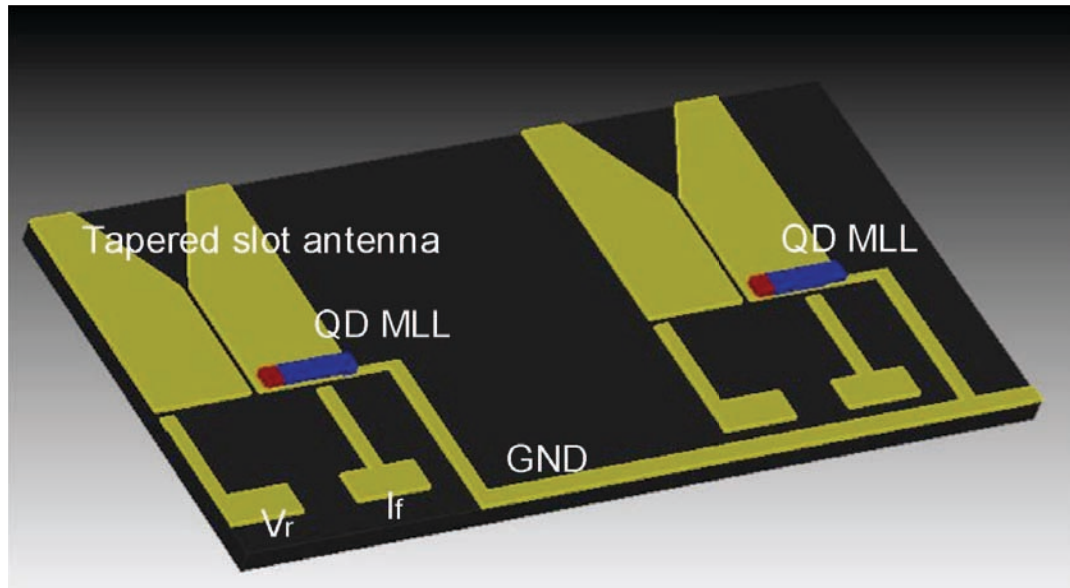
Fig. 5.1 The schematic drawing of a QDMLL-integrated-phased antenna array (two elements). V_r: the contact pad for the reverse voltage bias of the absorber. I_f: the contact pad for the forward current bias of the gain section. GND: the contact pad for the common ground of the laser chips.

References:

1. M. T. Crowley, N. Patel, D. Murrell, M. Breivik, C.-Y. Lin, Y. Li and L. F. Lester, "Modeling the temperature performance of monolithic mode-locked quantum dot lasers," *IEEE Lester Eastman Conference on High Performance Devices*, (2010).

2. J-H. Kim, C-Y. Lin, Yan. Li, N. Naderi, C. G. Christodoulou, and L. F. Lester, "Beam Steering of a Linearly Tapered Slot Antenna Array Integrated with Quantum Dot Mode Locked Lasers", *the 23rd Annual Meeting of the IEEE Photonics Society*, (2010).

3. A. W. Elshaari, A. A. Aboketaf, and S. F. Preble, "Controlled storage of light in silicon cavities" *Opt. Express*, vol. 18, pp. 3014–3022 (2010).

4. A. A. Aboketaf, A. W. Elshaari, and S. F. Preble, "Optical time division multiplexer on silicon chip," *Opt. Express*, vol. 18, pp. 13529–13535 (2010).